Aus dem Bereich der Physiologie
Theoretische Medizin und Biowissenschaften
der Medizinischen Fakultät
der Universität des Saarlandes, Homburg/Saar

Role of the SNAP-25 linker domain in calcium-triggered exocytosis

Dissertation
zur Erlangung des Grades eines Doktors der Naturwissenschaften
der Medizinischen Fakultät
der UNIVERSITÄT DES SAARLANDES
2019

vorgelegt von: Ahmed Shaaban
geb. am: 19 November 1986, Gizeh, Ägypten

Tag der mündlichen Prüfung: 02.12.2019
Dekan: Univ.-Prof. Dr. med. Michael D. Menger
Erste Berichterstater: Prof. Dr. Ralf Mohrmann
Zweite Berichterstater: Prof. Dr. Frank Schmitz

Doctoral supervisor: Prof. Dr. Ralf Mohrmann

Table of Contents

List of Figures

List of Tables

List of Abbreviations

µF: Microfarad

a.u.: Arbitrary units

ANOVA: Analysis of Variance

ATP: Adenosine triphosphate

BAPTA: 1,2-bis(o-aminophenoxy)ethane-N,N,N′,N′-tetraacetic acid

BoNT: Botulinium toxin

BSA: Bovine Serum Albumin

Ca^{2+}: Calcium

CCs: Chromaffin cells

Cpx: Complexin:

DMEM: Dulbecco's Modified Eagle Medium

DPTA: Diethylenetriaminepentaacetic acid

E18: Embryonic day 18

ECL: Enhanced chemiluminescence

ECS: Extracellular solution

fF/S: Femtofarad per second

fF: Femtofarad

g: Gram

GFP: Green Fluorescent Protein

Gm: Membrane conductance

Gs: Series Conductance

GST: Glutathione S-transferase

GTP: Guanosine triphosphate

h: Hour

H_2O: Water

HEPES: 2-[4-(2-hydroxyethyl)piperazin-1-yl]ethanesulfonic acid

ICS: Intracellular solution

JMD: Juxta-membrane domain

KCL: Potassium chloride

kDa: Kilodalton

Kg: Kilogram

KO: Knock out

LDCV: Large Dense Core Vesicles

m: Milli

M: Molar

mCh: mCherry

min: Min

ml: Milliliter

mM: Millimolar

n: number of cells

N: Number of experiments

Nm: Nanometer

NMJ: neuromuscular junction

NP-EGTA: Nitophenyl-EGTA

Oms: Osmol

P: Probability

PAGE: Polyacrylamide gel electrophoresis

PBS: Phosphate-buffered Saline

Pen/Strep: Penicillin/Streptomycin

pH: Potential Hydrogen

PMSF: Phenylmethylsulfonyl fluoride

pS: Picosiemens

PSF: Pre-spike foot

rpm: Revolutions per min

RRP: Ready releasable pool

SDS: Sodium dodecyl sulfate

SEM: Standard error of mean

SFV: Semliki-forest virus

SNAP-25: Synaptosomal associated protein 25

SNARE: Soluble NSF (N-ethylmaleimide-sensitive factor) Attachment Protein) Receptor

SR: Sustained release

SRP: Slowly releasable pool

Syb: Synaptobrevin

Syt: Synaptotagmin

Stx: Syntaxin

TBS: Tris-Buffered Solution

TBST: Tris-Buffered Solution containing 1% tween (20)

t-SNARE: Target SNARE

UV: Ultraviolet

V-SNARE: Vesicular SNARE

WT: Wild type

ΔC_M: Change in membrane capacitance

This work is dedicated to my entire beloved family, especially my Grandma who passed away 09.07.2009

Summary

Spatially and temporally controlled release of neurotransmitters, hormones, and neuropeptides is crucial for proper regulation of physiological processes. On the molecular level, exocytosis of secretory vesicles is driven by assembly of tetra-helical complexes out of the Soluble N–ethylmaleimide sensitive factor (NSF) attachment protein receptor (SNARE) motifs of synaptosomal associated protein-25 (SNAP-25), syntaxin-1a (Stx), and synaptobrevin-2 (Syb). The formation of membrane-bridging *trans*-SNARE complexes putatively brings vesicle and plasma membrane into close apposition against repulsive forces, thereby allowing for subsequent membrane merger and establishment of a fusion pore. While the structure of the core of the SNARE complex has been resolved on the atomistic scale, the functional implications of several structural features of SNARE proteins have remained poorly understood. In particular, the mechanistic function of the bidentate organization of SNAP-25 is still largely obscure: While Stx and Syb represent transmembrane proteins that contain a single SNARE motif in their cytosolic domains (Q_a and R; respectively), SNAP-25 comprises two SNARE motifs (Q_b and Q_c), which are connected by a 60 amino acid-long acylated linker peptide.

In this work, we have investigated the role of this unique SNAP-25 linker domain, which is highly conserved among all orthologs in vertebrates. Earlier studies have considered the linker as a functionally dispensable connector, as it lacks a detectable secondary structure and is not required for SNARE-mediated liposome fusion *in vitro*. Addressing the idea of an inert linker, we have performed an elaborated structure-function analysis introducing linker mutants into SNAP-25 knock-out chromaffin cells by means of a viral expression system. In particular, we tested whether SNAP-25 linker integrity is mechanistically important for secretion and found that co-expression of two complementing SNAP-25 fragments (each containing an intact SNARE motif) only reestablished a severely diminished, kinetically distorted secretory response – thus indicating a mechanistic requirement for a continuous SNAP-25 backbone. Substitution of the whole linker by an artificial, flexible peptide that was only composed of glycine and serine residues led to a completely dysfunctional SNAP-25 variant, which even caused a slight dominant-negative effect on secretion when expressed in wild type (WT) chromaffin cells. Similarly, partial substitution mutants, in which only N- or C-terminal linker segments was replaced by a flexible G/S peptide, exhibited strong functional deficits in primed pool maintenance and fusion triggering. As linker substitution mutants exhibited a delayed kinetics of SNARE assembly in biochemical assays, some of the functional defects might arise from altered SNARE interactions due to a loss of interaction motifs and/or changed conformational properties of the linker. In support of this idea, we found that mutation of four bulky hydrophobic residues that were postulated to mediate the association of the C-terminal linker section with the core complex induced the key phenotypical

traits of the larger C-terminal substitution mutant, albeit the overall phenotype was less severe. An incremental exacerbation of the functional deficits could be observed, when the last 9 amino acids of the C-terminal linker were replaced, supporting the view that C-terminal linker attachment to the core complex is essential for effective fusion.

Mutations targeting the N-terminal palmitoylation motif also had a strong impact on secretion: substitution of the acylated cysteine residues tremendously slowed-down release and decreased the size of the readily-releasable pool. Interestingly, we could exclude the possibility that compromised secretion was indirectly caused by a mislocalization of non-acylated SNAP-25, as the main functional deficits persisted even after retargeting mutant SNAP-25 (cysteine deficient) back to the plasma membrane via a secondary, N-terminal palmitoylation-motif. To investigate whether the acyl anchors of the linker contribute to force transfer from the assembling core complex onto the plasma membrane, we generated mutants, in which SNARE motif and linker were mechanically uncoupled by insertion of flexible spacer peptides of different lengths. While these mutants exhibited a mild fusion triggering phenotype, as would be expected for ineffective molecular straining of the membrane, spacer insertion in palmitoylation-deficient SNAP-25 also exacerbated defective triggering, which clearly contradicts the idea of SNARE force transfer. Thus, spatially defined linker:membrane contacts near the prospective fusion site at C-terminal end of the core complex are of crucial importance the fusion mechanism, while the mechanical coupling of SNARE complex and linker palmitoylation motif seem negligible.

In summary, our data uncover a mechanistic requirement for the SNAP-25 linker domain in fast Ca^{2+}-triggered exocytosis. The SNAP-25 linker primarily serves to functions: [1] it promotes SNARE complex nucleation and assembly by engaging in core complex interactions. [2] It mediates mechanistically important membrane interactions that potentially establish a favorable bilayer configuration for membrane merger. Thus, the linker domain is not just a flexible connector of SNAP-25 SNARE motifs, but itself acts as a functional component of the fusion machinery.

Zusammenfassung

Die räumlich und zeitlich kontrollierte Freisetzung von Neurotransmittern, Hormonen und Neuropeptiden ist entscheidend für die ordnungsgemäße Steuerung physiologischer Prozesse. Auf molekularer Ebene wird die Exozytose sekretorischer Vesikel durch den Zusammenbau von tetra-helicalen Komplexen aus den SNARE-Motiven von SNAP-25, Syntaxin-1a (Stx) und Synaptobrevin-2 (Syb) vorangetrieben. Die Bildung von Membran-verbrückenden trans-SNARE-Komplexen bringt Vesikel und Plasmamembran vermutlich gegen abstoßende Kräfte in enger Anordnung, wodurch eine anschließende Membranfusion und die Bildung einer Fusionspore ermöglicht werden. Während die Struktur des Kerns des SNARE-Komplexes auf atomarer Ebene aufgelöst wurde, sind die funktionalen Implikationen verschiedener Strukturmerkmale von SNARE-Proteinen bisher wenig bekannt. Insbesondere ist die mechanistische Funktion der zweizähnigen Organisation von SNAP-25 noch weitgehend unklar: Während Stx und Syb Transmembranproteine darstellen, die ein einzelnes SNARE-Motiv in ihren zytosolischen Domänen (Qa bzw. R;) enthalten, umfasst SNAP-25 zwei SNARE Motive (Qb und Qc), die durch ein 60 Aminosäuren langes acyliertes linkerpeptid verbunden sind.

In dieser Arbeit haben wir die Rolle dieser einzigartigen SN25-linkerdomäne untersucht, die bei allen Orthologen in Wirbeltieren hoch konserviert ist. In früheren Studien wurde der linker als funktionsfähig verzichtbarer Konnektor betrachtet, da ihm eine nachweisbare Sekundärstruktur fehlt und er für die SNARE-vermittelte Liposomenfusion in vitro nicht erforderlich ist. Um die Idee eines inerten linkers anzusprechen, haben wir eine ausführliche Struktur-Funktions-Analyse durchgeführt, bei der linker-Mutanten mittels eines viralen Expressionssystems in SNAP-25$^{-/-}$ (KO) - Chromaffinzellen eingeführt werden. Wir untersuchten insbesondere, ob die linkerintegrität für die Sekretion mechanistisch wichtig ist, und stellten fest, dass die co-expression von zwei komplementären SN25-Fragmenten (die jeweils ein intaktes SNARE-Motiv enthalten) nur eine stark verminderte, kinetisch verzerrte sekretorische Reaktion wieder herstellte für ein durchgehendes SNAP-25-Backbone. Die Substitution des gesamten linkers durch ein künstliches, flexibles Peptid, das nur aus Glycin- und Serinresten bestand, führte zu einer vollständig dysfunktionellen SNAP25-Variante, die bei Expression in WT-Chromaffinzellen sogar einen geringfügig dominanten negativen Effekt auf die Sekretion auslöste. In ähnlicher Weise zeigten partielle Substitutionsmutanten, bei denen nur N- oder C-terminale linker-Segmente durch ein flexibles G / S-Peptid ersetzt wurden, starke funktionale Defizite bei der Aufrechterhaltung und Fusionsauslösung des Primed Pools. Da linker-Substitutionsmutanten in biochemischen Assays eine verzögerte Kinetik der SNARE-Assemblierung zeigten, könnten einige der Funktionsdefekte auf veränderte SNARE-Wechselwirkungen aufgrund eines Verlusts von Interaktionsmotiven und / oder geänderten Konformationseigenschaften des

linkers zurückzuführen sein. Zur Unterstützung dieser Idee haben wir herausgefunden, dass die Mutation von vier sperrigen hydrophoben Resten, die postuliert wurden, um die Assoziation des C-terminalen linker-Abschnitts mit dem Kernkomplex zu vermitteln, die phänotypischen Schlüsselmerkmale der größeren C-terminalen Substitutionsmutante induziert, wenn auch insgesamt Der Phänotyp war weniger schwerwiegend. Eine schrittweise Verschlimmerung der funktionellen Defizite konnte beobachtet werden, als die letzten 9 Aminosäuren des C-terminalen linkers ersetzt wurden. Dies unterstreicht die Ansicht, dass die Anbindung des C-terminalen linkers an den Kernkomplex für eine effektive Fusion unerlässlich ist.

Mutationen, die auf das N-terminale Palmitoylierungsmotiv abzielten, hatten ebenfalls einen starken Einfluss auf die Sekretion: Die Substitution der acylierten Cysteinreste verlangsamte die Freisetzung enorm und verringerte die Größe des schnell freisetzbaren Pools. Interessanterweise konnten wir die Möglichkeit ausschließen, dass die beeinträchtigte Sekretion indirekt durch eine Fehllokalisierung von nicht acyliertem SNAP-25 verursacht wurde, da die Hauptfunktionsdefizite auch nach dem Retargeting von mutiertem SNAP-25 über eine sekundäre N-terminale Palmitoylierung zur Plasmamembran bestehen blieben -Motiv. Um zu untersuchen, ob die Acylanker des linkers zur Kraftübertragung vom Assemblierungskernkomplex auf die Plasmamembran beitragen, wurden Mutanten generiert, bei denen SNARE-Motiv und linker durch Einfügen von flexiblen Spacerpeptiden unterschiedlicher Länge mechanisch entkoppelt wurden. Während diese Mutanten einen milden fusionsauslösenden Phänotyp zeigten, wie dies bei einer ineffektiven molekularen Dehnung der Membran zu erwarten wäre, verstärkte die Spacer-Insertion in palmitoylationsdefizientem SNAP-25 auch das fehlerhafte Triggern, was der Idee der SNARE-Kraftübertragung eindeutig widerspricht. So ist räumlich definierter linker: Membrankontakte in der Nähe der voraussichtlichen Fusionsstelle am C-terminalen Ende des Kernkomplexes sind von entscheidender Bedeutung für den Fusionsmechanismus, während die mechanische Kopplung von SNARE-Komplex und linker-Palmitoylierungsmotiv vernachlässigbar erscheint.

Zusammenfassend zeigen unsere Daten eine mechanistische Anforderung an die SN25-linkerdomäne bei schneller Ca^{2+}-gesteuerter Exozytose. Der linker dient in erster Linie den Funktionen: [1] Er fördert die SNARE-Komplex-Nukleation und -Montage durch Einbindung in komplexe Interac-Interaktionen [2] Er vermittelt mechanistisch wichtige Membranwechselwirkungen, die möglicherweise eine günstige Doppelschichtkonfiguration für die Membranfusion ergeben. Die Linkerdomäne ist somit nicht nur ein flexibler Konnektor von SNAP-25-SNARE-Motiven, sondern fungiert selbst als funktionaler Bestandteil der Fusionsmaschinerie.

Introduction

Organisms need to generate proper physiological responses to external and internal stimuli. The necessary integration of information is accomplished by intricate intercellular signaling pathways, which transmit information between cells via release of messenger substances. Exocytosis represents a fundamental cellular mechanism, by which a vesicle or secretory organelle fuses with the plasma membrane in order to release its molecular cargo into extracellular space. Temporally and spatially regulated exocytosis is of paramount importance for intercellular communication processes like synaptic transmission and hormone secretion. Since exocytosis was shown to have a critical role in both physiological and pathophysiological events, many research groups have focused on this process since its discovery by the end of the nineteenth century (Ivanov, 2014).

1.1 Regulated vs. constitutive exocytosis

Trafficking of vesicles towards the cell surface is an essential process for eukaryotic cells for normal cell function as well as proper intercellular communication. In fact, two main pathways by which the cell can transfer certain substances towards the cell membrane or the extracellular matrix. First pathway is the canonical pathway known as “constitutive” pathway. In this pathway, continuous vesicle supply from the *Trans-Golgi Network* (TGN) takes place towards the plasma membrane. The constitutive pathway is used by all cells mainly to insert new cell membrane patches, lipids, extracellular molecules and glycoproteins to the cell surface. However, these pathways can be used to secrete extracellular molecules such as glycoproteins, lipids, and antibodies (Alberts et al., 2015; Wilson and Hunt, 2015). Regulated exocytosis is the other pathway by which cells can release certain cargo stored in vesicles to the extracellular milieu. Regulated exocytosis is a tightly regulated way to release cargo that only takes place under certain circumstances. It takes place in secretory cells such as neurons, neuroendocrine or exocrine cells. Regulated exocytosis starts when a cell is activated either chemically, mechanically or electrically. This activation would eventually lead to raise in the intracellular calcium which in turn will cause cascade of events that finally leads to the fusion of the vesicle membrane with the plasma membrane releasing the vesicle’s cargo to the outside of the cell.

1.2 Vesicle pools, docking, and priming

To study this highly regulated cellular process of exocytosis, Erwin Neher and Thomas Voets pioneered the field of understanding different pools of vesicles in chromaffin cells. They were able to describe and analyze different types of vesicles pools. Since spatial distribution of calcium inside a chromaffin cell is not homogenous, this would result in different release probabilities of the large dense core vesicles according to their proximity to the calcium channels. To circumvent this factor, Voets and colleagues developed a technique by which, calcium ions could be homogenously distributed across the cell. The calcium is chelated using the chelator NP-EGTA (Voets, 2000; Voets et al., 1999). The chelated calcium is then introduced inside the cell in an intracellular solution (ICS) through a patch pipette. After ensuring homogenous spatial distribution of the pipette solution (intracellular solution) across the cell, the calcium was then uncaged using a strong UV-flash light, and exocytosis was measured as the increase in the total cell capacitance via the stimulating/recording electrode. Fura dyes were also introduced within the intracellular solution in order to estimate the calcium concentration inside the cell before and after the uncaging of the calcium. Chromaffin cells express different types of voltage-gated calcium channels (Garcia-Palomero et al., 2000). Thus, induced depolarization would lead to the activation of these channels raising local calcium concentrations to higher levels (micro-molar range) creating "calcium-microdomains". This high local calcium concentration would lead to the fusion of vesicles in proximal vicinity to these activated channels. It was shown that the fusion of large dense core vesicles from adrenal chromaffin slices is biphasic; an initial fast phase of catecholeamine release that is followed by a later slower phase. The fast phase was initiated by either a fast (18 Hz) depolarization trains (from -80 to -5 mV), or via low frequency stimulation (3 Hz).

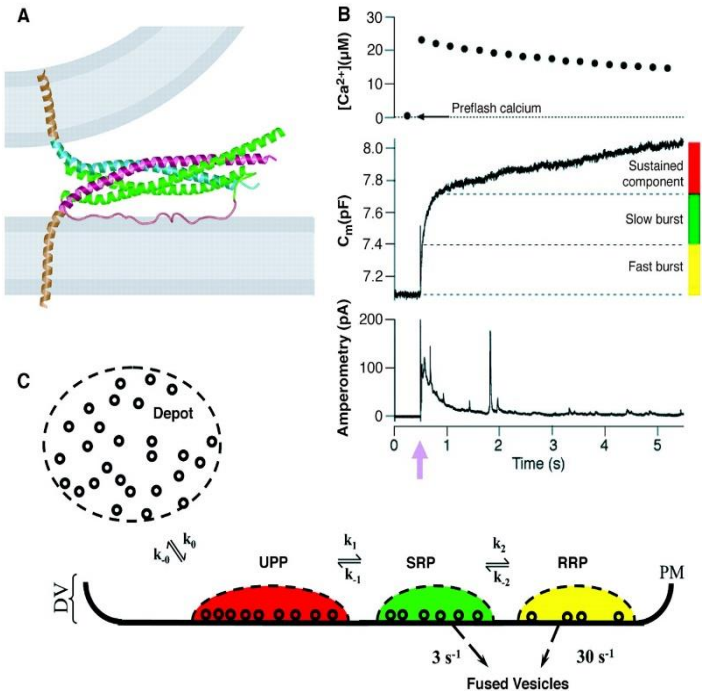

Figure 1 release of vesicle pools upon UV-flash Ca^{2+}-uncaging.

(A) Cartoon showing the overall structure of the SNARE complex. (B) Typical capacitance recording (middle panel) combined with carbon fiber amperometry (lower panel) while monitoring calcium concentration before and after flash (upper panel). (C) A model depicting different LDCVs pools in a chromaffin cell. Adapted from (Rettig and Neher, 2002).

However, they were only able to induce the slow phase under high frequency stimulation and failed to see it under low frequency depolarizations. Interestingly, when the duration of the low frequency stimulus was prolonged from 10 ms to 100 ms. Subsequently, they switched from depolarization to stimulation via calcium uncaging where increased global calcium in a chromaffin cell resulted in three distinct pools of vesicles. Fitting the capacitance trace (ΔC_M) was best achieved using a triple exponential function. The three pools were named the readily releasable pool (RRP), the slowly releasable pool (SRP) and sustained release (SR) with time constants of 27, 290, and 5600 ms, respectively (Figure 1B). Both the RRP and SRP were collectively named "the exocytotic burst". It was found that with a stronger pre-flash stimulus, the exocytotic burst was decreased without affecting the slow (sustained) component. Similar experiments were performed a year later using mouse instead of bovine adrenal chromaffin cells and it yielded very similar results showing consistency of the release pools and kinetics across different organisms (Voets, 2000; Voets et al., 1999). The sustained component is known to arise from docking and priming (terms that will be explained later) of the unprimed pool (UPP). This UPP was estimated to be situated nearly 200 nm away from the plasma membrane (Figure 2). The UPP is replenished through a major pool of vesicles in a chromaffin cell; named as Depot pool (DP). DP represents the group of vesicles >200 nm away from the plasma membrane (Becherer and Rettig, 2006). The three vesicle pools were then represented in an equation with triple exponential components representing RRP, SRP, and the sustained release rate) as follows:

$$\mathbf{C_{M(t)} = A_0 + A_{RRP}\,(1 - e^{-t/\tau_{RRP}}) + A_{SRP}\,(1 - e^{-t/\tau_{SRP}}) + A_{SR}\,(1 - e^{-t/\tau_{SR}})}$$

Where $C_{M(t)}$ is the capacitance of the cell at a given point (after 5 s of calcium uncaging), and A_0 is the capacitance of the cell before stimulation. A_{RRP} is the RRP value, A_{SRP} is the SRP value and the third component is calculated as a rate of release (i.e. fF per second).

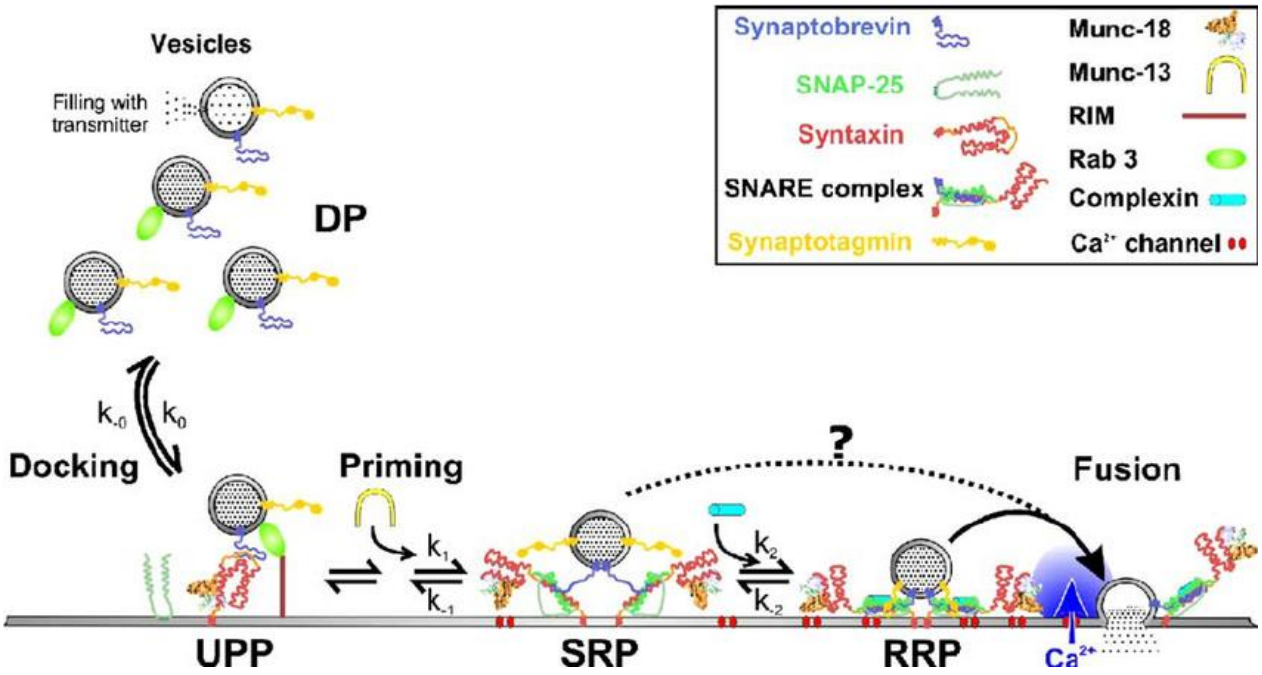

Figure 2 SNAREs and SNARE regulatory proteins involved in regulated exocytosis.
The depot pool (DP) is group of vesicles that are mature, filled with transmitter but far from the plasma membrane. From the DP comes a group of unprimed vesicles called unprimed pool (UPP) that approach the plasma membrane in a process called docking. Mammalian uncoordinated (Munc) -18 helps stabilize the docked vesicles by reducing the backward rate k−0. Priming is the transfer of vesicles from the UPP to the slowly releasable pool (SRP) due to "half zippering" of the SNARE complex from the individual SNAREs SNAP-25, syntaxin, and synaptobrevin. Munc13 is a priming factor that enhances the forward rate k1. The equilibrium between SRP and RRP could be controlled by complexin, Calcium-dependent secretion activator (CAPS) and other proteins, which decrease the k−2 rate. Synaptoagmin initiates the vesicle merging with the membrane upon binding to Ca^{2+}. Adapted from (Becherer and Rettig, 2006).

1.3 SNAREs as core components of the membrane fusion machinery

Soluble N-ethylmaleimide sensitive factor attachment protein receptors (SNAREs) form a large protein family, whose members are primarily characterized by 60-70aa long, α-helical segments that are referred to as SNARE motifs (Jahn and Scheller, 2006; Kloepper et al., 2007; Weimbs et al., 1997). Four of these SNARE motifs can interact with each other and assemble into a helix bundle with parallel orientation, which is primarily stabilized by internal hydrophobic interactions (Poirier et al., 1998; Sutton et al., 1998). Structural studies have shown that the four interacting amphiphatic helices are aligned in a way that the side-chains at the core of the rode-like SNARE complex face each other in 15 hydrophobic interaction layers (Fasshauer et al., 1998b). According to the crystal structure, the fully-formed SNARE complex is around 12 nm long (Sutton et al., 1998) with hydrophobic layers numbered from -7 to + 8. Interestingly, the central "0"-layer accommodates conserved polar residues - one arginine and three glutamine residues. The identity of theses amino acids in the different SNARE motifs has led to the classification of "R" and "Q"-type

SNAREs (Jahn and Scheller, 2006). There are more than 60 identified members of the SNARE superfamily in mammals and more than 20 members in the yeast (Karp, 2013). Based on the homology of SNARE motifs four major subgroups can be distinguished: Q_a, Q_b, Q_c, and R (Fasshauer et al., 1999). While SNARE complexes typically contain a single member of each subgroup, there is substantial promiscuity with respect to the possible combinations of cognate SNAREs that can successfully engage in complex formation *in vitro* (Fasshauer et al., 1999; Pabst et al., 2002).

While prototypical SNAREs represent regular transmembrane proteins carrying only a singular SNARE motif, Q_b and Q_c motif-containing SNAREs have evolutionary fused and formed an additional group of the so-called Q_{bc} SNAREs (Fasshauer et al., 1999). This is particularly evident when considering that the yeast homologs of the mammalian Q_{bc}-SNARE *synaptosome associated protein* (SNAP)-25: sec9 and Spo20 are plasma membrane-localized, separate Q_b- and Q_c-SNAREs, that serve core functions in yeast sporulation (Fukuda et al., 2000; Weimbs et al., 1997) , while the related SNARE motifs in SNAP-25 are interconnected by a linker domain in tandem-like organization (Figure 7). Though Q_{bc} SNAREs generally lack a transmembrane domain, several isoforms associate with membranes via side-chain modifications. In particular, the Q_{bc} SNAREs SNAP-25 and SNAP-23 contain clusters of cysteine residues within the linker domain that allow for acylation and effective membrane anchorage (Bark and Wilson, 1994; Shukla et al., 2001).

The formation of SNARE complexes between lipid bilayers has been implicated in membrane fusion processes and likely represents the most prominent mechanism for physiological fusion of cellular organelles (Jahn and Sudhof, 1999; Sollner et al., 1993a; Sollner et al., 1993b). It is well established that SNARE proteins exhibit a specific subcellular distribution, with complex-forming sets of SNAREs residing on membranes of different cellular compartments (Chen and Scheller, 2001). For regulated exocytosis, i.e. the Ca^{2+}-dependent fusion of secretory organelles with the plasma membrane, the predominant set of SNARE proteins in vertebrates consists of synaptobrevin-2 (R), syntaxin-1 (Q_a), and SNAP-25 (Q_{bc}). Indicating the direction of exocytosis, SNAREs are commonly subdivided in vesicular (v)-SNAREs and target (t)-SNAREs on the plasma membrane (Rothman, 1994; Sollner et al., 1993b). As the first t-SNARE, SNAP-25 was identified in neurons in 1989 (Oyler et al., 1989), while the second t-SNARE syntaxin (Stx) was discovered in the lab of Richard Scheller in 1992 (Bennett et al., 1992). The v-SNARE was named vesicular-associated integral membrane protein (VAMP)-2 or synaptobrevin-2 (Syb) and was first described in 1988 (Trimble et al., 1988). Orthologs of these SNARE proteins were also discovered in yeast cells and were shown to participate in the yeast secretory pathway (Novick et al., 1980).

The central role of SNARE proteins in exocytosis has been established by a wealth of experimental evidence, including knockout mouse models (Bronk et al., 2007; Schoch et al., 2001; Sharma et al., 2012),

antibody infusion (Xu et al., 1999), reconstitution experiments, and neurotoxin-mediated proteolytic degradation (Binz et al., 1994; Blasi et al., 1993; Schiavo et al., 1993; Yamasaki et al., 1994). According to the most popular mechanistic scenario, the forming SNARE complex is envisioned as a molecular motor that forces lipid bilayers into close apposition, thereby enabling membrane merger and the formation of a fusion pore (Hanson et al., 1997; Jahn et al., 2003). The free energy to overcome membrane repulsion is putatively generated by formation of the thermodynamically stable tetrahelical SNARE assembly, which needs to be actively disassembled under ATP consumption by the ATPAse *N*-ethylmaleimide sensitive factor (NSF) after fusion (Brunger et al., 2009; Jahn and Scheller, 2006; Rizo and Sudhof, 2002; Sudhof and Rizo, 2011). The free energy production of SNARE complex formation has been estimated by calorimetry (Pabst et al., 2002; Wiederhold and Fasshauer, 2009) and force microscopy (Montana et al., 2008, 2009), yielding values in the range of 40 k_BT (k_B = Boltzmann constant, and T = Temperature) . Theoretical considerations of bilayer fusion at distance of about 1 nm (same distance experimentally observed during stalk formation) have pointed to an energy demand in the same range (~30 k_BT) for the establishment of a fusion pore , indicating that formation of a single or a few SNARE complexes might be sufficient to successfully induce membrane merger (Mohrmann and Sorensen, 2012; Zhang et al., 2016). In line with this, experimental data confirmed that the minimum SNARE stoichiometry for fast efficient secretion requires 2-3 SNARE complexes (Mohrmann et al., 2010; Shi et al., 2012; Sinha et al., 2011).

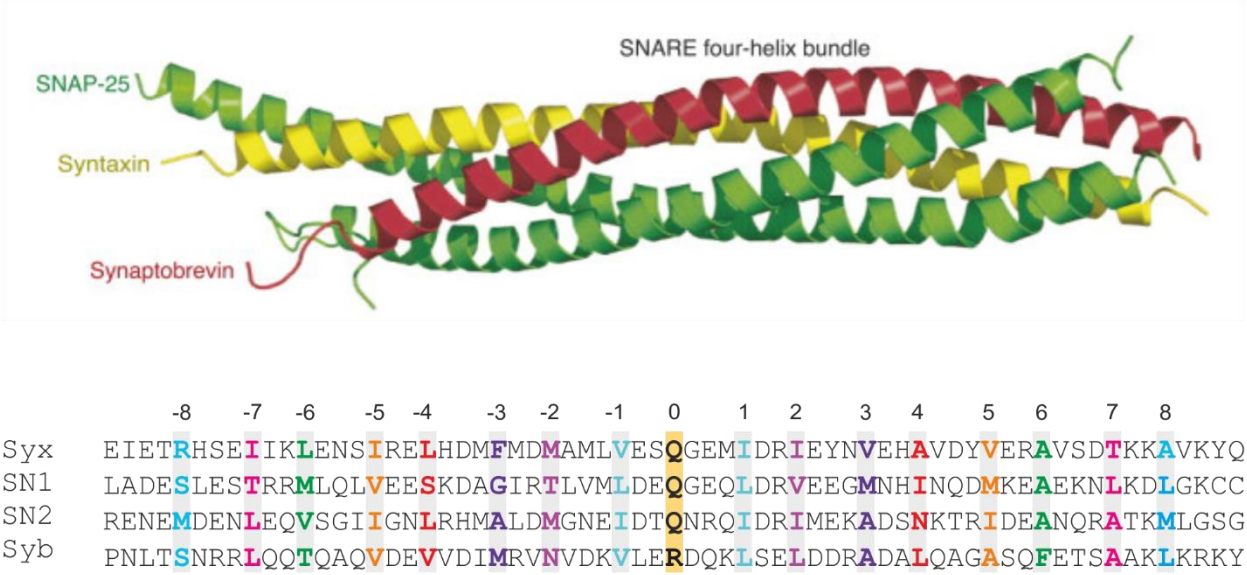

Figure 3 Layers of the SNARE complex.
Top: predicted helices from the crystal structure shown as SNAP-25 (green), syntaxin (yellow), and Synaptobrevin-2 (blue). Bottom: aligned sequences of different SNARE proteins and different layers ranging from -7 to + 8. Adapted from (Weber et al., 2010).

The actual folding pathway, by which the four SNARE motifs assemble into a complex, has not been completely elucidated. Mutational studies in chromaffin cells have delivered strong evidence that SNARE assembly involves different intermediates, as mutations that target different hydrophobic layers induce distinctive phenotypes (Sorensen et al., 2006; Walter et al., 2010; Weber et al., 2010; Weber et al., 2014). While the previous models suggested a lipidic fusion pore, another model was proposed suggesting a parallel organization of the transmembrane domains (TMDs) forming a fusion pore of proteinacious nature (Jackson, 2010). Generally, N-terminal layer mutations in the SNARE motifs do not cause severe secretion deficits, while central mutations seem to impair priming, and C-terminal mutations primarily affect fusion triggering. These findings suggest that the complex likely forms in a progressive fashion from N- to C-terminus involving functionally divergent stages (Pobbati et al., 2006). In line with this idea, biochemical experiments using different SNARE fragments also indicated that the N-terminal region of the complex is first formed, while C-terminal assembly correlates with the final stages of membrane fusion (Fasshauer and Margittai, 2004). SNARE complex assembly and disassembly profiles measured by force microscopy further indicated the existence of metastable assembly states, in which SNARE motifs were only partially assembled (Gao et al., 2012; Kyoung et al., 2011). However, when purified SNAREs were mixed in solution (Fasshauer et al., 1999) or used for liposome fusion assays (Weber et al., 1998), SNARE motifs are constitutively active, and no assembly intermediates could be identified. Thus, it appears likely that additional accessory factors retain the SNARE complex in a partly-assembled prefusion state in order to prevent premature secretion.

1.3.1 v-SNAREs in secretory cells and neurons

In neurons and neuroendocrine cells of mammals, four different Syb/VAMP isoforms (Syb-1, 2, 7, and 8) have been identified (Ren et al., 2007; Schoch et al., 2001; Sudhof et al., 1989; Trimble et al., 1990). The VAMP2 isoform is involved in synaptic (SV) release in neurons (Baumert et al., 1989; Trimble et al., 1988), insulin secretion from ß-cells of the pancreas, release of zymogen granules from pancreatic acinar cell, and catecholamine secretion from adrenal chromaffin cells (Gaisano et al., 1994; Misonou et al., 1997). VAMP2 is sensitive to botulinum neurotoxin (serotypes B, D, F and G) while VAMP1, its closest isoform, as well as VAMP8 are neurotoxin insensitive (Pitzurra et al., 1996; Rossetto et al., 1996) (refer to Figure 4).

VAMP7, another toxin insensitive variant, is present at the apical membrane of epithelial cells and it is mainly involved in constitutive exocytosis (Galli et al., 1998). VAMP8, also named endobrevin, localizes with transferrin receptors at early endosomal compartments. In adrenal chromaffin cells, cellubrevin, also known as VAMP3, was shown to be functionally redundant to VAMP2 (McMahon et al., 1993). On the other hand, cellubrevin and synaptobrevin were showed to be located differently to either synaptic vesicles

(Syb) or dense core vesicles (cellubrevin) having two distinct functions in the modulation of synaptic transmission in astrocytes (Schwarz et al., 2017).

All of these VAMP isoforms are about 120 amino acids in size and constitute type II membrane proteins. The isoforms are comprised of an N-terminal region of 25-35 amino acids, the SNARE motif, a short juxta-membrane segment, the TMD, and a very short luminal motif. While the cytosolic section of isolated Syb-2 has been considered largely unstructured (Fasshauer and Margittai, 2004), recent work on the membrane-embedded protein suggested the presence of two folded helical regions, one within the SNARE motif and another at the transition to the juxta-membrane domain (Ellena et al., 2009). The TMD is located at the carboxyl end, localizing the protein to synaptic vesicles or large dense core vesicles (Gerst, 1997; Grote et al., 1995; Regazzi et al., 1996).

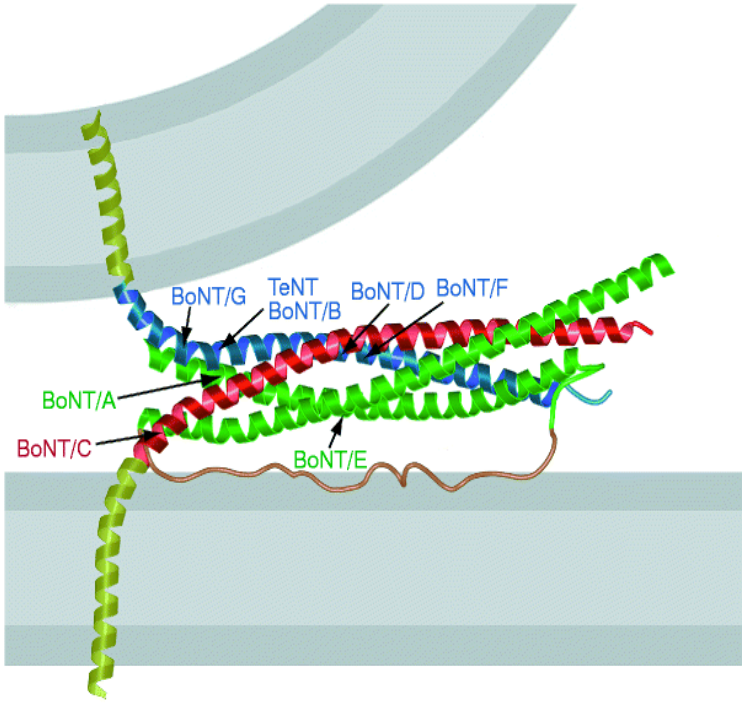

Figure 4 Neurotoxins cleavage sites in different SNARE proteins.
Cartoon showing susceptibility of different SNAREs to different tetanus as well as botulinum neurotoxins. While BoNT/A and E are the main effectors on SNAP-25 (two green helices connected by an orange linker), BoNT/C acts on Stx and BoNT/B, D, F, and G act on different sites in Syb (blue). Adapted from (Sutton et al., 1998).

In yeast, Snc1 and Snc2 are the two Syb homologs that are found in two types of secretory vesicles in yeast aiding in delivery of new lipids, enzymes and membrane proteins constitutively towards the plasma membrane (Gerst et al., 1992). These v-SNAREs were also shown to interact with their v-SNARE homologs Sec9, a SNAP-25 homolog, and SSo1 and SSo2 (Stx homologs) to form a ternary SNARE complex (Rossi et al., 1997). In principle, the Syb family is structurally as well functionally conserved during evolution.

1.3.2 t-SNAREs

1.3.2.1 Syntaxin isoforms in neuroendocrine cells and neurons

In mammals, there are at least 16 different members of the Stx family, thus representing the largest group of SNARE proteins. Stx-1A and Stx-1B are the main isoforms expressed in neurons and neuroendocrine cells (Bennett et al., 1993). Stx is an integral protein inserted in the plasma membrane via its TMD (Bennett et al., 1992; Bennett et al., 1993; Inoue et al., 1992) as shown in Figure 4. Structurally, Stx consists of 3 coiled-coil helices named H1, H2, and H3 as well as a TMD (Bennett et al., 1992). "H3" is the SNARE motif, by which Stx contributes to the SNARE complex (Kee et al., 1995) (Figure 5A, B). The H1 and H2 helices are believed to be intramolecular regulators of the Stx activity through inhibiting the H3 domain from binding to SNAREs (Nicholson et al., 1998). Stx function is orchestrated by a major accessory protein named Munc-18. Munc-18 is one of the members of the Sec1/Munc-18-like SM family of proteins known for their important role in intracellular membrane trafficking (Carr and Rizo, 2010). Munc-18 is crucial for the Stx function. Munc-18 strongly binds to the closed form of Stx (at its N-peptide region) through its arch-shaped cavity (Dulubova et al., 1999; Misura et al., 2000). This conformation not only hinders SNARE assembly and stops uncontrolled exocytosis but also helps in the stability of both proteins (Burkhardt et al., 2008). With the aid of another accessory protein, named Munc-13, conformational change of Munc-18:Syntaxin complex occurs to render the Stx in the open conformation, allowing other SNARE proteins to bind the complex and promote fusion (Ma et al., 2011).

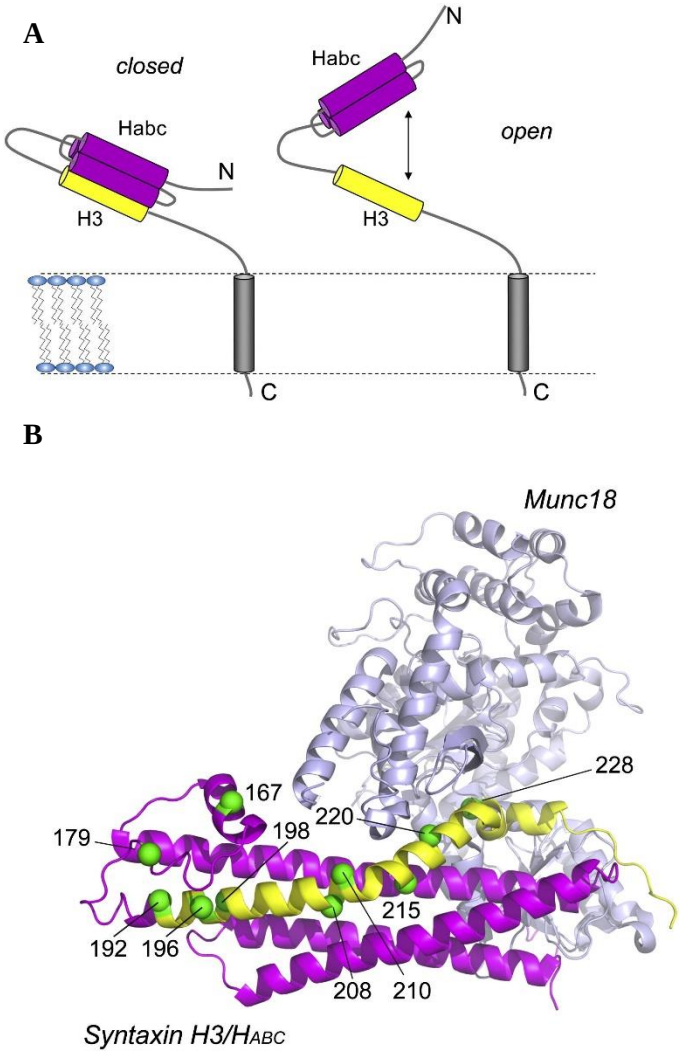

Figure 5 Schematic figure of Stx1a-Munc18 complex. (a) Different motifs of Stx either in the closed (left) or the open (right) conformation (b) Crystal structure of the syntaxin 1a/Munc18-1 complex. Adapted from Dawidowski and Cafiso (2013).

Stx-1A is sensitive to botulinium neurotoxin C (BoNT/C) evidenced by completel abolishment of insulin release from secretory granules in ß-cells upon application of BoNT/C (Figure 4) (Land et al., 1997). Stx-2 and 3 were present in polarized epithelial cells specifically localized to the apical membrane (Delgrossi et al., 1997; Fujita et al., 1998), while Stx-4 was found to localize at the apical membrane of the renal collecting duct cells (Mandon et al., 1996). Other Stx family members are possibly playing role in the early stages of the secretory pathway such as endoplasmic reticulum (ER)-Golgi transport, or endosomal transport (Prekeris et al., 1999).

Sso1 and Sso2 are the two main Stx homologs in yeast. Knocking out both genes expressing these homologs completely blocked the secretory pathway, confirming the same function observed in mammals (Aalto et al., 1993). Another Stx-1 homolog was observed in *C. elegans* (the gene is encoded by the unc-64 locus) (Saifee et al., 1998). The null mutant of Stx-1 is paralyzed and the hypomorphic mutants possess behavioral defects and changed mode of neurotransmitter secretion. A Stx-1A homolog, denoted as Dsynt1, is also expressed also in drosophila and is targeted to axons and synapses of the central nervous system (Broadie et al., 1995; Cerezo et al., 1995). Loss of function mutations yielded lethal drosophila embryos. Spontaneous neurotransmitter release as well as evoked response was completely abolished when measured using electrophysiological recordings (Schulze et al., 1995). Moreover, Stx-1A is required at the blastoderm stage of development of the drosophila embryos (Burgess et al., 1997). Thus, Stx is crucial not only for synaptic transmission, but also for ensuring proper development.

1.3.3 Q_{bc}-SNAREs and exocytosis

1.3.3.1 Q_{bc}-SNAREs in neurosecretory cells and neurons

The primary Q_{bc}-SNAREs involved in secretion are SNAP-25 and SNAP-23; with SNAP-25 being the main isoform in neurons (Delgado-Martinez et al., 2007; Hess et al., 1992). SNAP-25 exists in two splice variants, denoted a and b. The primary sequence of SNAP-25 a and b is completely conserved between the orthologs of human, mouse and chicken (Bark and Wilson, 1994; Oyler et al., 1989). In dissected brains of mice and chicken, SNAP-25a is highly expressed during embryonic stage while SNAP-25b levels dramatically increased during postnatal life (Bark et al., 1995; Bark and Wilson, 1994). The same was also shown to occur in different brain regions in humans (Prescott and Chamberlain, 2011).

SNAP-25b was shown to mediate generally higher secretory response to the same stimulus than SNAP-25a, as shown by expression of both isoforms in SNAP-25 knock-out (SNAP-$25^{-/-}$) mouse adrenal chromaffin cells (Nagy et al., 2005). The primary sequence of the splice isoforms differ in 9 amino acid positions, 4 at the linker region and 5 at the first SNARE motif (denoted Q_b or SN1). The increase in secretion observed

with SNAP-25b was attributed to the two amino acids Q66, K69 (H66 and Q69 for SNAP-25a isoform; respectively) (Nagy et al., 2005). SNAP-23 is a constitutively expressed Q_{bc}-SNARE that shares around 60% sequence identity with SNAP-25(Nagy et al., 2008). It is expressed in neuronal as well as non-neuronal cells, where it functions in constitutive and regulated exocytosis (Guo et al., 1998; Leung et al., 1998; Ravichandran et al., 1996). While SNAP-23 is sufficient to drive insulin secretion in BoNT/E-treated pancreatic B cell line (HIT) (Sadoul et al., 1995), SNAP-23 failed to functionally substitute for SNAP-25 in mouse adrenal chromaffin cells, as over-expression of SNAP-23 in mouse adrenal SNAP-$25^{-/-}$ cells did not restore the exocytotic burst and had a dominant negative effect when over-expressed in WT cells (Sorensen et al., 2003). Later experiments indicated that the limitation of SNAP-23-mediated secretion is caused by a sequence variation in the C-terminal linker segment, but not due to difference in SNARE motifs (Nagy et al., 2008). Currently, no specific function could be attributed to the corresponding SN25 linker motif (V^{120}VDEREQMAI^{129}), which lacks any particular secondary structure.

A classic SNAP-$25^{-/-}$ mouse model was generated byWashbourne et al. (2002), targeting exons 5a and 5b that would normally undergo alternative splicing. SNAP-25 deficient mice exhibit late embryonic lethality but appear largely morphologically normal at embryonic days 17.5-18.5 (E17.5-18.5). As most obvious phenotypical traits, homozygous null mutants develop a dorsal hunch and show neither spontaneous movements nor sensory motor reflexes, when mechanically stimulated. Heterozygous SNAP-$25^{+/-}$ animals were functionally and morphologically indistinguishable from the WT mice, albeit protein expression is roughly halved in comparison to WT mice in Western Blots. A functional characterization of the null mutants demonstrated that genetic ablation of SNAP-25 results in dysfunctional transmission at the neuromuscular junction (Washbourne et al., 2002), diminished secretion of catecholamines from adrenal chromaffin cells (Sorensen et al., 2003), and abolished synaptic transmission at central synapses (Delgado-Martinez et al., 2007). Noteworthy, SNAP-$25^{-/-}$ neurons show a strongly reduced survival in culture, with residual neurons exhibiting decreased dendritic arborizations (Delgado-Martinez et al., 2007). These phenotypes can be differentially rescued by expression of Q_{bc}-SNARE isoforms: introducing either SNAP-25a, SNAP-25b, or SNAP-23 restored neuronal survival, arborization as well as the frequency and amplitude of spontaneous release in cultured neurons (Delgado-Martinez et al., 2007). However, in cultured SNAP-$25^{-/-}$ chromaffin cells, expression of SNAP-23 could not reinstate normal priming of large dense-core vesicles, while expression of SNAP-25a fully rescued secretion, and expression of SNAP-25b boosted the secretory response over the wild type level (Sorensen et al., 2003).

1.3.3.2 Membrane-anchorage of SNAP-25

The N-terminal linker region of several Q_{bc}-SNAREs contains a cluster of 4-5 cysteine residues that can be modified by S-acylation. SNAP-25 isoforms have four cysteine residues (Figure 6) that are palmitoylated by acyltransferases of the *aspartate-histidine-histidine-cysteine* (DHHC) family, thereby ensuring the correct localization of the SNAP-25 at the plasma membrane (Gaisano et al., 1994; Greaves et al., 2010a; Greaves et al., 2009). Truncated SNAP-25 variants have indicated that about two thirds of the linker sequence (aa 85-120) are required for efficient acylation and membrane anchorage of the protein (Greaves et al., 2010b) (Figure 6). It has been speculated that this minimal SNAP-25 fragment can transiently localize to the plasma membrane, thus allowing for interaction with membrane-associated DHHC acyltransferases and thereby facilitating membrane anchorage. In line with this idea, it has recently been proposed that electrostatic anchoring of SNAP-25 by positively charged residues around the cysteine cluster precedes the acylation step (Weber et al., 2017). Though interactions of SNAP-25 with other t-SNARE proteins are not absolutely necessary for palmitoylation, as facilitating effect of Stx-1A on SNAP-25 has been proposed (Gonelle-Gispert et al., 2000).

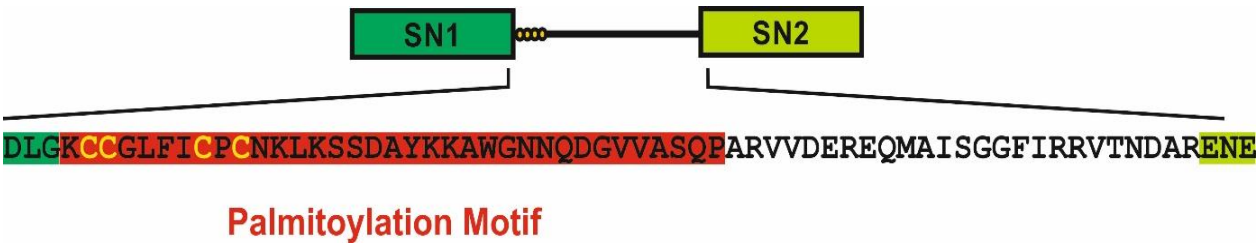

Figure 6 Structure of the SNAP-25 a isoform.
Cartoon showing the tandem sequence of the SNAP-25 a isoform; dark green is the first SNARE motif (Qb or SN1), light green is the second SNARE motif (Q_c or SN2) spaced by a 60 amino acid linker comprising the motif needed for DHHC acyltransferase recognition (highlighted in red). The figure was kindly provided by Prof. Ralf Mohrmann.

The presence of all cysteine residues seems to be critical for the correct localization of SNAP-25, as mutation of only a single cysteine already significantly impacts membrane anchorage (Washbourne et al., 2001). A complete cysteine deficient mutant showed more than 90% loss of membrane anchorage (Nagy et al., 2008). While the specific acylation pattern of the four cysteine residues is still unclear, there is evidence suggesting that not all residues are indeed S-acylated in the naive protein (Foley et al., 2012; Veit et al., 1996). The positioning of cysteines is slightly altered in SNAP-25b in comparison to isoform a, but this alteration seems to be inconsequential for the function (Nagy et al., 2005).

Membrane-bound SNAP-25 has been proposed to partially (20%) localize in lipid rafts (Chamberlain et al., 2001; Garcia-Martinez et al., 2015), but the functional implication of its presence within the cholesterol-

rich patches is not clear. SNAP-25 forms clusters on the plasma membrane (Zhao et al., 2013), and the clustered distribution pattern of SNAP-25 has been shown to depend on the presence of cholesterol (Lang et al., 2001). Interestingly, it has been demonstrated that SNAP-23, a Q_{bc}-SNARE, with 5 potential acylation positions is even more tightly associated with lipid rafts than SNAP-25, suggesting that the extent of acylation determines the specific localization within lipid environments (Salaun et al., 2005). Given a negative correlation between raft-association and secretion, it has been speculated that only SNAP-25 at the borders of lipid rafts might actively engage in vesicle fusion (Salaun et al., 2005). Thus, SNAP-25 acylation and available lipid domains could spatially define release sites.

Depending on the experimental system and expression level, elimination of the cysteine residues in SNAP-25 mutants has been reported to affect secretion to different extents: In some models systems no secretion could be detected (Washbourne et al., 2001), while in others the size of secretory responses largely persisted, but release kinetics were dramatically slowed down (Nagy et al., 2008). Moreover, amperometric recordings in SNAP-25$^{-/-}$ chromaffin cells that express acylation-deficient variants also displayed a decelerated transmitter discharge due to a prolonged life-time of the initial fusion pore state (Nagy et al., 2008). Thus, SN25-mediated membrane contacts are involved in fusion pore evolution.

1.3.3.3 SNAP-25 associated diseases

On the pathophysiological level, several neuropsychiatric diseases are associated with mutations in SNARE proteins. A single nucleotide polymorphism (rs363043) in the SNAP-25 intron 1 region has been linked to hyperactivity in patients with autism (Guerini et al., 2014). In schizophrenic patients, it was reported that the ventral caudate expressed in total 30% less SNAP-25 compared to controls, indicating a strong link between the incidence of schizophrenia and expression of SNAP-25 (mainly isoform a) in a specific brain region (Barakauskas et al., 2016). Moreover, SNAP-25 single nucleotide polymorphisms were also linked to attention deficit hyperactivity disorder when tested in Chinese subjects (Zhang et al., 2011). Interestingly, increased amounts

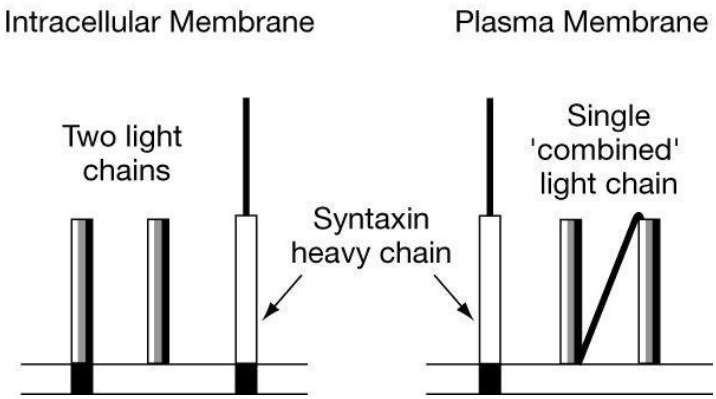

Figure 7 proposed model for intracellular arrangement of t-SNAREs.
The plasma membrane t-SNARE is composed of one syntaxin heavy chain, which contributes one α-helix, and one combined light chain, SNAP-25, which contributes two α-helices. In comparison, most intracellular t-SNAREs are composed of one syntaxin heavy chain and two associated light chains. In the case of vacuolar homotypic fusion, Vacuolar morphogenesis protein (Vam) 3 functions as a syntaxin heavy chain, and Vesicle Transport through t-SNARE Interaction (Vti)1 and soluble Vam7 act as two light chains. In contrast to Vam7, most light chains are probably integral membrane proteins. Adapted from Fukuda et al. (2000).

of SNAP-25 fragments were detected0 in cerebrospinal fluid in Alzheimer's disease patients by mass spectrometry, possibly even serving as a marker for the disease at the very early stages (Brinkmalm et al., 2014). Reduced levels of SNAP-25 in SNAP-$25^{+/-}$ mice were also associated with moderate hyper-excitability, higher sensitivity to kainate induced seizures and problems in the learning and memory processes (Corradini et al., 2014). The spontaneous mutation $I^{67}T$ was reported to cause ataxia as well as distorted sensory motor gating in "blind-drunk" mutant mice (Jeans et al., 2007). Thus, understanding the full function of SNAP-25 protein would help in developing new therapies for the neuropsychiatric disorders.

1.3.4 SNARE accessory proteins

Although SNARE proteins can efficiently drive liposome fusion in the absence of other factors in reduced model systems (Schuette et al., 2004; Tucker et al., 2004), regulatory proteins are crucial for exocytosis in neurons and neuroendocrine systems (Gerst, 1999). These regulatory proteins perform wide range of functions in the secretory pathways. Some regulatory proteins and their roles in exocytosis will be highlighted:

As regulated exocytosis is a well controlled process based on a Ca^{2+}-stimulus to trigger secretion, a large protein family called synaptotagmin (Syt) were discovered to be the primary calcium sensors in different secretory systems. Seventeen members of the synaptotagmin family have been identified, of which several of them undergo alternative splicing yielding different splice variants. Different synaptotagmin isoforms are expressed in neurons as well as cells (Mizuta et al., 1994; Perin et al., 1991). Synaptotagmin associates with the vesicular membrane and possess two calcium binding motifs named C2A and C2B domains (Geppert et al., 1991). These domains are preceded by α-helical coiled coil domain. C2A binds in a calcium dependent fashion to phospholipids, specifically to the negatively charged head groups. C2B binds to different inositol polyphosphates; however, with phosphatidyl-inositol-4,5-bisphosphate (PIP_2) in a calcium independent manner and with phosphatidyl-inositol-3,4,5-triphosphate (PIP_3) independently (Schiavo et al., 1996). Syt affinity to Stx significantly increases upon binding of Syt to Ca^{2+} (Chapman et al., 1995). Additionally, Syt interacts with voltage gated calcium channels regulating their gating properties (Charvin et al., 1997; Leveque et al., 1994; Petrenko et al., 1991). Another important feature is that Syt can interact with SNAP-25 via its C2B domain (Schiavo et al., 1997).

In chromaffin cells, the two main isoforms expressed are Syt-1 and Syt-7 (Schonn et al., 2008). Syt-7 can bind up to seven Ca^{2+} ions, while Syt-1 is able to bind to only five Ca^{2+} ions (Ubach et al., 1998) with Syt-7 showing almost ten folds more sensitivity for calcium in comparison to Syt-1 (Bhalla et al., 2005). These observations explain why Schonn and his colleagues saw a complete loss of the fast component of released vesicles upon stimulation in mouse chromaffin cells when Syt-7 isoform was knocked out (Schonn et al.,

2008). When Syt-1 and Syt-7 were both deleted, the secretion in chromaffin cells was nearly abolished while a significant amount of secretion was still observed in single knock out mutants with different release kinetics (Schonn et al., 2008). The PIP_2 binding domain can also bind SNAREs specifically to Stx and SNAP-25 (Rickman et al., 2004). Later, Mohrmann and his colleagues found out that this Syt-1:SNAP-25 interaction is crucial for vesicle docking, priming and fusion indicating the importance of the Syt-1 not only as a calcium sensor at the late stages of fusion but also in pool stability (Mohrmann et al., 2013).

There are many reported accessory proteins that help in vesicles docking, priming, or fusion. Some also act post fusion to disassemble the SNARE complex. As mentioned previously, NSF/SNAP are other protein families that use ATP, mainly acting like chaperones to regulate SNAREs and vesicle formation (Fleming et al., 1998). Ras-associated binding (Rab) proteins are another family of guanosine triphosphatase (GTPase) proteins that use energy and link vesicles to the cytoskeleton or to other components of the fusion machinery (Li et al., 1994). Double C2-like domain-containing protein beta (DOC)-2 proteins are thought to play role in exocytosis as low affinity calcium sensors since they possess a C2 domain that could bind Ca^{2+} (Orita et al., 1995). Recently, it was shown that DOC2b knock out mouse chromaffin cells have a defect in secretion. The exocytotic burst was shifted to sustained release in the DOC2b deficient cells indicating a role of DOC2b in calcium triggered LDCV release in adrenal chromaffin cells (Pinheiro et al., 2013). CAPS is another cytosolic protein known for its function in priming of SVs in neurons and LDCVs in neuroendocrine cells (Jockusch et al., 2007; Nguyen Truong et al., 2014). In summary, SNARE mediated membrane fusion is a very complicated, tightly regulated, and system specific mechanism that uses groups of proteins to ensure the precise response to a certain defined stimulus.

Aim of the Work:

Although the importance of membrane-bridging SNARE complexes for exocytosis is very well established, the exact pathway of complex assembly, the identity of intermediates, and the nature of SNARE:lipid interactions during membrane merger are still obscure. Interestingly, very little insight has so far been gained into the preferential usage of structurally specialized Q_{bc}-SNAREs in exocytosis. To learn about the functional implications of the tandem-like structure of Q_{bc}-SNAREs, we have investigated potential mechanistic functions of the "linker" domain, which connects the two SNARE motifs in SNAP-25. Performing a detailed structure-function analysis, we planned to evaluate several mechanistic ideas about the role of the SN25 linker:

1. **Is SNAP-25 linker integrity important for the function of SNARE complexes?**
   Earlier reconstitution studies postulated that complementary SNAP-25 fragments without a physical connection between both SNARE motifs can mediate secretion as efficient as the wildtype protein (Chen and Scheller, 2001; Wang et al., 2009) thus objecting the need for a continuous SNAP-25 backbone. However, the used test paradigms only involved assays in cracked/permeabilized, Botulinum Toxin /E-treated cells, which may have promoted non-canonical transmitter release. As secretion was only assayed on the population level with little temporal resolution in older work, we aimed here to evaluate the ability of different combinations of SNAP-25 fragments to reinstate release in SNAP-25$^{-/-}$ neurosecretory cells using high-resolution electrophysiological techniques (membrane capacitance measurements and amperometry) to assay release properties on the level of single cells.

2. **Does SNAP-25 linker contain mechanistically relevant motifs?**
   As the linker domain does not exhibit a detectable secondary structure, it has been primarily considered as an inert connector without specific mechanistic function. That said, a recent characterization of different SNAP-23/25 chimera pointed out that sequence variations in the C-terminal linker section may account for functional differences between both isoforms (Nagy et al., 2008). To explore the possibility that the linker is indeed functionally relevant and contains mechanistically important motifs for protein and/or lipid interactions, we set out to generate and functionally characterize a set of novel linker mutants. For this purpose, the whole linker domain or respective subregions should be substituted by a flexible connector peptide of equal length comprising only glycine and serine residues. Moreover, we planned to specifically target bulky non-polar amino acids in the C-terminal linker region that have previously been suspected to associate

with a hydrophobic groove on the surface of the SNARE complex (Sutton et al., 1998). The electrophysiological experiments should be complemented by biochemical assay, testing the SNARE interactions of the generated SNAP-25 mutants.

3. **Are linker-mediated lipid interactions critical for the fusion mechanism?**
   Acylation-deficient SNAP-25 variants have been reported to alter secretion properties (Nagy et al., 2008), but it has remained unclear to what extent these functional deficits are simply induced by a mislocalization and decreased plasma membrane expression of the mutant protein. Therefore, mutant SNAP-25 should be re-targeted to the plasma membrane via an artificial, secondary palmitolyation motif attached to the N-terminus. If the functional deficits would persist under these circumstances, it must be assumed that specific linkler:membrane contacts are required during the final fusion steps. To elucidate whether the observed slow-down of secretion in the presence of non-acylated SNAP-25 is caused by ineffective force-transduction of the SNARE complex (due to the loss of the acyl anchors), the effects of spacer insertions between SN1 and the linker acylation site should be tested, as such modification should mechanically "uncouple" the membrane attachment site within the linker.

With the proposed experiments, we should be able to collect sufficient evidence to conclude whether and how the SNAP-25 linker mechanistically supports the fusion machinery.

Materials and Methods

The used materials were mainly available at the department of Univ.-Prof. Dr. Dieter Bruns and to lesser extent at the department of Univ.-Prof. Dr. Jens Rettig. The devices were mostly used in Prof. Dieter Bruns lab, otherwise it is stated.

1.4 Chemicals

Product	Company
Acetic acid	Roth
Acrylamide mix (30%)	Roth
Albumin	Thermo Fisher
Ammonium persulphate	Thermo Fisher
BAPTA	Sigma Aldrich
Cocktail protease inhibitor	Thermo Fisher
DMEM	Linaris Biologische Produkte
EDTA	Sigma Aldrich
Ethanol	Roth
Fura-4F, Pentapotassium Salt	Thermo Fisher
Glycine	Merck
HEPES	Sigma Aldrich
KCL	Merck
Mag-Fura-2, Tetrapotassium Salt	Thermo Fisher (molecular probes REF M1290)
Methanol	Roth
Fat-free Milk	Merck
Na_2HPO_4 x $2H_2O$	Merck
NaCl	Merck
NaH_2PO_4 x H_2O	Merck
Optimem	Life Technologies

Papain extract	Worthington Biochemical, Lakewood, NJ, USA
Penicillin	Life Technologies
PMSF	Thermo Fisher
Ponceau	Thermo Fisher
PVDF	Thermo Fisher
SDS	Merck
Streptomycin	Life Technologies
TEMED	Thermo Fisher
Tris-Base	Thermo Fisher
Triton-X	Thermo Fisher
Trypsin inhibitor	Thermo Fisher
Tween20	Thermo Fisher

1.5 Cell culture

1.5.1 Solutions

1.5.1.1 Dulbecco's Modified Eagle's Medium (DMEM)

- 500 µl Penicillin (10000 units/mL) /Streptomycin (10,000 µg/mL) mix was added to 250 ml DMEM then sterile filtered. Afterwards, 2.5 ml of Insulin-Transferrin-Selenium-Ethanolamine (ITSX)
- ITSX was added (i.e. 0.2% Penicillin-Streptomycin and 1% ITSX) and the medium was stored at 4 °C for maximum of two weeks.

1.5.1.2 10X Locke's solution

- 1.5 M NaCl
- 56 mM KCl
- 8.5 mM NaH_2PO_4 (anhydrous)
- 21.5 mM Na_2HPO_4X (H_2O)
- 100 mM D-Glucose
- pH was adjusted to 7.0 and diluted in double distilled water (ddH_2O) to 1X to be ready for use.

1.5.1.3 Extracellular solution

- 145 mM NaCl = 8.474 gm
- 2.8 mM KCl = 2.8 ml (1M KCl)
- 2 mM $CaCl_2$ = 2 ml (1M $CaCl_2$)
- 1 mM $MgCl_2$ = 1 ml (1M $MgCl_2$)
- 10 mM HEPES = 2.383 gm
- pH = 7.2 (Using NaOH)
- until 1000 ml ddH_2O

  1 g of D-Glucose was added before adjusting the osmolarity. The osmolarity was raised to roughly 300 mOsm using Mannitol if needed.

1.5.1.4 Intracellular solution

- 110 mM Cs-glutamate (20 µl in 80 µl total volume)
- 8 mM NaCl
- 25 mM HEPES

- 4 mM $CaCl_2$ (13 µl of 25 mM stock solution in 80 µl total volume)
- 5 mM NP-EGTA (8 µl of 50 mM stock solution in 80 µl total volume)
- 0.4/0.4 mM Fura-4F/Furaptra (6.4 µl of Fura mixture in 80 µl total volume)
- ddH_2O (ad to 80 µl total volume)
- 0.3/2 mM Na_2GTP/MgATP (10 µl of ATP/GTP mixture in 80 µl total volume)
- 1 mM Ascorbic acid (adjusted pH to 8)

1.5.1.5 Enzyme solution (sterile filtered)

- 2 mg cysteine aliquot (755/752 sigma)
- 10 ml DMEM (invitrogen 31966-021)
- 0.1 ml 100 mM $CaCl_2$ (1M $CaCl_2$ stock)
- 0.1 ml 50 mM EDTA
- sterile filter

1.5.1.6 Inactivation solution (sterile filtered)

- 25 mg Albumin (Sigma A-4503)
- 25 mg Trypsin inhibitor (Sigma T-9253)
- 10% FCS-DMEM
- Sterile filter

1.5.1.7 Chymotrypsin (2 mg/ml) (sterile filtered)

- 2 mg chymotrypsin
- 1 ml OptiMEM
- Aliquots of 105 µl were stored at -20 °C.

1.5.1.8 Aprotonin (6 mg/ml) (sterile filtered)

- 6 mg Aprotonin
- 1 ml OptiMEM
- Aliquots of 105 µl were stored at -20 °C.

1.5.1.9 BSA (6.5% w/v) (sterile filtered)

- 13 mg BSA
- 2 mL OptiMEM
- Aliquots of 105 µl were stored at -20 °C.

1.5.1.10 Homogenization buffer

- 130 mM NaCl
- 50 mM HEPES
- 1 mM EDTA
- pH = 7.3

Then 5 ml of the buffer were taken and added to them ½ of a pellet of the cocktail protease inhibitors and 50 µl PMSF (100 mM stock) together with 2% triton. The whole mix was kept to get mixed in a cold room for 30 min.

1.5.1.11 Stacking gel (for two gels)

- 4.1 ml H_2O
- 1 ml 30% acrylamide mix
- 1M Tris (pH 6.8)
- 10% SDS
- 10% ammonium persulfate
- 6 µl TEMED

1.5.1.12 Separating gel (12% for two gels)

- 3.3 ml H_2O
- 4 ml 30% acrylamide mix
- 2.5 ml of 1.5M Tris (pH 8.8)
- 0.1 ml 10% SDS
- 0.1 ml 10% ammonium persulfate
- 4 µl TEMED

1.5.1.13 10X Semi-dry (Transfer) buffer

- 200 mM Tris-Base
- 1.5 M Nacl
- pH = 7.5

1.5.1.14 1X transfer buffer (TBS)

- 100 ml 10X transfer buffer
- 200 ml methanol
- 700 ml dH_2O

1.5.1.15 0.1% TBST

- add 1 ml of Tween20 to the 1X TBS

1.5.1.16 1% Milk TBST

- add 1g free fat milk powder to 100 ml 0.1% TBST

1.5.1.17 10X SDS electrophoresis (running) buffer

- 60 mM Tris-Base (30 g in 1 l)
- 1% (1 g per 100 ml) SDS (10g in 1 l)
- 1.92 M Glycine (144 g in 1 l)
- pH = 8.8

1.5.1.18 1X SDS running buffer

- 100 ml 10X running buffer
- 900 ml distilled water

1.5.1.19 10X TBS

- 1X TBST (tween 20 is added to remove any antibody that non-specifically binds to the blot which results in good signal to noise ratio)

1.5.1.20 Ponceau solution

- 1 g Ponceau powder
- 5 ml acetic acid
- 495 ml DDW

1.5.1.21 Antibodies

- Monoclonal α-SNAP-25 from synaptic systems clone 71.1 (1:1000)
- Polyclonal α-SNAP-25 C-terminus from millipore (AB1762) (1:500)
- Goat anti-mouse (1:5000)
- Goat anti-rabbit (1:5000)

1.5.2 Extraction of chromaffin cells from mouse adrenal glands

Freshly prepared Dulbecco's Modified Eagle Medium (DMEM) was sterile-filtered shortly before the preparation. Twenty units of papain extract were added to 1 ml of enzyme solution and incubated at pH = 8 and 9% CO_2, then sterile filtered. The coverslips and the 6-well dishes were kept under UV-radiation

for 20 min to ensure sterilization of the coverslips. The mouse was then sacrificed via inhalation of CO_2, followed by cervical dislocation. A Cesarean-section was made to extract the litter at the embryonic day 18 (E18) out of the mother and separate them from the embryonic sac. The embryos were decapitated and opened at the abdominal area. The muscle tissue underneath the skin was also removed to allow access to adrenal glands. The adrenal glands were carefully extracted one by one and transferred to pre-cooled Locke's solution. The glands were then cleaned from the surrounding connective tissue and blood vessels via micro-scissors and were washed shortly in a drop of enzyme solution and then incubated in 300 µl enzyme solution at 37 °C for 30-45 min under continuous shaking. The enzyme solution was then completely removed, replaced with 300 µl of inactivation solution and incubated for 5 min. The inactivation solution was then completely removed and the adrenal glands were washed in 500 µl DMEM. The medium was removed and 200 µl fresh media were then added and the chromaffin cells inside adrenal medulla were dissociated through triturating the glands 10-20 times using a 200 µl pipette tip. Additional 100 µl of medium were added to reach a final volume of 300 µl, mixed, and then seeded on glass coverslips in a 6-well dish with a drop of 50 µl per coverslip. The cells were allowed to settle for 30 min under 5% CO_2, 37 °C. After 30 min, 2 ml of DMEM was added to each coverslip and left for 48 h before performing any electrophysiological recordings.

1.5.1 Semliki-forest virus (SFV)

SFV belongs to the α-viruses family, with a single stranded RNA having its first two thirds at the 5' end, encoding the proteins needed for the virus replication. The RNA is enveloped by structural proteins that are encoded in the last third of the virus genome. This technique was then adopted to insert genes of interest encoding proteins for expression in chromaffin cells. Ashery et al. (1999) used SFV to encode the cDNA of proteins of interest and were able to efficiently infect mouse adrenal chromaffin cells.

The cDNA of the protein of interest was sub-cloned into the pSFV1 plasmid. The plasmid was then linearized using its specific restriction enzymes. The linearized plasmid together with the helper plasmid, pSFV-helper2, were mixed (10 µg from each plasmid) and electroporated into Baby Hamster Kidney (BHK) cells, incubated at 37 °C for 24 h. When both plasmids come into contact, a fully functional virus is made which will eventually lead to the death of the BHK cells and the release of virons into the culture medium, in which the BHK cells are incubated. The supernatant, containing the virons, is then collected and separated from the cell debris using low speed centrifugation. A modification was made in the pSFV-helper plasmid that would stop the virus from being infective unless the coat spine protein (P62) is cleaved using a protease. The virus is then snap-frozen in liquid nitrogen and stored in aliquots at -80 °C.

1.5.1.1 Virus activation

100 µl of chymotrypsin were added to the 450 µl of virus and incubated for roughly 45 min at room temperature. The chymotrypsin was then inactivated by adding 100 µl Aprotonin and 100 µl of Bovine Serum Albumin (BSA), then incubated for 5 min. The virus was then ready to use. During the day of measurement, the virus was kept in a +4 °C fridge and was valid to use for 48 h after activation.

.

1.5.2 Patch clamp

1.5.2.1 Membrane capacitance measurements via patch clamp in adrenal chromaffin cells

Capacitance measurements in chromaffin cells (CCs) were introduced and accurately measured by Neher and Marty in 1982. These measurements are performed by attaching the stimulating recording electrode via the patch pipette to the cell and adjusting the patch-clamp configuration to the whole cell. A sine wave is then applied to measure the amount of current needed to be injected to "clamp" the cell at the command voltage. When this sinusoidal wave is applied frequently enough, it can directly correlate to the exact size (surface area) of the cell. For this purpose, a lock-in amplifier is used to provide a high frequency sine wave that is considered to be the command signal to the voltage clamp (Figure 8). One main advantage of voltage clamp is that it prevents the cells from becoming depolarized or hyperpolarized. This prevents opening and/or closing of ion channels which would in turn affect the electrical properties of the cell. If we consider that each electrically conducting substance has a so-called "specific capacitance", this specific capacitance was calculated for the cell membrane considering it to be electrically active. As the cell acts as a parallel capacitor, the capacitance would be directly proportional to the surface area of this cell with the equation $C = \varepsilon_0 A/d$, where C is the capacitance, ε_0 is the di-electric constant, A is the area of the plates of the capacitor and d is the distance between the two plates. The specific conductance of the cell membrane was calculated according to this equation to be 1 $\mu F/cm^2$ (Cole, 1968). Considering this law and implementing it on a chromaffin cell with an average diameter of around 10 µm, we can deduce its overall capacitance calculated to be around 3.14 pF considering the spherical nature of a chromaffin cell.

From these calculations, it is inevitable that there is a direct correlation between the surface area of the cell and its total capacitance. When a stimulus arrives at the chromaffin cells, it leads to opening of voltage gated calcium channels that in turn lead to an increase in the intracellular calcium concentration. This calcium rise will cause fusion of vesicles with the plasma membrane and increase in the total capacitance of the cell. The challenge is to accurately estimate this slight increase in the total surface area as a direct measure to the membrane capacitance. In order to accurately measure this change in the cell surface area, the whole cell patch clamp technique was applied to chromaffin cells. Patch clamp technique was developed first in 1976

in order to be able to study ion channels activity in live intact cells. Six years later, Neher and Marty (1982) showed that this technique, with some modifications, can be used for measuring membrane capacitance changes at high temporal resolution. In patch clamp, a glass pipette is filled with the solution of interest (intracellular solution) into which a stimulating recording electrode is inserted such that the intracellular solution and the electrode are in direct contact. Then, the pipette is guided to touch the cell with positive pressure pre-applied on the pipette. When the pressure is released, a very tight seal between the plasma membrane and the pipette tip is formed which is known as a Giga-Ohm (GΩ) seal (Sigworth and Neher, 1980). This high seal is crucial to greatly improve the signal to noise ratio. Now, this small contact between the membrane and the pipette, the membrane patch, was used initially to study single ion channel activity and this configuration was termed "cell-attached" patch clamp configuration. The technique was modified in such a way where this patch was perforated and the pipette had access to the whole interior of the cell in a configuration known as "whole-cell patch clamp". As the GΩ seal must be maintained for high quality recordings, the resistance of the pipette itself should not be of high resistance due to two main reasons. First is to allow for efficient perfusion of the intracellular solution to the inside of the cell. Second, to avoid the voltage drop that could happen under high resistance since the pipette in the circuit is connected in series with the cell.

By maintaining the voltage at the resting potential, current would be injected to compensate for any increase (i.e. exocytosis) or decrease (i.e. endocytosis) of the total capacitance (surface area) of the cell. When this voltage is applied, the capacitive component will rise instantaneously then start in the decay while the resistive component will start to rise after a certain delay from the capacitive one. Thus, a phase shift between the voltage and current occurs.

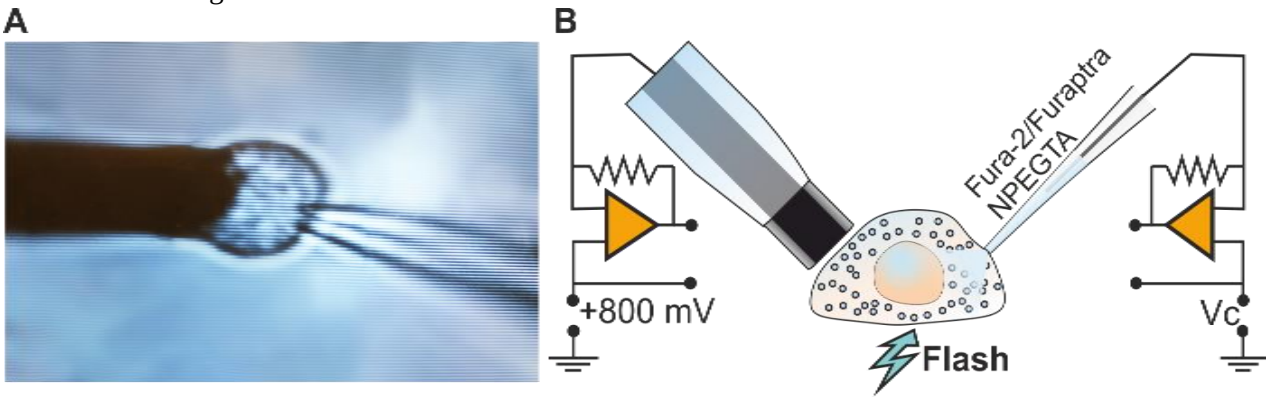

Figure 8 Experimental setup of a voltage-clamped chromaffin cell.
(A) Microphotograph shows a cultured chromaffin cell (CC) in the typical recording configuration, in contact with carbon fiber and patch pipette. Catecholamine secretion was stimulated by flash photolysis of infused caged-calcium compound Nitrophenyl-EGTA (NPE). (B) Schematic diagram of a cultured chromaffin cell prepared from SNAP-25$^{-/-}$ mice at E18. After two days *in vitro*, cells were infected by Semliki-Forest viruses engineered to express either wildtype or mutant SNAP-25. All electrophysiological recordings were done 5-7 h post viral infection. For the characterization of the release properties, amperometric and capacitance measurements were performed in parallel.

1.5.2.2 Calibration curve

The flash-photolysis experiment is based on fully controlling the calcium levels in the cells before and after stimulation (Ca^{2+}-uncaging). Therefore, calcium indicators are crucial for such an experiment. The range of calcium to be detected is fairly big. The chromaffin cells have a calcium concentration of about 100 nM under resting conditions. To prime vesicles for release, the calcium levels have to be increased to 600-800 nM and the release of vesicles occurs upon uncaging of calcium from 800 nM up to 20-30 µM. Two FURA dyes were used for these experiments as there is no single FURA dye that could cover this wide range of calcium detection. FURA-4F was used to detect the lower range of calcium as it has a dissociation constant (Kd) of 0.77 µM detecting roughly from 77 nM up to 7.7 µM (10 times above and below the Kd value of the dye). For the upper range of calcium, Furaptra (Mag-Fura-2) was used due to having a Kd value of 25 µM detecting a lower range from 2.5 µM and an upper range of 250 µM. Combining both dyes will cover the entire range of calcium concentrations needed to be detected for this experiment. In order to use these dyes accurately a calibration curve, with pre-defined calcium concentrations, had to be established. Eight calibration solutions were prepared as shown in Table 1 having the concentrations (µM): 0, 0.330, 0.737, 3.28, 11.585, 23.186, 71.041, and 12500 estimated by the Freecon calcium calculator. 1,2-bis(o-aminophenoxy)ethane-N,N,N′,N′-tetraacetic acid (BAPTA) was the Ca^{2+}-chelator used for solutions with low calcium concentration (solutions 1 to 3), due to its high affinity to calcium. As Ca^{2+} concentration in the calibration solutions reached the micromolar range or higher (solutions 4 to 8), BAPTA was exchanged with Diethylenetriaminepentaacetic acid (DPTA) that has a lower affinity to calcium and better buffer capacity at these concentrations. At the end of the calibration process, the ratios obtained from each calibration solution were inserted in an Igor function that plotted two logarithmic plots representing both FURA dyes to obtain one final calibration curve (Figure 9). The calibration solution could be stored in the Igor directory where the pre/post flash calcium concentrations of each experiment could be extracted and plotted directly using this calibration file.

In the present experiments, holding potential was adjusted to -70 mV, and a 1 KHz sine wave stimulus with a 35 mV peak to peak amplitude. Ratiometric Ca^{2+} imaging was performed using the mix of Fura-4f and Furaptra (Magfura, Invirogen). The cells were patched-clamped at the whole cell configuration using borosilicate glass patch pipettes (GC150F10, Harvard). The pipettes were pulled using P-1000 puller (Sutter Instruments) followed by heat polishing. The patch pipettes were adjusted to be of 3-5 mΩ resistance. After stabilizing the Giga-seal configuration, the cell was opened and the flash Ca^{2+}-uncaging stimulus was applied after the FURA dye has efficiently been infused to the cells (takes roughly 1-2 min). Parallel to capacitance measurements via the patch pipette, a carbon fiber microelectrode was set to +800 mV and approached to

touch the cell from the opposite side of the patch pipette. Amperometric currents were sampled at 1 KHz to be simultaneously measured with the capacitance response.

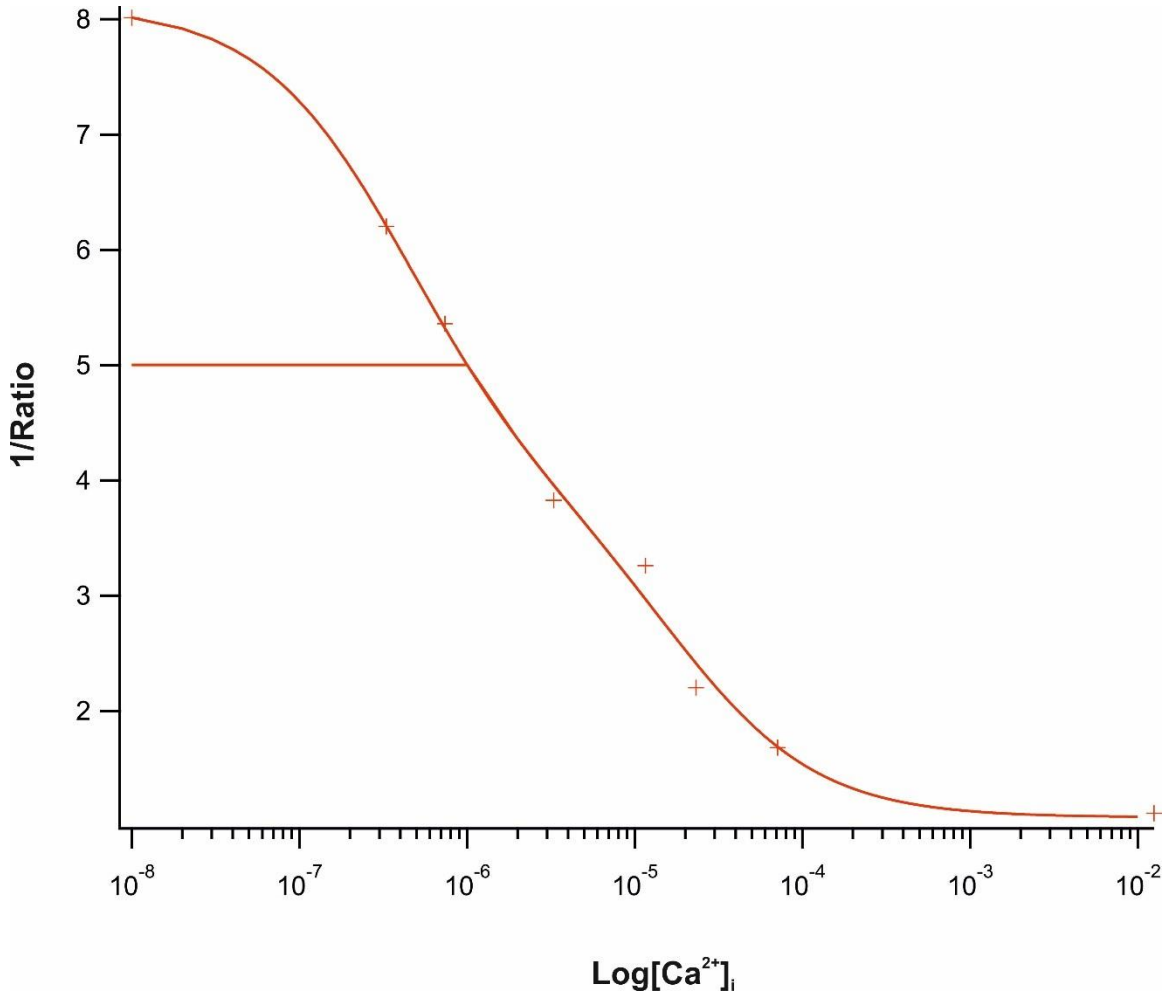

Figure 9 Ca^{2+}-calibration curve for flash-photolysis experiments.
Table showing different calibration solutions having calculated free calcium $[Ca^{2+}]_i$. ranging from 0 nM to 12.5 mM. Free $[Ca^{2+}]i$ was estimated using the Igor macro "Freecon". On the x-axis, plotted the inverse of the ratio (1/R) obtained from each calibration curve. On the y-axis, plotted the free $[Ca^{2+}]_i$ on a logarithmic scale.

Solution	1	2	3	4	4a	5	6	7	8
2xBP	14.5	10	11	11.5		10	9	10	20
MgATP/Na_2GTP (20/3mM)	4	4	4	4	4	4	4	4	4
BAPTA (86mM)	9.3 (20mM)	4.5 (9.68mM)	3.1 (6.67mM)	-	1.7 (3.66mM)	-	-	-	-
CaBAPTA (100/86mM)	-	4.8 (10.32mM)	6.2 (13.33mM)	-	7.6 (16.34mM)	-	-	-	-
DPTA (100mM)	-	-	-	15.2 (38.1mM)	-	13.8 (34.5mM)	12.2 (30.5mM)	8.2 (20.5mM)	-
CaDPTA (100/100mM)	-	-	-	0.8 (1.9mM)	-	2.2 (5.5mM)	3.8 (9.5mM)	7.8 (19.5mM)	-
$CaCl_2$ (100mM)	-	-	-	-	-	-	-	-	5
Vitamin C (40 mM)	1 (1 mM)	1	1	1	1	1	1	1	1
H_2O (filtered Milipore)	8	11	11.7	4.3		5.8	6.8	9.8	6.8
DyeMix (5/5mM)	3.2	3.2	3.2	3.2	3.2	3.2	3.2	3.2	3.2
Free [Ca^{2+}]	0	330nM	737nM	3.282µM	3.129µM	11.585µM	23.186µM	71.041µM	12.5mM

Table 1 Ca^{2+}-calibration curve for flash-photolysis experiments.
A table showing different calibration solutions having calculated free calcium ranging from 0 nM to 12.5 mM. Free $[Ca^{2+}]_i$ was estimated using the Igor macro "Freecon".

1.5.2.3 Fabrication of carbon fibers

Neuronal and neuroendocrine cells communication occure via the release of biogenic amines and other neurotransmitters e.g. catecholamines, such as norepinephrine and epinephrine from adrenal chromaffin cells via exocytosis (Eguiagaray et al., 2004; Suudhof, 2008). One characteristic feature of these catecholamines is their electrochemical activity allowing them to be oxidized and subsequently detected with amperometric measurements using carbon fiber microelectrodes in chromaffin cells (Bucher and Wightman, 2015; Mundroff and Wightman, 2002). Nearly 30 years have passed since amperometric measurements were first established, and now these measurements are mainly used due to the high sensitivity of the carbon fiber and the high acquisition rate (temporal resolution) that allow for detailed analysis of single fusion events of vesicles (Amatore et al., 2008; Wang et al., 2009).

The carbon fibers were fabricated according to Bruns (2004). In details, 10 µm carbon fibers a few centimeters long were cut and separated under a light microscope, then the tip of the fiber was glued against a copper wire using highly conductive silver glue (Busch Silber-Leitlack). In parallel, a glass capillary (GC150F-10, Harvard apparatus, USA) was polished by flaming its tip against a Bunsen burner to smooth

the sharp end. The copper wire attached to the carbon fiber was then inserted from the copper wire end towards the tip of glass capillary until the copper wire exits the capillary from the other side leaving the carbon fiber roughly in the middle of the glass capillary. The copper wire and the glass capillary were glued together at the end of the capillary using a two component epoxy glue (2-K-epoxidkleber, UHU© plus) and left for around 4 h to harden. After the glue had dried, the capillary was pulled using the P-1000 puller (Sutter Instruments, USA). The puller was adjusted to pull roughly 0.5 cm after the connection between the fiber and the wire. Each capillary was then checked under the microscope to ensure the carbon fiber was attached to the copper wire. For a better signal to noise ratio, the carbon fiber has to be insulated. This is done via electroplating an anionic polymer (Glassophor ZQ 84-3211) over the carbon fiber by applying a voltage of 5 V through a platinum electrode. This applied voltage would render the carbon fiber to act as an anode and the platinum electrode to be the cathode. Electro-coating takes place at the surface of the anode where hydrolysis of water and production of protons takes place. These produced protons are important to catalyze the deposition of the anion electrophoretic deposit. A 40-50 s deposition time was enough time to form a uniform insulating coat around the fiber (note: the duration and applied voltage could be changed in order to reach the proper coat thickness and uniformity). The carbon fibers were heat treated in an oven at roughly 155 °C for 20 min. Finally, the tip of the pipette where the carbon fiber protruded was sealed using Sylguard and applying heat for couple of seconds to allow for the Sylguard to polymerize and harden. The fibers were ready then to be connected to the head stage of the amplifier for electrophysiological measurements.

1.5.3 Confocal microscopy

Images were acquired using a laser scanning microscope LSM 710 (Carl Zeiss Microimaging GmbH). The confocal images were acquired using an oil based Plan-Apochromat 100x/1.4 NA DIC M27 objective. The focal plane was set at near the equatorial plane of live chromaffin cells. All confocal images were acquired at a pinhole of 1 airy unit size, a bit depth of 16 bits per pixel, and an image format of 253x352. Green fluorescent protein (GFP) fluorescence was detected by exciting with Argon laser at 488 nm at a 5% laser intensity. The Master gain was fixed at 751 and the Digital gain was adjusted to 1.0. The protein distribution near the membrane was quantified using linear line scans of 3 µm length and a thickness of 1 pixel. The resulting fluorescence profiles were aligned at the position of the maximal fluorescence intensity using an in-house written marco for IGOR (Wavemetrics).

1.5.4 Protein quantification using western blot analysis

1.5.4.1 Sample collection and preparation

To collect enough sample for western blot analysis, five newborn (postnatal day 1-2) mice were sacrificed and chromaffin cells from these animals were seeded on a 5 cm petri dish and left for two days at 37 °C, 9% CO_2 (day of preparation and the next day and then the day after they were used). After 2 days of incubation, each dish of cells was infected with 500 µl of the SFV of choice for the experiment for around 6 h. The cells in the dish were then washed 2 times with ice-cold Phosphate-buffered Saline (PBS). 150 µl of homogenization buffer were then added and the cells were detached from the dish using a sterile cell scraper. The scraped cells with the buffer were transferred to a 1.5 ml Eppendorf tubes and 2-3 trituration steps were performed to ensure proper lysis of the cells. Then, the lysate was kept on ice for 1 h. The Eppendorf tubes were centrifuged for 5 min at 4 °C, 13000 rpm. The supernatant was placed in a fresh Eppendorf tube and the pellet containing cell debris and intracellular compartments was discarded. The sample was then stored for later usage at -80 °C.

1.5.4.2 Bradford protein assay

The Bradford assay is used to detect the concentration of total protein in a sample of interest. The principle of the assay is based on the change of the color of the Coomassie dye inside the Bradford solution from brown to green/blue when it binds to protein molecules under acidic conditions. We used this technique to ensure equal loading of our samples used for western blot analysis. 1 µl of each sample was added to 999 µl of Bradford solution and incubated for 10 min, at room temperature. For a negative control (blank), 1 µl of the homogenization buffer was also added to 999 µl of Bradford solution. The absorbance was measured using a spectrophotometer at wave length of 595 nm and the samples absorbance was compared to a preestablished calibration curve of known protein concentrations to determine each sample's protein concentration. Upon usage, the sample was diluted in ß-mercapto-methanol and sample buffer to a final volume of 20 µl to be loaded in the SDS-PAGE gels.

1.5.4.3 Sample loading

15 µl of each sample (if needed the sample was diluted using the sample buffer to reach equal concentration) was added to 4X ß-mercapto-methanol sample buffer. Then, the samples were heated at 95 °C for 5 min for protein denaturation and then shortly centrifuged to collect the sample. The samples were loaded into the SDS-PAGE gel, and then run at 100 V for 20 min at 160 V for 50 min. Then transfer was done to transfer the proteins on the SDS-PAGE gel to the nitrocellulose membrane. The membrane was run for 2 h at 250 mAmp. The membranes were stained with Ponceau dye for 10 min under shaking then

washed with Tris-Buffer solution containing 1% Tween-20 (TBST) until the stain was cleared from the membrane. The membrane surface was then blocked with 5% milk in TBST and left for 1 h under shaking at room temperature. The primary antibodies (detecting either N- or C- terminal end of the SNAP-25) were diluted in 1% milk in TBST and incubated overnight at 4 °C (dilution 1:1000). The membrane was washed with 1% milk in TBST 3 times with 15 min time interval between each wash. The secondary antibody was then added at room temperature for 1 h. (dilution 1:5000). The membrane was finally washed 3 times with TBST (no milk) with 10 min time interval between each wash at room temperature. For development of the blot, the membrane was incubated in ECL developing solution from Pierce (1:1 premixed white/brown solutions) for 5 min under shaking at room temperature. All pictures were developed using the gel doc machine (from Biorad).

To identify the concentrations of different over-expressed SNAP-25 variants, a calibration curve with defined protein concentrations was performed for the N- and C- terminus antibodies that were used. For the antibody binding at the N-terminal end of the SNAP-25 (aa 20-40), fluorescence intensity measured in arbitrary units (a.u.) was linear up to 210 ng of purified SNAP-25 protein. C-terminus antibody showed linearity relationship between the protein concentration and fluorescence intensity only at concentrations less than 150 ng, after which, the signal was saturated. From this control experiment, we concluded that all over-expressed mutants will be run parallel to purified protein concentrations that don't exceed 150 ng.

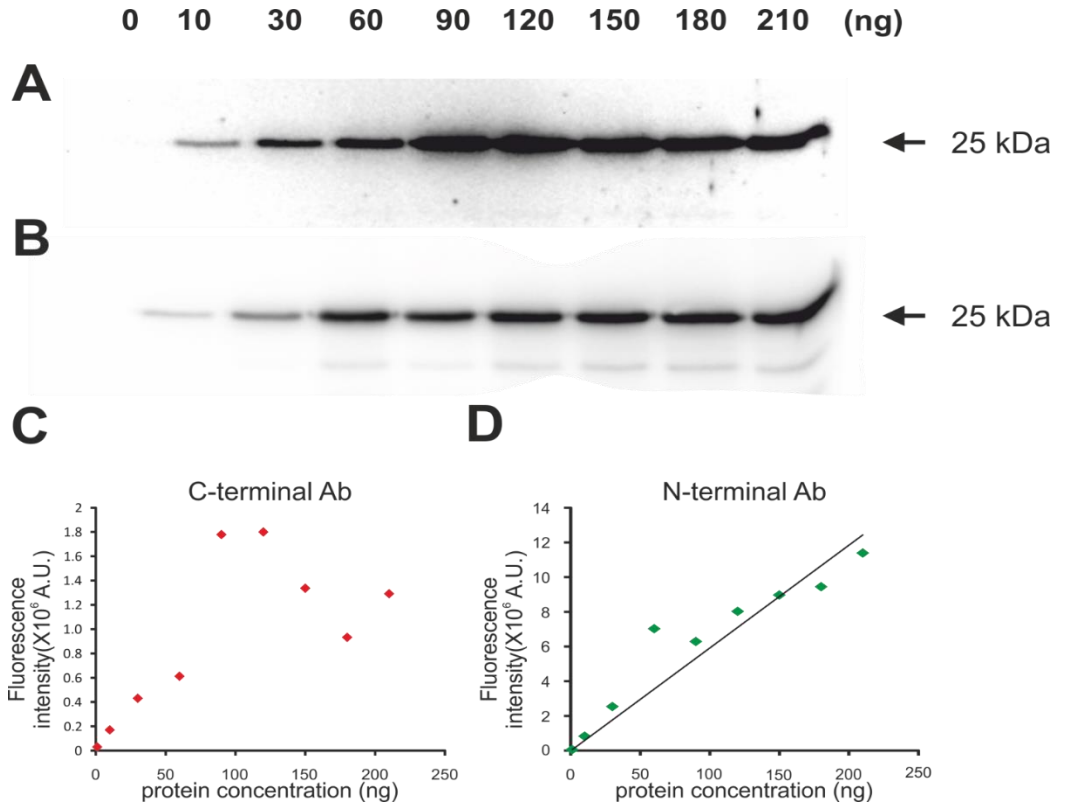

Figure 10 Checking linearity of different SNAP-25 antibodies using western blot analysis.

(A) Western blot showing purified WT SNAP-25 protein using antibody (Ab1762, Millipore) detecting the C-terminal end of the SNAP-25 (amino acids 190-206). (B) Western blot showing purified WT SNAP-25 protein using antibody (71.1, Synaptic Systems) detecting the N-terminal end of the SNAP-25 (amino acids 20-40). (C) Fluorescence intensity (in a.u.) plotted vs different protein concentrations using C-terminal antibody detecting amino acids 190-206. (D) Fluorescence intensity plotted vs different protein concentrations using N-terminal antibody detecting amino acids 20-40. For C-terminal Ab, the fluorescence/protein concentration ratio was linear only at concentrations less than 150 ng, while it was completely linear for the N-terminal Ab.

1.5.5 SNARE complex assembly assay

SNAP-25 WT or mutants were His-tagged, bacterially expressed in E. coli (BL21DE3). The proteins were then purified using a nickel-nitrilotriacetic acide column (Qiagen). Dialysis of SNAP-25, Stx-1A$^{1-262}$, and GST-Syb2$^{1-116}$ was done in dialysis solution composed of: 100 mM NaCl, 20 mM Tris, 1 mM DTT, 1 mM DTT, 1 mM EDTA, 0.5% Triton X-100 and pH was adjusted to 7.4. Around 3 µM protein from SNAP-25 (WT or mutants), Syb2 or Stx-1A was mixed in 80 µl test volume. The mix was then incubated for different time intervals under gentle agitation and 25 °C. After incubation, the SNARE complex assembly was stopped by adding SDS-containing sample buffer. The samples were then run without boiling on SDS-PAGE gel and protein bands were stained with Coomassie blue dye. The gels were scanned and quantified by densitometry using ImageJ. All SNARE complex assembly assays were kindly performed and provided by Walentina Frisch, data was analyzed by Prof. Dr. Ralf Mohrmann.

1.5.6 Stx-1A binding assay

25 µM of GST-Stx-1A$^{1-262}$ was incubated with glutathione-sepharose beads for 2 h at 4 °C for immobilization. The beads were extensively washed and incubated in binding solution with 5 µM SNAP-25 WT or mutant protein for 20 h at 4 °C. The binding solution contained in mM: 100 NaCl, 20 Tris, 1 DTT, 1 EDTA, 0.5% Triton X-100, and the pH was adjusted to 7.4. Afterwards, the beads were washed four times, then resuspended in a fresh binding buffer. The retention efficiency was tested by running SDS-PAGE followed by Coomassie blue dye staining. The protein bands were analyzed by densitometry using ImageJ. As Coomassie staining and protein size are directly proportional, the molar ratio n_{bound}/n_{stx1A} reflecting different molecular weights of different proteins used was calculated.

1.5.7 Epifluorescence microscopy

Adrenal chromaffin cells were cultured on coverslips as described before and left for 48 h at 37 °C, 9% CO_2. Each coverslip was infected for about 5.5 h with the protein of interest using Semliki-forest virus. The coverslips were then inserted in the measuring chamber and 1 ml of ECS was added prior to the measurements. All images were captured under 70.44 ms exposure time.

1.5.8 Transgenic mice

All experiments were performed on mouse chromaffin cells at embryonic days 17-19. All of the recordings are performed on SNAP-25$^{-/-}$ mouse cells unless stated otherwise. Animals were handled in compliance with the federal German animal welfare act and local regulations of the University of Saarland. The SNAP-25 knock-out mice were initially made by (Washbourne et al., 2002). The mice were maintained by backcrossing with C57BL/6 WT mice in the local animal facility.

1.5.9 Statistical analysis

Data are presented as mean values ± the standard error of the mean (SEM) unless stated otherwise. For analysis of amperometric spikes, median was selected as these spike have a skewed distribution and then the mean of the medians was calculated for statistical comparisons. All statistical tests were done using the *SigmaPlot* software and each test is mentioned according to the experiment in the figure legends. Significance was evaluated according to the following categorization of P-values (P): * for $P < 0.05$, ** for $P < 0.01$, and *** for $P < 0.001$. For detailed statistical analysis of each experiment, please refer to the complete information in the **Appendix** (directly after the conclusion).

Results

1.6 SNAP-25 co-expression of separated SN1- and SN2-containing SNAP-25 fragments inefficiently reconstitutes secretion

In SNAP-25, the two SNARE motifs (SN1 and SN2) are connected by a linker domain of roughly 60 amino acids. The functional requirement of a linkage between the two SNARE motifs has remained controversial (Chen et al., 1999; Wang et al., 2008). Chen and colleagues infused cracked, BoNT/E toxin-treated pheochromocytoma cell line (PC12) with SN2 fragments (SNAP-25$^{141-206}$) and reported an almost full restoration of secretion in a [^{3}H]norepinephrine radioactivity assay. However, this result was later challenged when Wang et al. (2008) demonstrated that an analogue rescue of release in permeabilized bovine chromaffin cells was only possible under specific conditions, after previous run-down of secretion. Thus, we were interested in testing the importance of a continuous SNAP-25 backbone in neuro-endocrine secretion using intact mouse chromaffin cells. For this purpose, truncated SN25 Lacking the last 26 amino acids (aa), named "SNAP-25Δ26" and SN2 fragments were co-expressed in SNAP-25$^{-/-}$ chromaffin cells using a bicistronic Semliki-forest virus (SFV) in order to detect any gain of function (Figure 11A). As we noticed in preparatory experiments (Figure 12) that an isolated SN2 fragment could not be stably expressed in chromaffin cells, we relied on N-terminally tagged SN2, which was fused to the fluorophore mCherry (mCh) and appeared to be protected from degradation. We aimed for an excess expression of the mCh-SN2 fragment to counter the low membrane association of SN2 lacking the palmitoylation motif. Also, a high mCh-SN2 level is probably required to facilitate its incorporation into ternary SNARE complexes, displacing the truncated SN2 motif of SNAP-25Δ26. To accomplish an imbalanced expression ratio, mCh-SN2 was inserted into the first open reading frame of the bicistronic viral expression vector, while translation of SNAP-25Δ26 in the second open reading frame was controlled by a polio virus internal ribosome entry site (IRES) (Figure 11 A and B). This polio virus IRES has previously been shown to have a weak driving efficiency in chromaffin cells (Mohrmann et al., 2010).

To confirm the anticipated expression ratio, mCh-SN2 and SNAP-25Δ26 levels were analyzed in cell lysates by Western Blot. In order to detect both fragments, different antibodies recognizing either N-terminal (71.1, Synaptic Systems) or C-terminal epitopes (AB1762, Millipore) were used. The monoclonal 71.1 antibody binds to amino acids 20-40 in the SNAP-25 WT protein, while the polyclonal AB1762 antibody binds to amino acids 190-206. The absolute concentration of each fragment in the same lysate was separately estimated using calibration curves with defined amounts (5, 40 and 120 ng) of bacterially purified SNAP-25 WT protein and the expression ratio was calculated. Linearity of the calibration curve was confirmed in

preparatory experiments (see materials and methods; Figure 10). This analysis revealed a 6.77 ± 0.75-fold (n = 6) excess of the mCh-SN2 fragment over the SNAP-25Δ26 (Figure 11 B).

To study secretion properties, membrane capacitance changes as well as amperometric currents upon photolytic calcium uncaging were simultaneously measured. Cells were infused via patch pipette with intracellular solution (ICS) containing ≈ 600 nM free Ca^{2+} and $[Ca^{2+}]_i$ was further elevated to 800-900 nM with brief uncaging UV pulses before application of the main UV flash, ensuring maximal vesicle priming. By this paradigm, a step like increase in $[Ca^{2+}]_i$ reaching 20-30 µM was accomplished allowing for synchronous release of LDCVs. No rescue was observed in SNAP-$25^{-/-}$ cells co-expressing SN25Δ26 and mCh-SN2 fragments, while WT SNAP-25 fully restored the secretory response. In fact, the total exocytotic burst was significantly suppressed under the level of residual release observed in uninfected SNAP-$25^{-/-}$ cells (ΔC_M(WT) = 390 ± 29 fF, n = 30; ΔC_M(KO) = 30 ± 2.9 fF, n = 23; and mCh-SN2/SN25Δ26ΔC_M = -0.4 ± 2.5 fF, n = 27; P < 0.05 for all comparisons; Dunn's test). This indicates that the SN25Δ26 fragment has a dominant negative effect on exocytosis, as previously shown (Sorensen et al., 2006), which could not be overcome by the 7-fold overexpression mCh-SN2 under our conditions

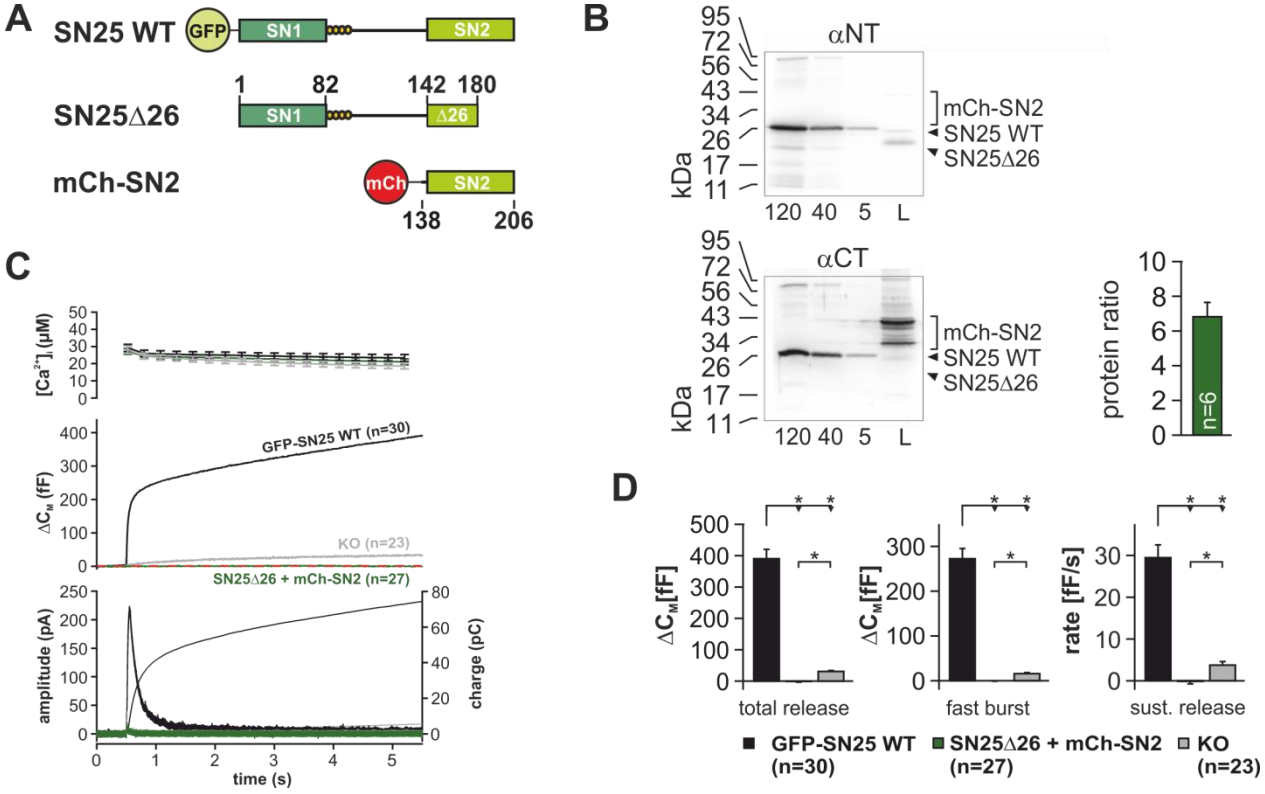

(Figure 11 C and D).

Figure 11 BoNT/E SNAP-25 product acts as dominant negative in SNAP-$25^{-/-}$ chromaffin cells.
(A) Cartoon showing the rescue paradigm: SNAP-25Δ26 (1-180) was co-expressed with mCh-SN2. (B) Expression analysis of SNAP-25Δ26 and mCh-SN2 fragments yielded a ratio mCh-SN2/SNAP-25Δ26 of 6.5:1, resulting from

the use of a different internal ribosomal entry site (polio virus) for the translation of the second reading frame. (C) Electrophysiological characterization of secretion in uninfected KO cells (grey), KO cells co-expressing SNAP-25Δ26 and mCh-SN2 (dark green), and KO cells rescued with WT protein (black). (D) Quantitative analysis of capacitance measurements for total release (left figure), fast burst (middle figure), and sustained release (right figure). All data is given as Mean ± SEM. n is depicted in each panel. Statistical testing was done by ANOVA with Tukey post-hoc test.

In an alternative rescue paradigm, a shorter SNAP-25 fragment lacking the entire SN2 motif (SNAP-25$^{1-141}$) was coexpressed with mCh-SN2 in SNAP-25$^{-/-}$ cells (Figure 13A). The bicistronic virus carried an encephalomyocarditis virus IRES to drive the second open reading frame containing SNAP-25$^{1-141}$. Analysis of expression levels revealed a 1.73 ± 0.4-fold excess of the mCh-SN2 fragment over SNAP-25$^{1-141}$ (Figure 13B). The functional characterization by membrane capacitance measurements and Ca^{2+}-uncaging showed that this combination of fragments was indeed able to reinstate release, but total release by far did not reach the level of WT controls (ΔC_M(WT) = 323 ± 29.3, n = 27; ΔC_M(KO) = 29.6 ± 5.3, n = 32; ΔC_M(mCh-SN2/SNAP-25ΔC) = 111 ± 17.6 fF, n = 21; P < 0.001 comparing either the KO or the mutant to the WT and p = 0.013 for the mutant vs KO, ANOVA Tukey test was applied). Notably, the response mediated by the two separate fragments lacked any fast component in contrast to controls (Figure 13C and D).

Since fitting the response of the mutant with a tri-exponential function was not possible due to small capacitance signal in this experimental setup, secretory burst was estimated by measuring the ΔC_M at 1 s (ΔC_M(WT) = 273 ± 22.8; ΔC_M(KO) = 15 ± 2.2, and ΔC_M(mCh-SN2/SNAP-25ΔC) = -0.015 ± 1.07 fF, n = 21;for total release) and sustained release rate was determined between the 1 s and 5 s releases as WT = 23 ± 2.8 fF/s, n = 27; KO = 4.2 ± 1 fF/s, n = 32; and mCh-SN2/SNAP-25ΔC = 11.3 ± 1.8 fF/s, n = 21 for the sustained release rate P < 0.05 for all comparisons; Dunn's test). Thus, separate SNAP-25 fragments failed to efficiently rescue release; concluding that an intact SNAP-25 backbone is essential for fast SNARE-mediated exocytosis.

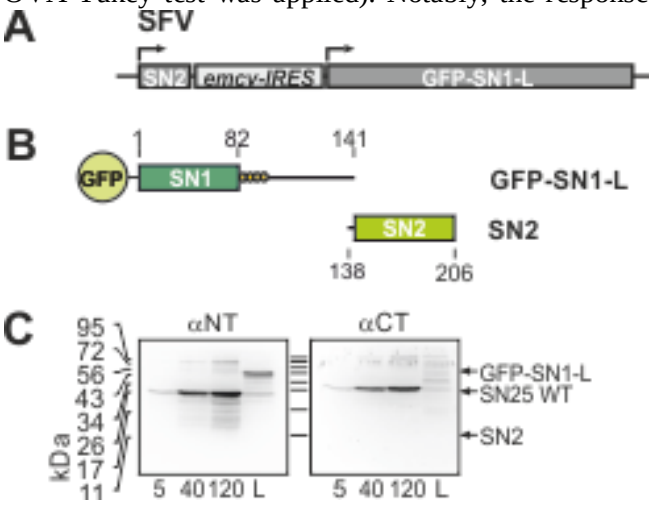

Figure 12 SN2 fragment undergoes degradation when expressed unprotected.
(A) Schematic diagram of the bicistronic construct with EMCV IRES to induce the expression of the second open reading frame. (B) The first open reading frame expressed the SN2 fragment of the SNAP-25 (aa 138-206) while the first second open reading frame expressed GFP-SN1 + L (aa 1-141) fusion protein. (C) Westernblot of cell lysate expressing the bicistronic construct using either N- (*left*) or C- (*right*) terminal SNAP-25 antibodies. SN2 was not expressed as shown on the gel at the right side.

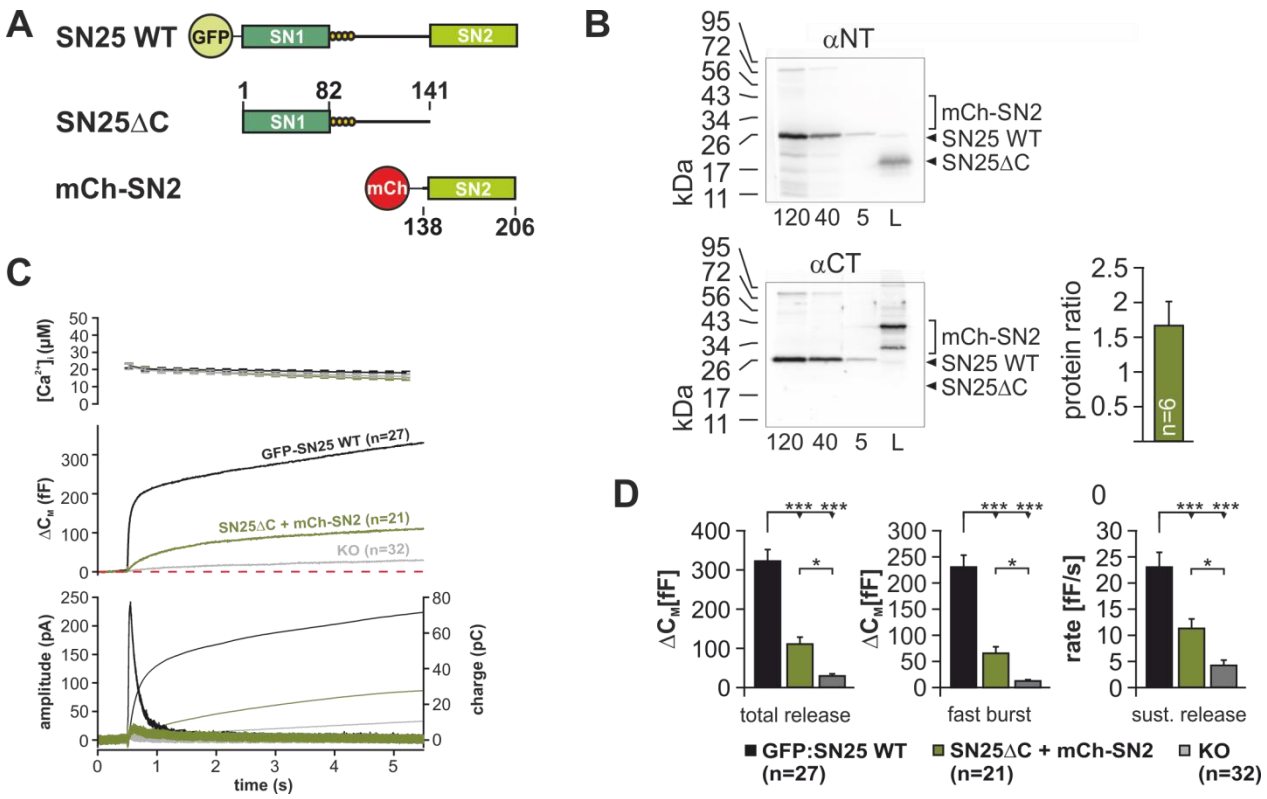

Figure 13 Discontinuous SNAP-25 is not capable of fully restoring exocytosis in SNAP-25$^{-/-}$ chromaffin cells.

(A) Cartoon showing the rescue paradigm, SNAP-25ΔC (aa 1-141) was coexpressed with mCh-SN2. (B) Expression analysis of SNAP-25ΔC and mCh-SN2 fragments yielded a ratio of mCh-SN2/SNAP-25ΔC 1.7:1, resulting from the use of an internal ribosomal entry site, encephalomyocarditis virus, for the translation of the second reading frame. (C) Electrophysiological characterization of secretion in uninfected KO cells (grey), KO cells co-expressing SNAP-25Δ26 and mCh-SN2 (dark green), and KO cells rescued with WT protein (black). (D) Quantitative analysis of capacitance measurements for total release (left figure), fast burst (middle figure), and sustained release (right figure). All data is given as mean ± SEM. Number of cells (n) is depicted in each panel. Statistical testing was done by ANOVA with Tukey post-hoc test.

Since expression of SNAP-25$^{1-141}$ in combination with mCh-SN2 partially rescued release, we wondered whether the SN2-detached linker in this situation would be still of any relevance for the reconstitution of secretion. To investigate this, we shortened the linker by removing its C-very terminal region and expressed the resulting SNAP-25$^{1-118}$ variant together with mCh-SN2 in SNAP-25$^{-/-}$ cells. This truncation was motivated by previous work of Nagy et al. that indicated the C-terminal linker in the kinetic control of fast calcium triggered exocytosis (Nagy et al. 2008). While expression of SNAP-25 WT could fully rescue the secretory burst, expression of the truncated SNAP-25$^{1-118}$ together with mCh-SN2 still only partially restored exocytosis in SNAP-25$^{-/-}$ cells. The relative rescue of total release by SNAP-25$^{1-118}$ was undistinguishable from the value previously found for the longer SNAP-25$^{1-141}$ fragment ΔC_M(mCh-SN2/SNAP-25$^{1-118}$) = 87.6 ± 11.6, n = 36; ΔC_M(mCh-SN2/SNAP-25$^{1-141}$) = 110 ± 17.5 fF, n = 21; p = 0.257; Figure 13D, Figure 14C). However, the relative rescue at 1 s post-flash using SNAP-25$^{1-141}$ was significantly higher than that observed

for SNAP-25$^{1-118}$, indicating that the loss of the C-terminal linker region in SNAP-25$^{1-118}$ had a detrimental effect on the fast-secretory burst (ΔC_M(mCh-SN2/SNAP-25$^{1-118}$) = 28.9 ± 4.2, n = 36; ΔC_M(mCh-SN2/SNAP-25$^{1-141}$) = 65.6 ± 12 fF, n = 21; p = 0.00142; Figure 13D, Figure 14D). Sustained release was not significantly different (mCh-SN2/SNAP-25$^{1-118}$) = 14.6 ± 1.9 fF/s, n = 36; and mCh-SN2/SNAP-25ΔC = 11.3 ± 1.8 fF/s, n = 21; p = 0.262). Western blot analysis showed a mCh-SN2:SNAP-25$^{1-118}$ ratio of 2.12 ± 0.09 (Figure 14D); four preparations were used, 5 adrenal glands for each preparation. Thus, we conclude that the full linker still plays a facilitating role in exocytosis even if the physical linkage between SNARE motifs is dissolved with it C-terminal region having a boosting effect on the fast release.

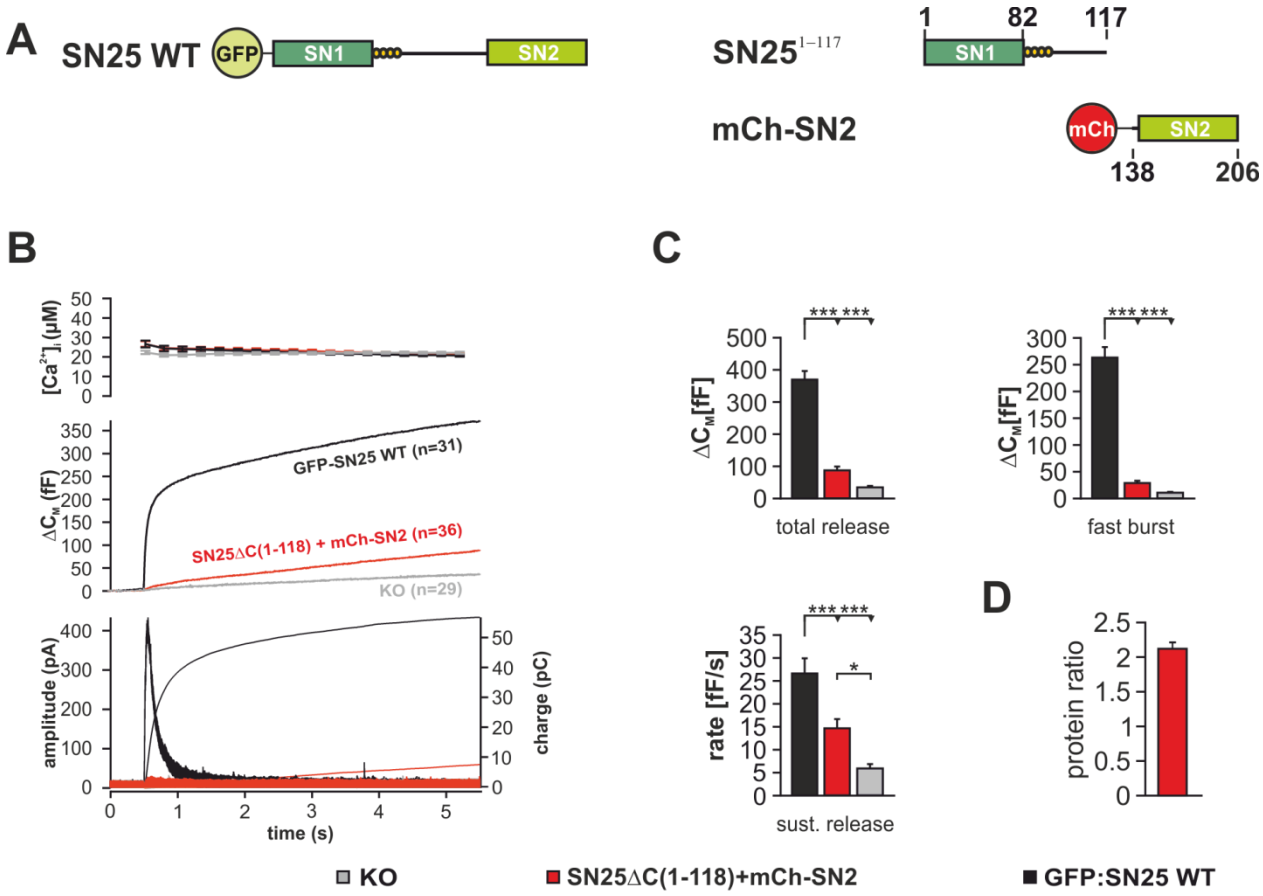

Figure 14 Incomplete linker further deteriorates LDCVs release.
(A) Cartoon showing the rescue paradigm: SNAP-25$^{1-118}$ was co-expressed with mCh-SN2. (B) Electrophysiological characterization of secretion in uninfected KO cells (grey), KO cells co-expressing SNAP-25ΔC$^{(1-118)}$ and mCh-SN2 (dark green), and KO cells rescued with WT protein (black). (C) Quantitative analysis of capacitance measurements for total release (top left figure), fast burst (top right figure), and sustained release (buttom right figure). (D) Expression analysis of SNAP-25$^{1-118}$ and mCh-SN2 fragments yielded a ratio of mCh-SN2/SNAP-25ΔC 2.12:1, resulting from the use of an internal ribosomal entry site encephalomyocarditis virus for the translation of the second reading frame. All data is given as mean ± SEM. n is depicted in panel B. Statistical testing was done by ANOVA with Tukey post-hoc test.

1.7 Substitution of the SN25 linker with a flexible peptide result in a fusion-incapable SNAP-25 variant

Our previous results delivered intriguing clues that not only the integrity of the linker domain but also the presence of specific linker motifs are critical for efficient fusion, in particular for the maintenance of high-fidelity burst secretion. To investigate the mechanistic function of the linker motifs in detail, we next generated a SNAP-25 mutant, SN25 L G/S, in which the complete linker was exchanged with a flexible peptide of equal length comprising only glycine and serine residues (varied sequences, ratio G/S ~2:1, Figure 15A). To estimate the expression level in infected cells, we N-terminally tagged WT and mutant SNAP-25 with GFP, which had been showed to have no detectable impact on its function (Delgado-Martinez et al., 2007). Viral expression of GFP-SN25 L G/S in SNAP-25$^{-/-}$ cells completely failed to rescue exocytosis, while WT SNAP-25 fully restored release (Figure 15B and C). Indeed, total secretion in cells expressing GFP-SNAP-25 WT was 325 ± 22 fF (n = 25), whereas overall release was as low as 43 ± 6.7 fF for GFP-SN25 L G/S-expressing cells (n = 26, P < 0.001 for SNAP-25 WT vs SN25 L G/S; uninfected cells: 36 ± 5.9 fF, n = 23). Burst release after 1 s and sustained release were undistinguishable between uninfected SNAP-25$^{-/-}$ and GFP-SN25 L G/S expressing cells (ΔC_M(WT) = 236 ± 18.8; ΔC_M(KO) = 20 ± 3.6, and ΔC_M(GFP-SN25 L G/S) = 18 ± 2.8 fF; P = 0.991 for uninfected vs SN25 LG/S; Figure 15C), again emphasizing that the mutant is incapable to reinstate secretion.

Expression of GFP-SN25 L G/S mutant in SNAP-25$^{-/-}$ cells also failed to rescue exocytosis to WT SN25 Levels when using longer-lasting stimuli (Figure 15D and E): Infusion of 19 µM free Ca^{2+} containing solution for 5 min via the patch pipette resulted in a ΔC_M of 2.5 ± 0.18 pF (n = 18) for WT SNAP-25, while SN25 L G/S expression yielded 0.386 ± 0.10 pF (n = 14), which was statistically not different from ΔC_M of uninfected cells (0.255 ± 0.08 pF, n = 11). Therefore, the diminished secretory response observed for SN25 L G/S within Ca^{2+}-uncaging experiments is not due to delayed release but rather indicates fusion incompetence. To test for a possible dominant-negative effect of the mutant protein, we also overexpressed GFP-SN25 L G/S mutant in SNAP-25 WT cells using 19 µM free Ca^{2+} to stimulate secretion for 5 min. Indeed, we found that overexpression of GFP-SN25 L G/S significantly decreased total release (1.85 ± 0.156 pF (n = 14); SNAP-25 WT overexpression: 2.63 ± 0.20 pF, n = 18, P < 0.05). Given this dominant-negative phenotype, it is expected that the mutant is still capable of substituting for endogenous SNAP-25 WT in the fusion complex but fails to drive exocytosis. Hence, the native primary structure and biophysical properties of the SN25 linker domain are critical for normal secretion, casting doubt on its postulated role as a simple connector peptide.

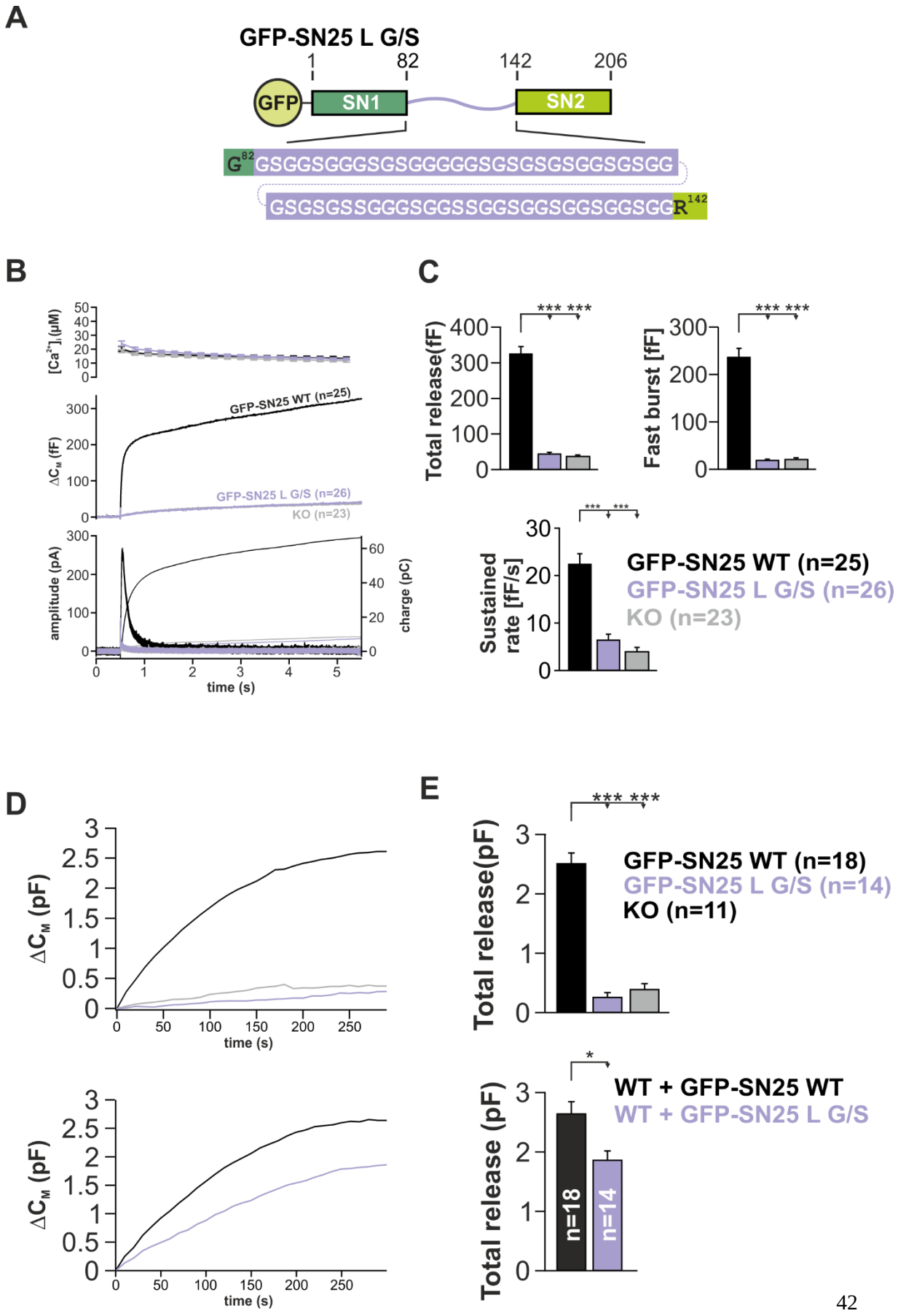
A
GFP-SN25 L G/S
1
82
142
206
GFP
SN1
SN2
G82GSGGSGGGSGSGGGGGSGSGSGSGGSGSGG
GSGSGSSGGGSGGSSGGSGGSGGSGGSGGR142
B
[Ca2+]i (μM)
ΔCM (fF)
GFP-SN25 WT (n=25)
GFP-SN25 L G/S (n=26)
KO (n=23)
amplitude (pA)
charge (pC)
time (s)
C
Total release(fF)
Fast burst [fF]
Sustained rate [fF/s]
*** ***
GFP-SN25 WT (n=25)
GFP-SN25 L G/S (n=26)
KO (n=23)
D
ΔCM (pF)
time (s)
E
Total release(pF)
GFP-SN25 WT (n=18)
GFP-SN25 L G/S (n=14)
KO (n=11)
*
WT + GFP-SN25 WT
WT + GFP-SN25 L G/S
n=18
n=14

Figure 15 Physical linkage between SNARE motifs is not enough for secretion.
(A) Cartoon showing the rescue paradigm: GFP-SN25 L G/S (exchange from aa 83-141). (B) Electrophysiological characterization of secretion in uninfected KO cells (grey), KO cells expressing GFP-SN25 L G/S (violet), and KO cells rescued with WT protein (black). (C) Quantitative analysis of capacitance measurements for total release (left figure), fast burst (right), and sustained release (bottom figure). All data are given as mean ± SEM. n is depicted in each panel. Statistical testing was done by ANOVA with Tukey post-hoc test. (D) Capacitance measurements upon overexpression of GFP-SN25 L G/S in SNAP-25$^{-/-}$ cells (higher panel) or WT cells (lower) and stimulation with 19 µM free Ca^{2+} for 3 min. (E) Quantitative analysis of capacitance measurements for total release in SNAP-25$^{-/-}$ (upper figure) or WT cells (lower figure).

1.8 The SN25 linker is essential for fast and efficient SNARE assembly

Given that SN25 L G/S failed to rescue exocytosis, we wondered whether the mutant protein is still capable to successfully engage in SNARE complex assembly. Formation of ternary SNARE complexes was biochemically assayed by mixing bacterially purified Stx-1A and Syb-2 together with SNAP-25 WT or SN25 L G/S mutant at equimolar concentrations (Figure 16). As an additional negative control, we also used a mixture of the separate SNAP-25 SNARE motifs, SN1 (aa 1-82) and SN2 (aa 142-206), instead of the SNAP-25 full length protein. All samples were incubated at room temperature under moderate agitation, and the assembly of SNARE complexes was terminated by addition of SDS containing sample buffer at different time points. SDS-resistant SNARE complexes were visualized on SDS-PAGE gels using coomassie brilliant blue dye. Interestingly, SN25 L G/S formed ternary complexes with Stx-1A and Syb-2 at rates that were significantly slower than WT SNAP-25, but still faster than the two separate SN1/SN2 motifs. Fitting the assembly curve with a biexponential function revealed that the initial onset rate was significantly decreased for the mutant compared with the WT protein (rate = $2.19*10^5 \pm 0.17*10e^5$ a.u. for SN25 L G/S and $4.37*10^5 \pm 0.52*10^5$ a.u. for WT; $P < 0.01$) (Figure 16 A-D). The absolute levels of SNARE complexes formed by SNAP-25 WT were slightly, but not significantly, higher than SN25 L G/S (Figure 16 D). That said, the final level as well as the initial rate of complex formation was significantly decreased for separate SN1 and SN2 fragments compared to SNAP-25 WT. These results indicate that the native linker can facilitate SNARE complex assembly, either by bringing SNARE motifs into an advantageous conformation for nucleation and/or by stabilizing interaction with other parts of the assembling complex.

SN25 L G/S as well as separate SNAP-25 SNARE motifs assemble into SNARE complexes with higher than usual molecular weight (~150kDa) (Fig. 16B,C). Fdez et al. (2008) previously reported this behavior for complexes composed of linker-less SN1 and SN2 fragments, demonstrating the formation of SNARE complex dimers, wherein the C-terminal ends of two fully-assembled complexes connect through interactions of the juxta-membrane domain of Syb-2. Interestingly, our experiments with SN25 L G/S now

suggest that linker motifs inhibit the SNARE interactions underlying dimerization, implying that the N-terminal linker region binds to and masks "sticky" surfaces on the C-terminal portion of the SNARE complex. In summary, our data show that the SN25 linker domain supports fast SNARE assembly and determines biochemical properties of such complexes.

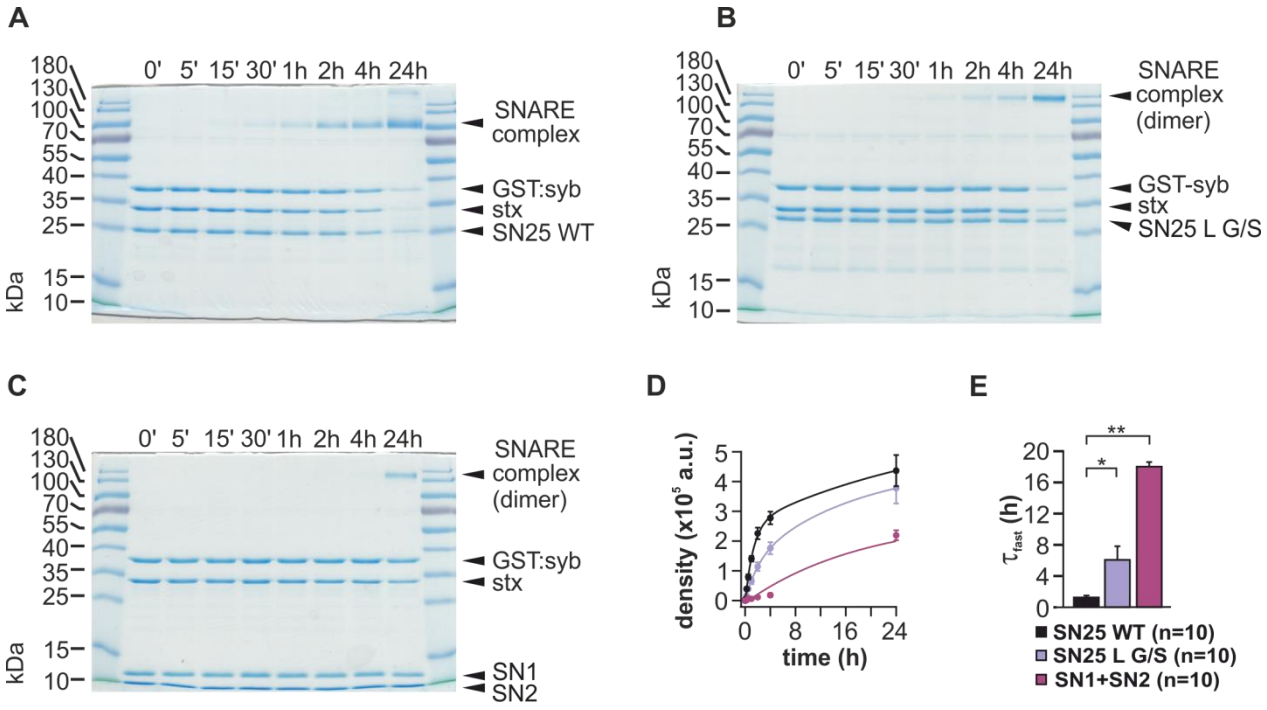

Figure 16 SNAP-25 linker speeds up SNARE complex formation.
Representative gels of ternary SNARE complex formation. Purified SNAP-25 WT (A), SN25 L G/S (B), or separated SN1 and SN2 (C) were mixed with equimolar amounts of Stx-1A and Syb-2, and SNARE complex formation was analyzed by SDS PAGE after different times (indicated above lanes). (D) Quantification of the amount of SNARE complexes formed at specific time points for each condition. (E) Time constants of formed SNARE complexes fitted with a biexponential function for each condition. All data are given as mean ± SEM. n is depicted in each panel. Statistical testing was done by ANOVA with Tukey post-hoc test.

1.9 The SN25 linker is involved in acceptor complex formation

According to current mechanistic models, SNAP-25 and Stx-1A initially form a so-called acceptor complex, which serves as a platform for Syb-2 binding and ternary complex nucleation (Chen et al., 2001; Fasshauer and Margittai, 2004; Ma et al., 2013). Since SN25 L G/S showed a decreased rate of SNARE complex formation, we then investigated whether this mutant can normally interact with Stx-1A. For this purpose, the retention of SNAP-25 WT, SN25 L G/S and complementary SNAP-25 fragments on immobilized Stx-1A was tested. A pull-down assay was established, wherein GST-Stx-1A was first bound to glutathione-sepharose beads, and WT or mutant protein were incubated with the beads for 20 h at 4ºC.

After extensive washing, retained proteins were analyzed by SDS-PAGE. We observed that WT SNAP-25 remained bound on immobilized GST-Stx with a molar ratio nSNAP-25/$n_{GST\text{-}Stx}$ of ~0.7 (n = 6, Figure 17A and B). As for the SN25 L G/S mutant, the fraction of retained mutant protein was significantly decreased compared to controls (around 50% lower molar ration compared to WT protein, Figure 17). When a mixture of linker-less SN1 and SN2 fragments was incubated with GST-Stx-1A beads, the SN1 fragment showed significantly lower but still substantial binding to Stx-1A, while SN2 was only retained in traces on the beads (Figure 17 A). Testing another set of SNAP-25 fragments, in which a continuous SN1-linker fragment (SN1-L) was combined with isolated SN2, yielded the same result. However, in the reverse situation, when SN1 was mixed with a continuous linker-SN2 (L-SN2) fragment, significant amounts of L-SN2 were found on beads, and the molar fraction of retained SN1 was almost increased to the level found for WT SNAP-25 (Figure 17 A, lower panel). The SN2 interaction with Stx-1A was dramatically increased from almost no interaction to ~ 0.5 relative molar retention on immobilized GST-Stx-1A (Figure 17 B). Moreover, the increased retention of L-SN2 in comparison to isolated SN2 was dependent on the presence of SN1, as only negligible amounts of L-SN2 were pulled down by GST-Stx-1A when SN1 was not in the mix.

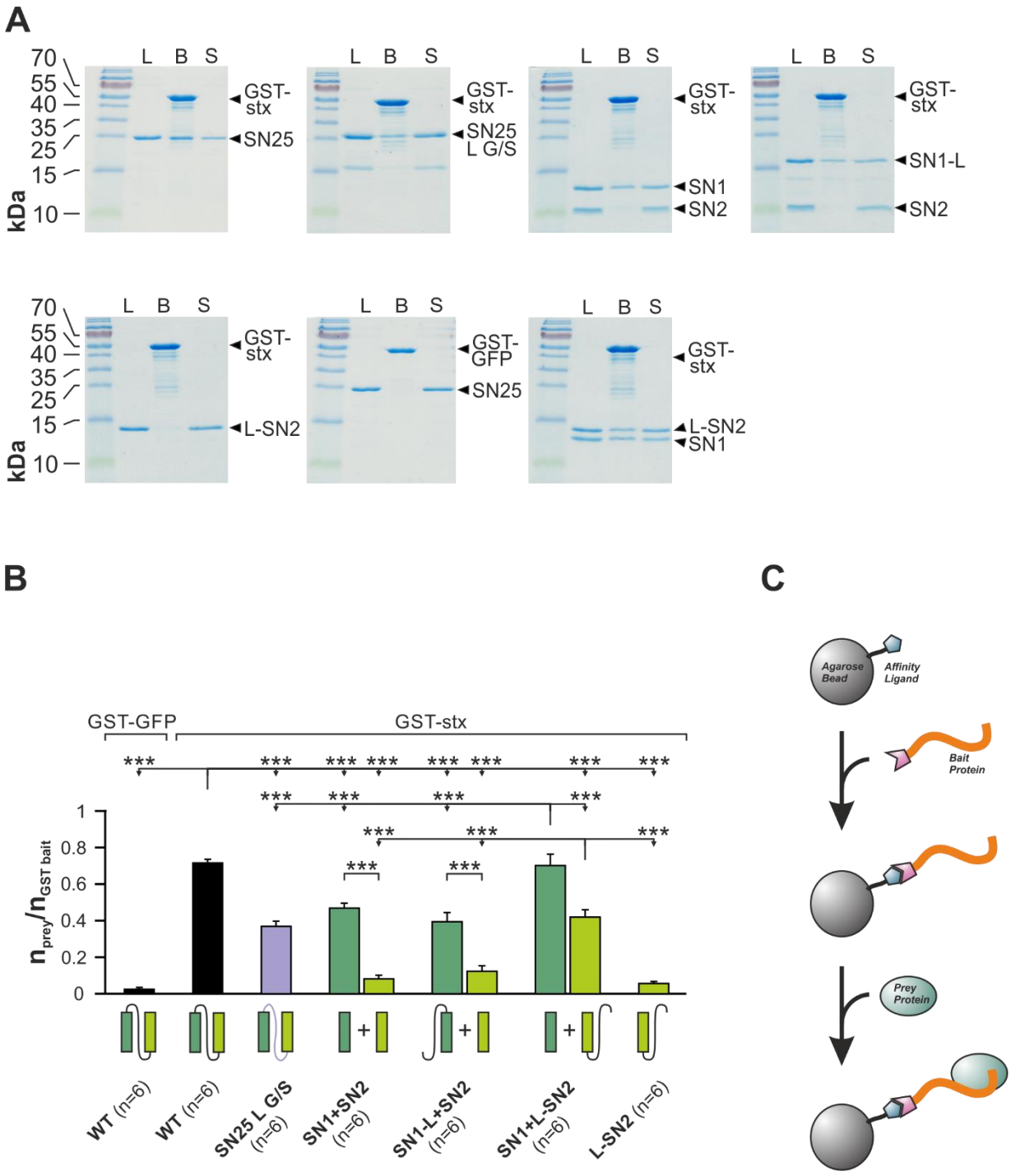

Figure 17 Pull down assay of SNAP-25 on immobilized GST-Stx1A.
(A) Coomassie stained gels showing the load (L) of SNAP-25 WT or SNAP-25 mutants on Stx1A containing beads (B) with bound SNAP-25 WT (or mutants) fraction and the supernatant (S). (B) Quantification of the SNAP-25 WT (or SNAP-25 mutants) retention on Stx1A GST beads. GST-GFP was used as a negative control for binding specificity. The average retention ratio nprey/nStx-1A was calculated for each protein/fragment. All data are plotted as mean ± SEM, Statistical analysis was done with ANOVA test. (C) Cartoon showing the schematic diagram of the

pull down experiment; WT or bacterially purified mutants were mixed with Syb-2 GST fusion protein as well as Stx-1A in 3 µM each and quantified the amount of SNARE complexes formed after incubation for 18 h, at RT.

In summary, we found that linker motifs are required for normal t-SNARE interactions. Our experiments with SNAP-25 fragments suggest the presence of certain functional units that interact with each other in binary acceptor complexes: SN1 can directly interact with the helical H3-domain of Stx-1A. The linker must be attached to SN2 in order to support its association with SN1:H3 complexes, possibly increasing the helicity of SN2 through direct interactions. The decreased Stx-1A interactions of SN25 L G/S might also hinder ternary SNARE complex nucleation and thus may account for the observed decrease in assembly rate.

1.10 Function of N- and C- terminal linker regions in LDCV exocytosis

To identify specific functions associated with different linker subregions, we constructed two additional linker mutants, in which either the N- (aa 83-118) or the C-terminal portion (aa 119-140) of was substituted by a flexible peptide. The subdivision of the linker in two parts was primarily based on earlier findings: The N-terminal two-thirds of the linker is responsible for proper acylation of the linker (Gonzalo and Linder, 1998). The C-terminal part has been associated with core complex binding (Sutton et al., 1998) and the expression of isoform-specific differences in secretion properties (Nagy et al., 2008). N- and C-terminal linker regions were exchanged with G/S repeats, called SN25 LN G/S and SN25 LC G/S respectively. The N-terminally GFP tagged mutants were expressed in SNAP-25$^{-/-}$ chromaffin cells in order to check their capability to rescue secretion (Figure 18A; Figure 19A). Cells expressing either mutant, SN24 LN G/S or SN25 LC G/S, showed very similar secretory responses upon stimulation by Ca^{2+}-uncaging. Most intriguingly, their phenotypes were characterized by a dramatically diminished RRP [RRP(SN25 LN G/S) = 0 vs WT = 91 ± 8.8, while RRP(SN25 LC G/S = 5 ± 2 vs WT = 125 ± 11.7 fF] and a significantly compromised SRP, indicating that both linker regions are important for proper exocytosis (Figure 18B; Figure 19B). The stimulation-secretion coupling for both mutants was weakened, as indicated by a significantly increased delayed onset of release after stimulation (Figure 18C; Figure 19C).

The cluster of four conserved cysteine residues in the N-terminal linker region was eliminated in SN25 LN G/S but not in SN25 LC G/S. As the loss of the membrane acyl-anchors should have dramatic consequences on the localization of SNAP-25, we investigated the subcellular distribution of GFP-tagged mutants using confocal microscopy. For this purpose we acquired confocal images near the equatorial plane of the near-spherical chromaffin cells and analyzed the protein distribution in the vicinity of the plasma membrane using “scanlines”, which were set in an orthogonal orientation onto the plasma membrane segment. All scanlines were aligned to the x-coordinate marking the maximum of the first derivative, which

should most closely reflect the outer perimeter of the cell. Our analysis revealed a similar fluorescence distribution for WT protein and SN25 LC G/S mutant, which exhibited undistinguishable fluorescence peak values at the presumed position of the plasma membrane (WT:16844 ± 1063 a.u., n = 23; SN25 LC G/S: 17848 ± 1227 a.u., n = 23). For reference we also included a non-acylated mutant SN25-cys, in which the four cysteines were substituted by serines residues. As expected, SN25 LN G/S as well as SN25-cys exhibited no obvious local fluorescence maximum near the putative position of the plasma membrane. Rather, fluorescence steadily increased until the cytosolic level was reached. At the presumed location of the plasma membrane the SN25-cys and SN25 LN G/S exhibited fluorescence intensities that were significantly smaller than in WT controls (SN25-cys: 12436 ± 1036; n = 23; SN25 LN G/S: 13200 ± 1046, n = 22; $P < 0.05$). Thus, we could confirm that acylation is important for membrane targeting of SNAP-25, as described before (Nagy et al., 2008). That said, it should be noted that the effective concentration of SNAP-25 at the plasma membrane was possibly only moderately decreased in these experiments, as the high expression level in our model system allows for a high supply of non-acylated protein in direct vicinity of the membrane.

To address whether the secretory phenotype of SN25 L G/S simply reflects the mislocalization and reduced availability of the mutant proteins at the plasma membrane, we comparatively characterized the secretion properties of the acylation-deficient mutant SN25-cys. In accordance with an earlier study (Nagy et al., 2008), we demonstrate here that expression of SN25-cys could restore around 70% of the total WT response under our experimental conditions (ΔC_M(SN25-cys) = 235 ± 16.8, and ΔC_M(WT) = 340 ± 22 fF; Figure 18B and C). As the phenotype of this minimal acylation mutant SN25-cys is relatively mild compared to the complete N-terminal substitution mutant, the severe secretion deficits of SN25 LN G/S cannot just be the sole result of protein mislocalization. Thus, the deficits observed in SN25 L G/S-expressing cells rather indicate a loss of functional motifs within the N-terminal linker region.

Despite relative high response from SN25-cys mutant, the SN25-cys exhibited certain release deficits. The ready releasable pool was significantly decreased and slowed down indicating a possible triggering phenotype. The sustained component, reflecting the priming process of newly docked vesicles, was also negatively affected. The first interpretation to such release inefficiency is due to the lack of stable interaction of the mutant with the plasma membrane. This could lead to a scenario, in which the SN25- cys mutant fails in properly pulling the membrane during the SNAREs zippering leading to hampered force transduction. The force transduction theory was then tested by following complementary experiments. The SNAP-25 WT ready releasable pool (WT_{RRP}) was 91 ± 8.8 fF while the SN25-cys_{RRP} 18 ± 5.2 fF and no RRP for the SN25 LN G/S mutant was detected ($P < 0.001$). The time constant of the RRP (WT_{TRRP}) was significantly faster than that of cysteine deficient mutants (SN25-cys_{TRRP}) yielding 12 ± 0.09 and 23 ± 0.29 ms respectively;

$P < 0.001$; Figure 18 B and C. WT_{SRP} was 97 ± 7.2 fF and SN25-cys_{SRP} was 113 ± 11 fF; that were both significantly higher than SN25 LN G/S_{SRP} that was 41 ± 14 fF ($P < 0.001$ and 0.01, respectively). WT_{TSRP} (130 ± 10 ms) was significantly faster than SN25-cys_{TSRP} (241 ± 33); $P < 0.01$. SN25 LN G/S_{TSRP} was significantly slower than WT_{TSRP} (307 ± 73); $P < 0.05$ (Figure 18 C). The sustained release rate of WT (WT_{sus}) was significantly higher than SN25-cys_{sus} and SN25 LN G/S_{sus} (30 ± 2, 19 ± 1.7, and 19 ± 2.8 fF/s respectively; $P < 0.01$ and 0.05 respectively) (Figure 18 C). The delay between onset of stimulation and secretion for SN25 WT (WT_{delay}) was 2 ± 0.4 ms while 6.5 ± 0.6 and 19 ± 3 ms for SN25-cys and SN25 LN G/S. WT_{delay} was significantly faster than SN25-cys_{delay} and SN25 LN G/S_{delay} ($P < 0.05$ and < 0.001, respectively) (Figure 18 C). SN25-cys_{delay} was significantly shorter than SN25 LN G/S_{delay} ($P < 0.001$) (Figure 18 C). On the other hand, WT_{RRP} was significantly higher than SN25 LC G/S_{RRP} (124 ± 11, 5.4 ± 2.7 fF, respectively; $P < 0.001$); Figure 19 B and C. WT_{TRRP} was significantly faster than SN25 LC G/S_{TRRP} (13 ± 0.7, 57 ± 8 ms, respectively; $P < 0.001$); Figure 19 C. WT_{SRP} was significantly higher than SN25 LC G/S_{SRP} (93 ± 10, 27 ± 8 fF, respectively; $P < 0.001$); Figure 19 C. WT_{TSRP} was significantly faster than SN25 LC G/S_{TSRP} (122 ± 10, 253 ± 55 ms, respectively; $P < 0.001$); Figure 19 C. WT_{sus} was significantly higher than SN25 LC G/S_{sus} (30 ± 3.4, 18 ± 3.1 fF/s) ; Figure 19 C. Finally, the delay of secretion for SNAP-25 WT was significantly shorter than that of SN25 LC G/S mutant (1.6 ± 0.3, 17.5 ± 4.6 ms, respectively; $P < 0.001$); Figure 19 C. Thus, the deficits observed by SN25 L G/S and SN25 LN G/S could be not only due to mislocalization of the proteins but rather due to loss of important amino acids needed for exocytosis to take place efficiently.

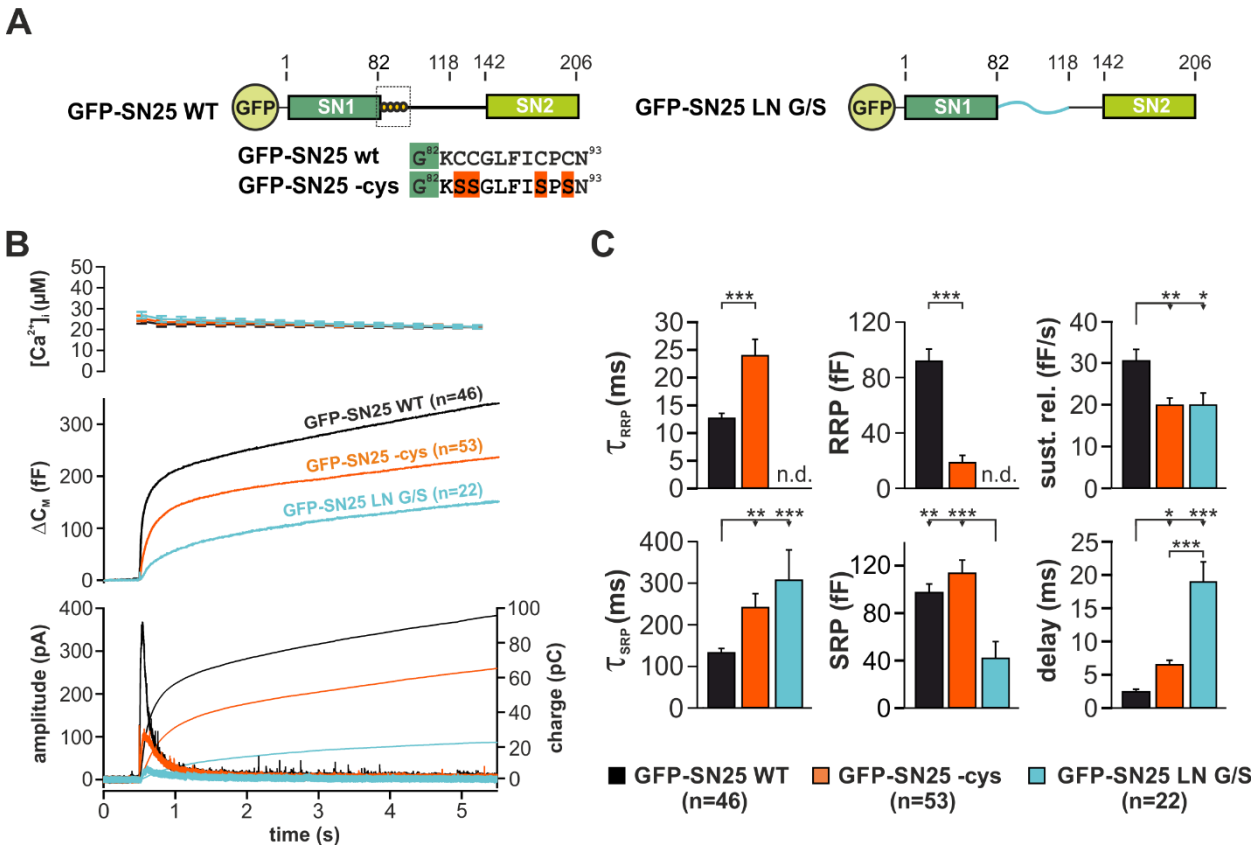

Figure 18 N-terminal linker regions promote secretion.
(A) Cartoon showing structure of the mutants: GFP-SN25 LN G/S where amino acids 82-118 were substituted with against Glycine-Serine residues while GFP-SN25-cys where cysteine residues of the linker were exchanged with Serine residues. (B) Electrophysiological characterization of secretion shown as averaged traces for $[Ca^{2+}]_i$ (top), capacitance measurements (middle) and amperometric recordings (bottom) in KO cells expressing GFP-SN25 LN G/S (cyan), GFP-SN25-cys (orange), or WT protein (black). (C) The mean amplitudes of RRP and SRP and their corresponding time constants τRRP and τSRP are depicted for the fast burst component. The mean sustained release rates describe the linear release component. The exocytic delay indicates the time interval between flash application and secretion onset. All data is plotted as mean ± SEM, statistical analysis was done with ANOVA test.

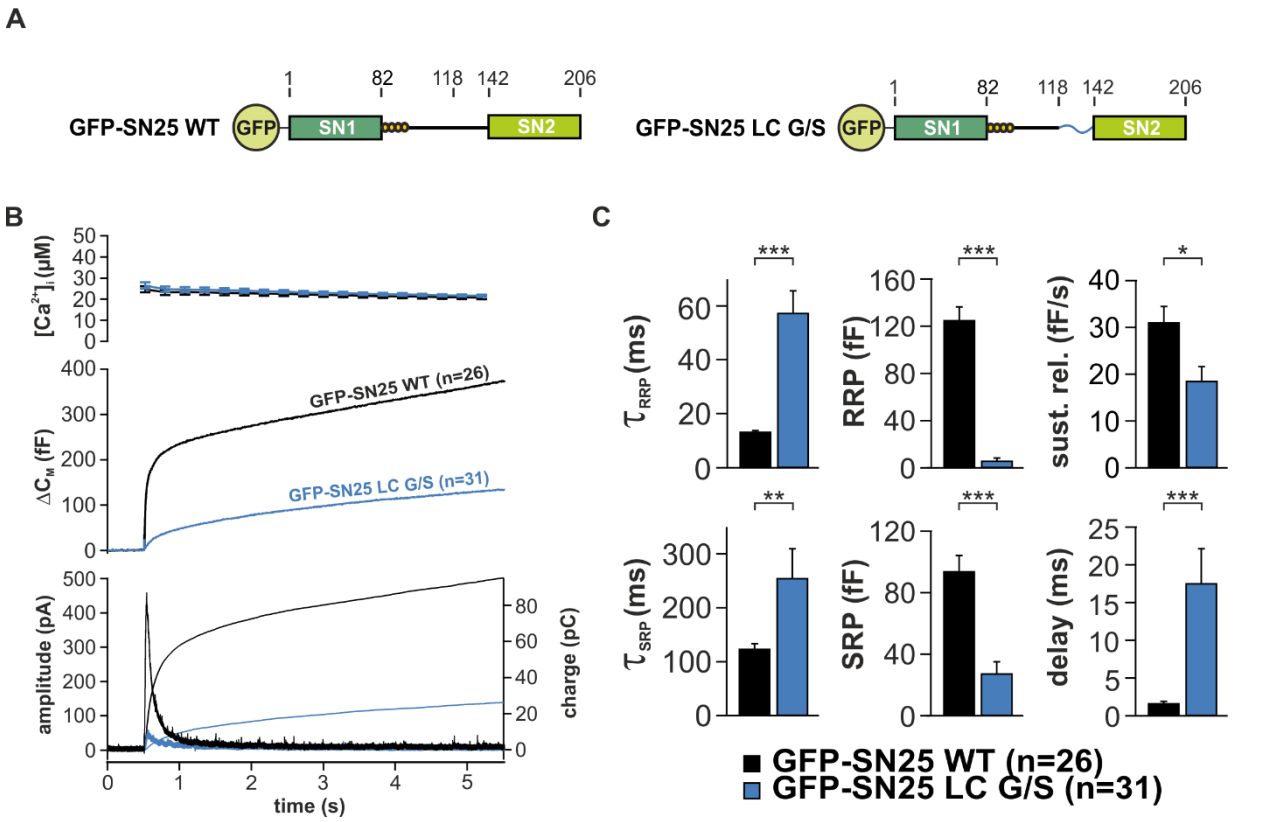

Figure 19 C-terminal linker stabilizes forward priming.
(A) Cartoon showing structure of the mutants: GFP-SN25 LC G/S where amino acids 118-142 were substituted with with glycine-serine residues. (B) Electrophysiological characterization of secretion shown as averaged traces for $[Ca^{2+}]_i$ (top), capacitance measurements (middle) and amperometric recordings (bottom) in KO cells expressing GFP-SN25 LC G/S (blue), or WT protein (black). (C) The mean amplitudes of RRP and SRP and their corresponding time constants τRRP and τSRP are depicted for the fast burst component. The mean sustained release rates describe the linear release component. The exocytic delay indicates the time interval between flash application and secretion onset. All data is plotted as mean ± SEM, statistical analysis was done with student's t-test.

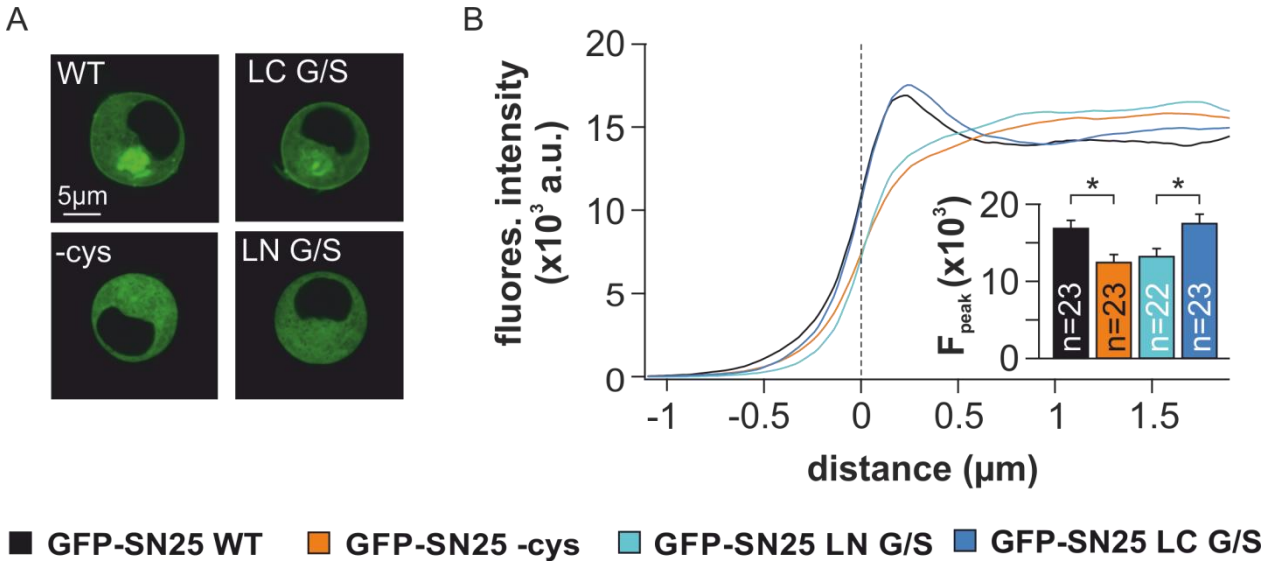

Figure 20 N-terminal linker region is responsible for anchorage of the SNAP-25 to plasma membrane.
(A) Confocal exemplary images of the four tested conditions; SNAP-25 WT, SN25-cys,SN25 LN G/S and SN25 LC G/S (B) Quantitative analysis of the concentration of the SNAP-25 WT and mutants on the plasma membrane. A set point of "0" was determined as the maximum slope of increase of fluorescence when a line of ~ 3.5 µM was taken across the plasma membrane. All data is plotted as mean ± SEM, statistical analysis was done with ANOVA via Tukey test.

1.11 N- and C- terminal regions of the linker have different effects on syntaxin interaction

Given our findings that the linker is involved in formation of stable binary t-SNARE complexes, we wondered whether the N- or C-terminal substitution of the linker regions affects SNAP-25:Stx-1A interactions. To address this question we employed a pull-down assay using immobilized GST-Stx-1A (Figure 21 A and B), as described before. Interestingly, we found that comparable amounts of protein were retained on beads after incubation with SN25 LN G/S or WT SNAP-25, suggesting that the N-terminal linker is dispensable for Stx-interactions. In contrast, the relative molar retention of the mutant protein was significantly lowered for SN25 LC G/S in comparison to WT protein (Figure 21 B). Thus, only the C-terminal linker segment seems to be critical for efficient t-SNARE interactions. As a complementary approach, we also investigated the retention of mutant L-SN2 fragments on immobilized Stx-1A in the presence of free SN1. In previous experiments, we established that the linker domain can facilitate the association of SN2 fragments with SN1:Stx H3-containing complexes. Somewhat incongruent to our experiments with full-length protein, we found that substitution of N- or C-terminal linker sections by a flexible peptide interfered with association of L-SN2 to Stx-1A. That said, it should be noted that in LN G/S-SN2 fragments two thirds of the attached linker is completely unstructured due to the substitution and could pose an obstacle for association with SN1:Stx-H3. This problem might be partly abated in the full-length protein, thus accounting for the apparent differences in Stx binding. In summary, our data points to a requirement for the C-terminal linker region in productive t-SNARE interactions. The role of the N-terminal section is presumably limited to providing an overall suitable linker conformation for C-terminal interaction with SN2 and/or the SN1:Stx-H3 assembly.

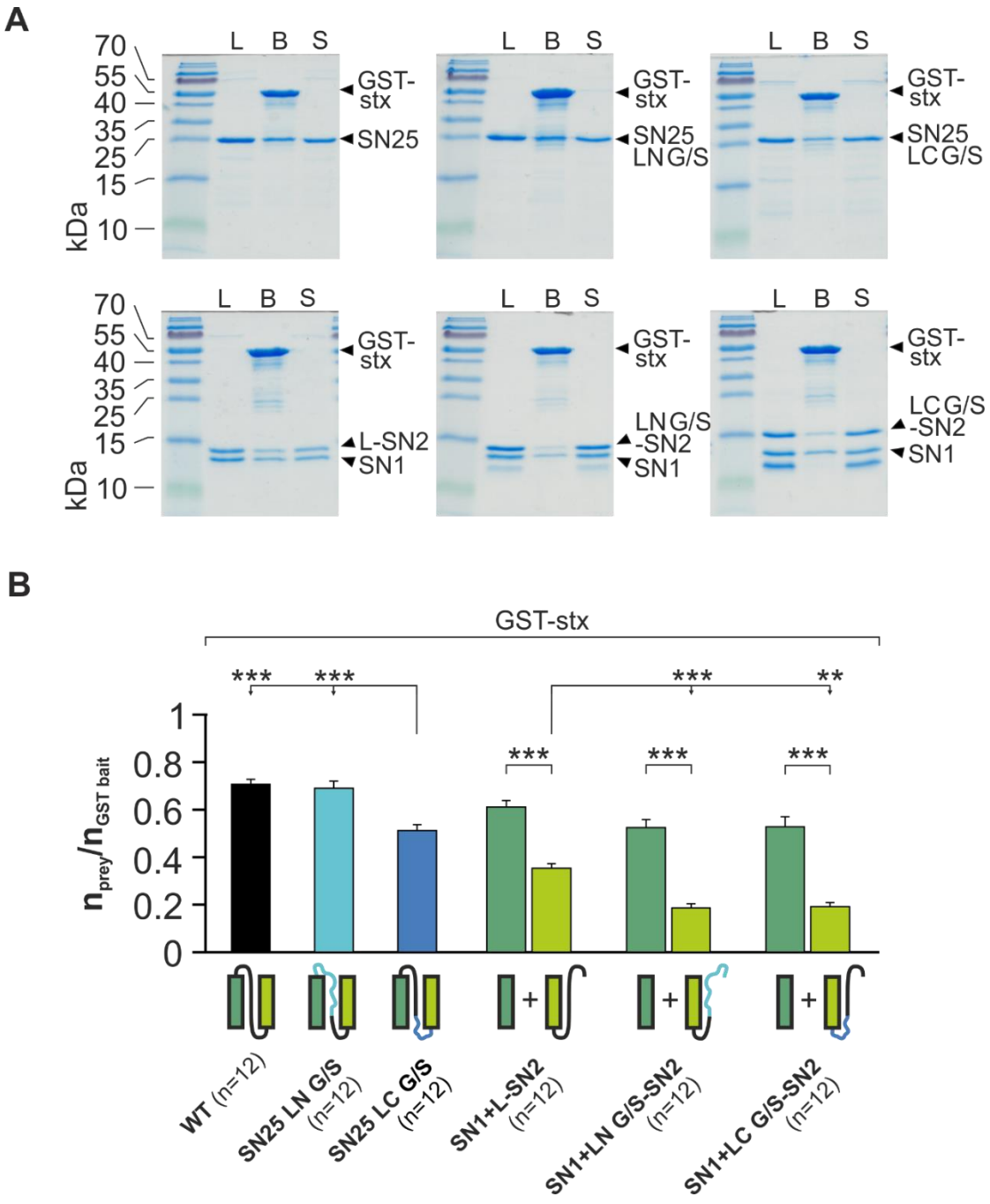

Figure 21 Differential role of SNAP-25 linker regions on SNAP-25:Stx1A interaction.
(A) Coomassie stained gels showing the load (L) as SNAP-25 WT or SNAP-25 mutants, Stx1A containing beads (B) with bound SNAP-25WT (or mutants) fraction and the supernatant (S). (B) Quantification of the SNAP-25 WT (or SNAP-25 mutants) retention on Stx-GST beads. GST-GFP was used as a negative control for binding specificity. The average retention ratio nprey/nStx-1A was calculated for each protein/fragment. All data is plotted as mean ± SEM, statistical analysis was done with ANOVA test.

1.12 Tension within the linker peptide is not critical for secretion

The SNARE core complex resembles a rod-like structure, whose total length of about 12 nm must be bridged by the SN25 linker (Sutton et al., 1998), so that SN1 and SN2 can enter the complex in parallel orientation. While the 60 aa long linker domain would be long enough to span the distance, molecular dynamic simulations have raised the idea that tension within the linker could interfere with SNARE assembly, if linker length is slightly shortened by crosslinking of cysteine residues by disulfide bridges (Bock et al., 2010). If light tension would indeed build up during SNARE complex formation due to the limited length of the linker, it could be an important determinant for the energetic landscape of core complex assembly. In order to investigate this idea, we generated and characterized two mutants, in which the linker was artificially extended. In one variant, denoted SN25 ext7aa, we extended the SN25 linker by seven amino acids using short inserts found in the slightly longer N-terminal linker segment of SNAP-23, the closest isoform to SNAP-25 (Figure 22A). A second extension mutant, called SN25 ext14aa, was generated by an additional insertion of seven amino acids before the beginning of the C-terminal linker region in SN25 ext7aa (Figure 22A). This inserted peptide in SN25 ext14aa contained a varied sequence of glycine and serine to avoid any possible formation of secondary structure. GFP-SN25 ext7aa did not show any signs of compromised or altered secretion when compared to corresponding WT controls [RRP(WT) = 139 ± 21 fF (n = 25) vs. RRP(SN25 ext7aa) = 144 ± 19 fF (n = 25); τ_{RRP}(WT) = 22.4 ± 2.1 ms vs. τ_{RRP}(SN25 ext7aa) = 24.8 ± 2.6 ms; SRP(WT) = 111 ± 23 fF vs. SRP(SN25 ext7aa) = 116 ± 25 fF; τ_{SRP}(WT) = 152 ± 20 ms vs. τ_{SRP}(SN25 ext7aa) = 173 ± 25 ms; sust.rate(WT) = 32 ± 2.9 fF/s vs. sust.rate(SN25 ext7aa) = 30 ± 3.6 fF; delay(WT) = 3.7 ± 0.77 vs. delay(SN25 ext7aa) = 4 ± 0.96]; Figure 22 A-C. Also in the GFP-SN25 ext14aa-expressing cells no significant deficits in release could be observed (Figure 23 A). [RRP(WT) = 173 ± 35 fF (n = 21) vs RRP(SN25 ext14aa) = 168 ± 28 fF (n = 17) τ_{RRP}(WT) = 30 ± 5.7 ms vs. τ_{RRP}(SN25 ext14aa) = 31 ± 3.4 ms; SRP(WT) = 89.5 ± 14.7 fF vs. SRP(SN25 ext14aa) = 79.9 ± 15.1 fF; τ_{SRP}(WT) = 154 ± 26 ms vs. τ_{SRP}(SN25 ext14aa) = 196 ± 33 ms; sust.rate(WT) = 30 ± 2.8 fF/s vs. sust.rate(SN25 ext14aa) = 42 ± 6 fF; delay(WT) = 4 ± 0.9 vs. delay(SN25 ext14aa) = 3.7 ± 0.7]; Figure 23 B and C. These results indicate that linker length is not a critical determinant for secretion. Clearly, linker tension is not required for the stabilization fusion intermediates, as might have been expected.

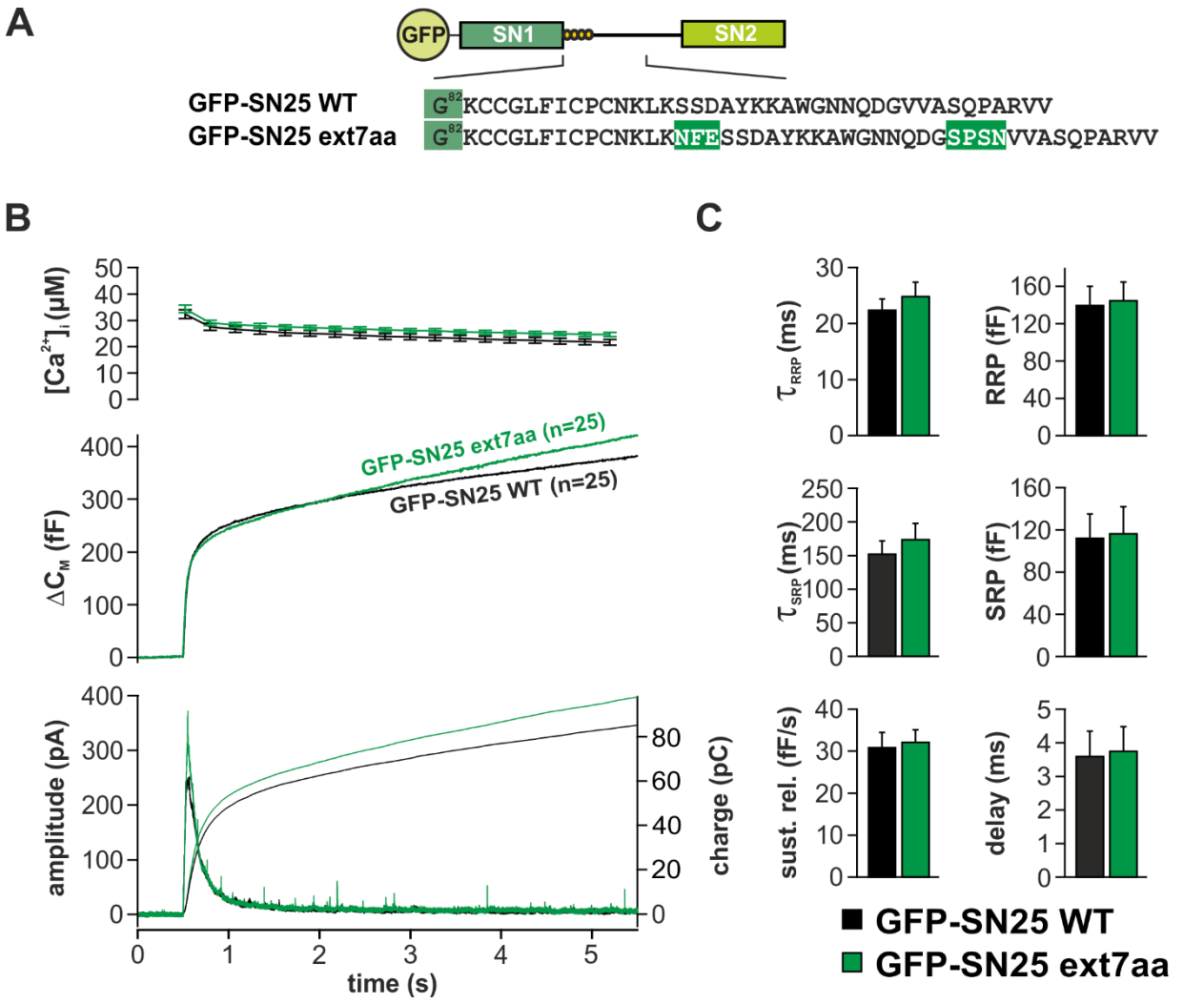

Figure 22 Overall extension of the linker does not change release properties.
(A) Cartoon showing GFP-SNAP-25 WT vs elongated mutant GFP-SN25 ext7aa. Extension was at the N-terminal linker region to match the corresponding sequence in SNAP-23, which is seven amino acids longer. (B) Electrophysiological analysis of secretion in SNAP-25 KO cells expressing GFP-SN25 ext7aa (green) or WT control (black). Averaged traces show $[Ca^{2+}]_i$ measurements (top), capacitance change (middle) and amperometric currents (bottom) in Ca^{2+}-uncaging experiments. No significant changes between WT and extension mutant. (C) Quantification of kinetic parameters. Mean amplitudes of RRP and SRP as well as their corresponding time constants τfast and slow, sustained release rate, and stimulation secretion delay were determined. Quantitative analysis showing no significant difference between extension mutant and its WT control. All displayed data are presented as mean ± SEM. n is depicted in panel B. Student's t-test was performed for each parameter.

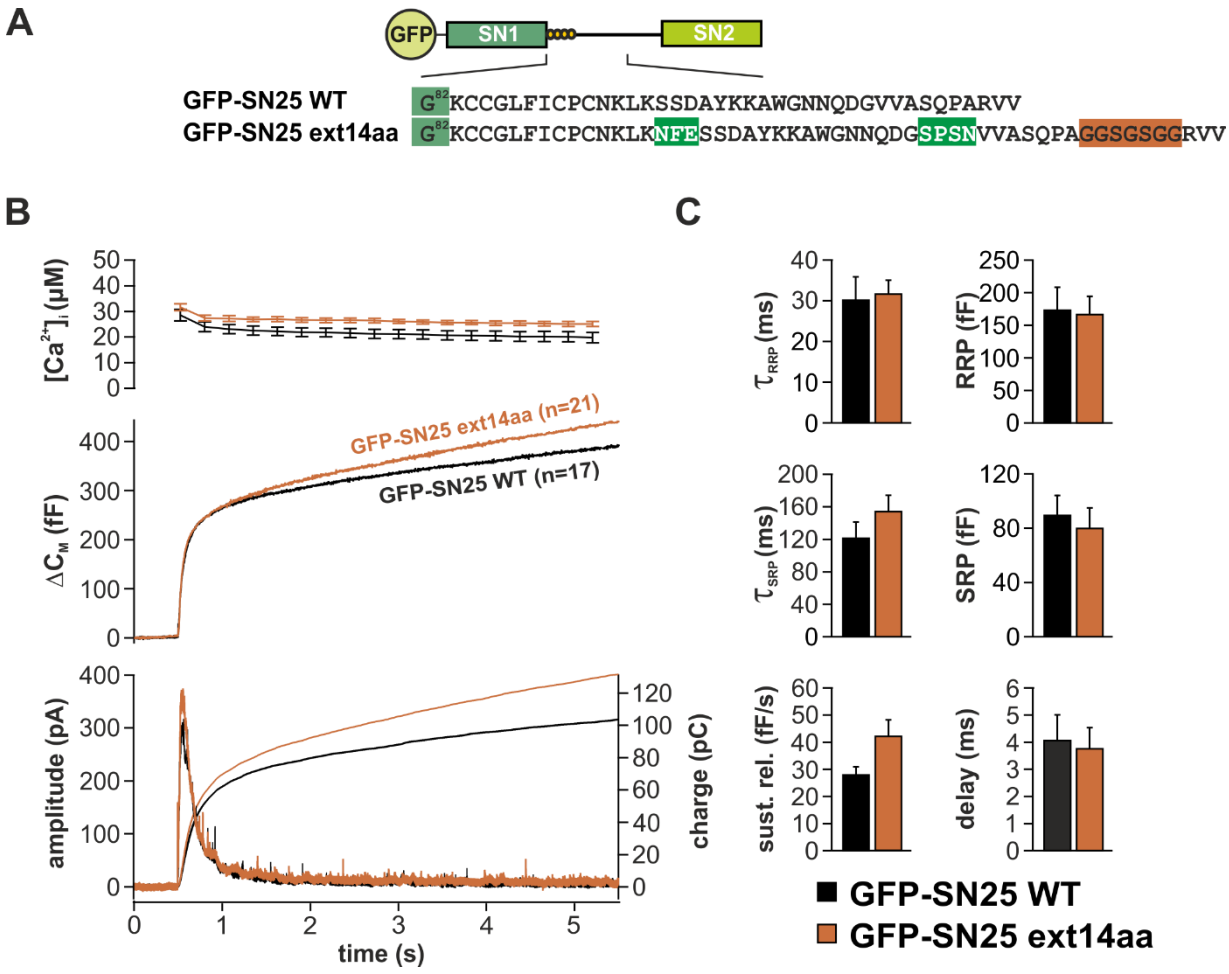

Figure 23 Overall extension of the linker does not change release properties.
(A) Cartoon showing GFP-SNAP-25 WT vs elongated mutant GFP-SN25 ext14aa. Extension was at the N-terminal linker region to match the corresponding sequence in SNAP-23 in addition to seven extra amino acids making the mutant fourteen amino acids longer. (B) Electrophysiological analysis of secretion in SNAP-25 KO cells expressing GFP-SN25 ext14aa (brown) or WT control (black). Averaged traces show $[Ca^{2+}]_i$ measurements (top), capacitance change (middle) and amperometric currents (bottom) in Ca^{2+}-uncaging experiments. No significant changes between WT and extension mutant. (C) Quantification of kinetic parameters. Mean amplitudes of RRP and SRP as well as their corresponding time constants τfast and slow, sustained release rate, and stimulation secretion delay were determined. Quantitative analysis showing no significant difference between extension mutant and its WT control. All displayed data are presented as mean ± SEM. n is depicted in panel B. Student's t-test was performed for each parameter.

1.13 Shortening of the linker boosts total secretion

As the extension of the SN25 linker is functionally well tolerated, we next wondered about the effects of linker shortening. Previous molecular dynamic simulations predicted that a decrease in linker length after formation of disulfide bridges would be detrimental to exocytosis (Bock et al., 2010), but the specific mechanistic effects on priming and triggering were unclear. To address this point, we generated a mutant variant with minor deletions in the N-terminal domain. For this purpose, we identified N-terminal linker

positions that exhibit noticeable variation in SNAP-25 orthologs throughout the animal kingdom (Figure 24). Four residues following the acylation motif were selected for elimination according to this conservation criterion: tyrosine[101], lysine[102], alanine[104], and asparagine[107] were the least conserved amino acids comparing SNAP-25 isoforms from the animal kingdom.

```
danio_sn25            GEQLERIEEGMDQINKDMKDAEKNLNDLGKFCGLCSCPCNKMK----SG-ASK-AWGNNQD
carassius_sn25        GEQLERIEEGMDQINKDMKDAEKNLNDLGKFCGLCSCPCNKMK----SGG-SK-AWGNNQD
cynops_sn25           GEQLDRVEEGMNHINQDMKEAEKNLKDLGKCCGLFICPCNKLK----SSDAYKKAWGNNQD
xenopus_sn25          GEQLERIEEGMEQINKDMKEAEKNLTDLGKFCGLCVCPCNKLK----SSDAYKKAWGNNQD
Gekko                 GEQLERIEEGMDQINKDMKEAEKNLTDLGKFCGLCACPCNKLK----SSDAYKKAWGNNQD
ophiophagus_sn25      GEQLERIEEGMDQINKDMKEAEKNLTDLGKFCGLCACPCNKLK----SSDAYKKAWGNNQD
hom_sn25              GEQLDRVEEGMNHINQDMKEAEKNLKDLGKCCGLFICPCNKLK----SSDAYKKAWGNNQD
rattus_sn25           GEQLDRVEEGMNHINQDMKEAEKNLKDLGKCCGLFICPCNKLK----SSDAYKKAWGNNQD
gallus_sn25           GEQLERIEEGMDQINKDMKEAEKNLTDLGKFCGLCVCPCNKLK----SSDAYKKAWGNNQD
mus_sn25              GEQLERIEEGMDQINKDMKEAEKNLTDLGKFCGLCVCPCNKLK----SSDAYKKAWGNNQD
pongo_sn25            GEQLERIEEGMDQINKDMKEAEKNSTDLGKFCGLCVCPCNKLK----SSDAYKKAWGNNQD
celegans_sn25         GEQLERCEGALDTINQDMKEAEDHLKGMEKCCGLCVLPWNKTDDFEK-TE-FAKAWKKDDD
dorytheutis_sn25      GEQLDRIEEGLDQINQDMKDAEKNLEGMEKCCGLCVLPWKRGKSFEKSGD-YANTWKKDDD
Drome_sn24            GEQLDRIEEGMDRINADMREAEKNLSGMEKCCGICVLPWKKVNI----KDDGESAWKANDD
ceratitis_Sn25        GEQLDRIEEGMDRINADMREAEKNLSGMEKCCGLCVVPWKKVAI----KDDGDHAWKANED
Procambarus_sn25      GEQLDRIEEGMDQINADMKEAEKNLTGMEKCCGLCVLPCNK----SSQFKEDESTWKGKED
drome_sn25            GEQLDRIEEGMDQINADMREAEKNLSGMEKCCGICVLPCNK----SQSFKEDDGTWKGNDD
```

Figure 24 SNAP-25 alignment between different species among the animal kingdom.
Alignment of the N-terminal sequence of the SNAP-25 between different isoforms in the animal kingdom. tyrosine[101]; lysine[102], alanine[104], and asparagine[107] were of the least conserved amino acids among the animal kingdom when comparing vertebrates' vs invertebrates. Thus, it was of the choice to be omitted. Lysine[102] was followed by another Lysine[103] and such amino acids were more prominent to omission.

The corresponding mutant was denoted SN25-4aa, as its linker was shortened by a total of four amino acids. Even though we expected an adverse effect on secretion, expression of GFP-SN25 -4AA in SNAP-25$^{-/-}$ cells significantly increased total release over the level of WT control cells (Figure 25A); ΔC_M5 s(WT) = 395 ± 34.9 vs ΔC_M5 s(SN25-4aa) = 565 ± 21.9 fF, P = 0.00265). This "boost" of the secretory response selectively elevated SRP-mediated release [SRP(WT) = 93.7 ± 10.1 fF, n = 29 vs. SRP(SN25-4aa) = 189.8 ± 16.5 fF, n = 32, $p < 0.05$], while the rate of SRP-mediated release was unchanged [τ_{SRP}(WT) = 121.1 ± 11.7 ms vs. τ_{SRP}(SN25-4aa) = 154.2 ± 15.7] (Figure 25 B). The RRP-mediated release component also remained unaltered [RRP(WT) = 195 ± 26.2 fF vs. RRP(SN25-4aa) = 225.2 ± 23.4 fF; τ_{SRP}(WT) = 19.4 ± 1.1 ms vs. τ_{SRP}(SN25-4aa) = 23.9 ± 1.6 ms]. Likewise, analysis of sustained release [sust. rel.(WT) = 21.8 ± 2.1 fF/S vs. sust. rel.(SN25-4aa) = 28 ± 3.3 fF/s] and exocytotic delay [delay(WT) = 3.3 ± 0.36 ms vs. delay(SN25-4aa) = 4.4 ± 0.42 ms] did not reveal any significant differences (Figure 25 C). Thus, our data suggests that slightly shortening the linker can selectively stabilize SRP vesicles, possibly by shifting the energetic landscape in a way that attenuates vesicle depriming. However, other mechanistic explanations including a specific function of the N-terminal linker segment in pool maintenance may also apply. In any case, the unique phenotypical combination of an increased SRP and an unchanged RRP also suggests that the

transition rate to the highly fusogenic mechanistic state is independent of the filling of the SRP, casting doubt that SRP vesicles simply mature into RRP vesicles over time.

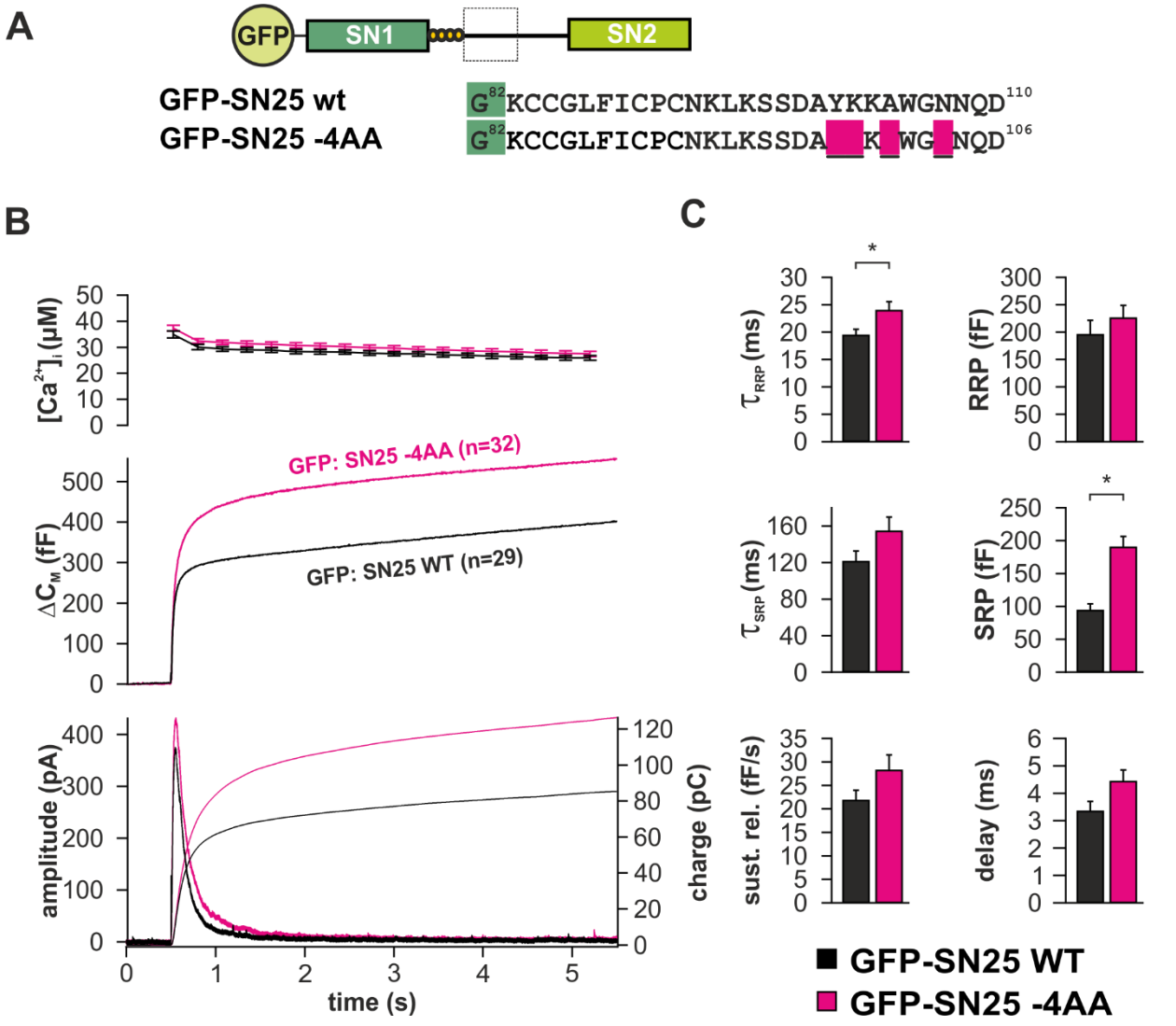

Figure 25 linker shortening caused significant increase of SRP size.
(A) Cartoon showing GFP-SN25 WT (black) vs GFP-SN25 -4AA (magenta). (B) Characterization of secretion in KO cells expressing GFP-SN25 WT or mutant. Shown are averaged $[Ca^{2+}]i$ measurements (top), capacitance traces (middle) and amperometric recordings (bottom). (C) Comparative electrophysiological analysis of secretion in GFP-SNAP-25 WT (black) and GFP-SN25 -4AA (purple) expressing KO cells. n is depicted in panel B. Comparison was performed using student's t test.

1.14 Mechanistic role of the acylation motif within the SN25 linker

The kinetic deceleration of secretion seen in acylation-deficient SNAP-25 mutants, especially in SN25-cys, may indicate that the N-terminal linker is mechanistically involved in fusion triggering. However, the interpretation of these phenotypes is complicated by mislocalization of the mutants, which cease to be membrane–anchored (Nagy et al., 2008). To clarify whether the loss of membrane localization is primarily responsible for the observed secretion deficits, we targeted the SN25-cys mutant back to the plasma membrane by a second acylation motif. For this purpose, we N-terminally fused the minimal acylation motif of SNAP-25 (aa 85-120) with the GFP-tag used to visualize the mutant (Figure 26A), resulting in P-GFP-SN25-cys.

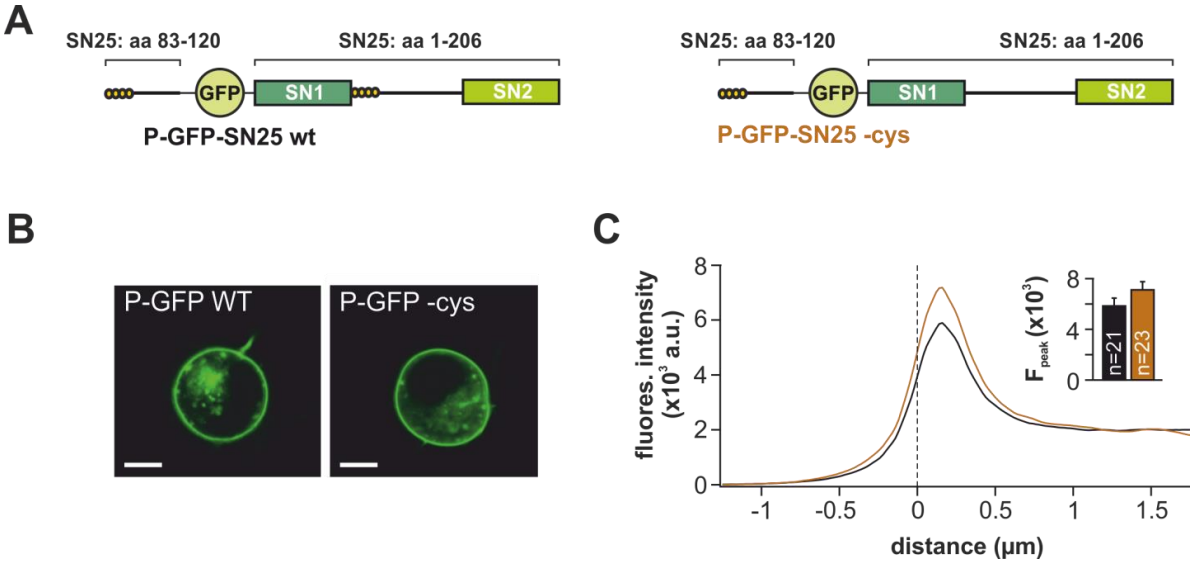

Figure 26 linker extra acylation site of the SNAP-25.
(A) Cartoon showing the rescue paradigm: extra acylated SNAP-25 WT (left panel), and SN25-cys (right panel) N-terminally to the GFP fluorophore. (B) Confocal exemplary images of the two conditions; P-GFP-SN25 WT, and P-GFP-SN25-cys (C) Quantitative analysis of the concentration of the SNAP-25 WT and mutants on the plasma membrane. A set point of "0" was determined as the maximum slope of increase of fluorescence when a line of ~3.5 µM was taken across the plasma membrane. n is depicted in panel C. All data is plotted as mean ± SEM, statistical analysis was done with student's t-test.

The same extra acylation sequence was also added to WT SNAP-25, generating P-GFP-SN25 WT as a control vector. Expression of retargeted WT and mutant SNAP-25 in SNAP-25$^{-/-}$ cells resulted in strong GFP fluorescence intensity at the plasma membrane, which suggests that both variants are efficiently acylated and membrane-anchored (Figure 26; B and C). We measured the peak fluorescence in aligned, orthogonal line scans and found no significant difference between retargeted mutant and WT protein [WT: 5845 ± 620 a.u., n = 21; SN25 LC G/S: 7680 ± 937, n = 23; P = 0.117].

On a functional level, P-GFP-SN25 WT fully restored secretion in SNAP-25$^{-/-}$ cells, reaching a similar level of release as GFP-SN25 WT without the second acylation motif (Figure 27 A-C). Intriguingly, P-GFP-SN25-cys mediated slower and lower secretory responses compared to controls, therefore largely retaining the key features of the secretion phenotype of the original SN25-cys mutant. A detailed kinetic analysis showed that the RRP in P-SN25-cys-expressing cells was significantly lower than in control cells expressing P-GFP-SN25 WT (60 ± 12.7 fF, n = 25 vs. 102 ± 11.9 fF, n = 26; P = 0.019) (Figure 27 B and C). Moreover, the RRP time constant τ_{RRP} in cells expressing the mutant was significantly higher than for controls (31 ± 5 ms vs. 18 ± 2 ms; P = 0.021). While the SRP component was similar for mutant and WT (138 ± 16 vs 107 ± 12 ms), the SRP time constant was however significantly increased in cells expressing the mutant in comparison to cells expressing WT SNAP-25 (214 ± 17 ms vs. 159 ± 18 ms; P = 0.04). As a deviation from the phenotypical profile of the original SN25-cys mutant, no significant difference in sustained rates of P-GFP SN25-cys and P-GFP-SN25 WT was observed, indicating that the aspect of the original phenotype might indeed be due to a reduction in the plasma membrane expression reducing forward priming.

In conclusion, our retargeting experiment points out that the exact position of acylation on SNAP-25 is mechanistically important. While a second N-terminal acylation motif can reestablish normal membrane localization, it is not sufficient to substitute for the original linker-based acylation site with respect to efficient secretion.

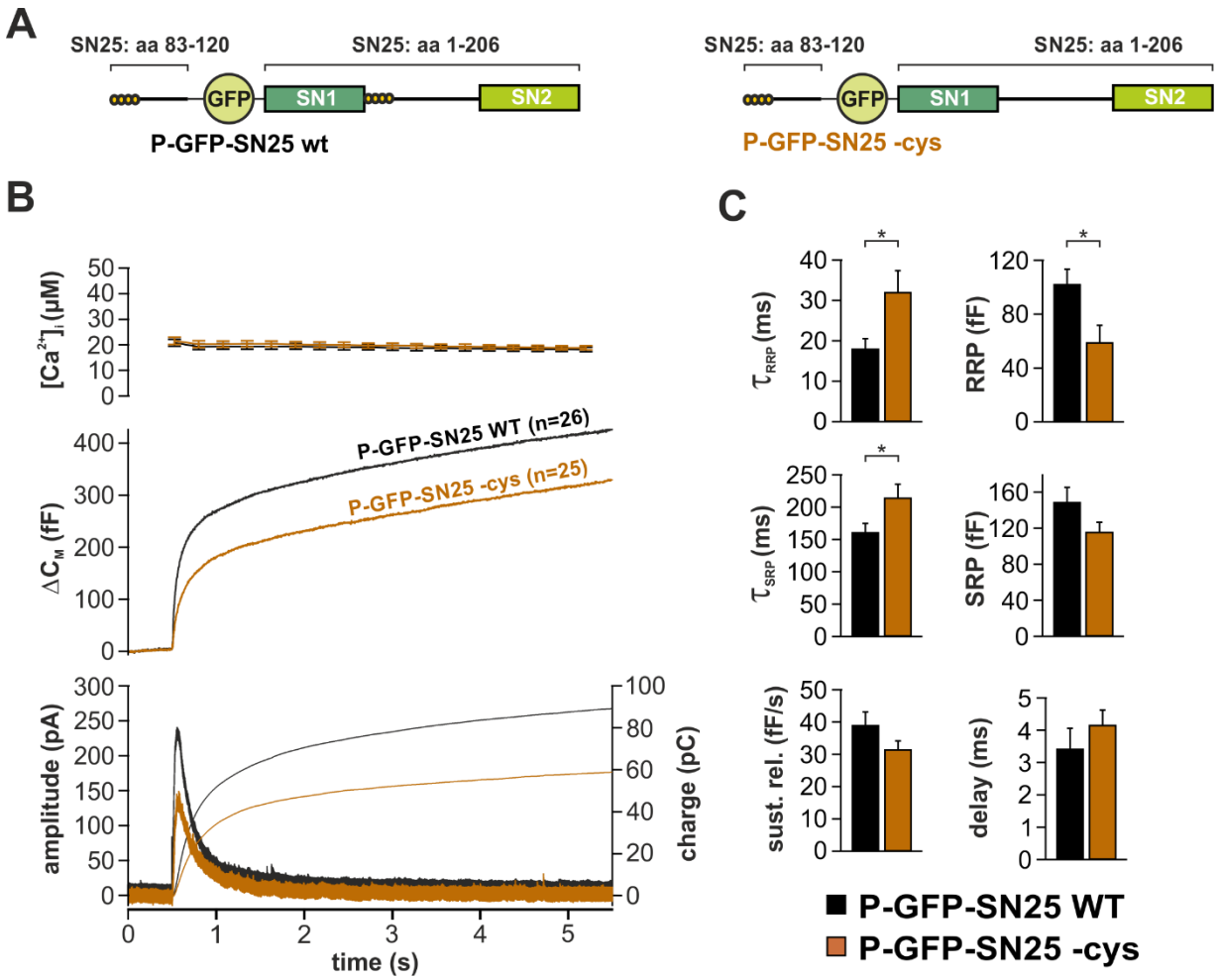

Figure 27 The role of linker acylation in exocytosis.
(A) Cartoon showing the design of extra acylation added to either WT or SN25-cys proteins (B) Averaged traces for $[Ca^{2+}]_i$ (top), capacitance measurements (middle) and amperometric recordings (bottom) in KO cells expressing P-GFP-SN25 WT or P-GFP-SN25-cys (Pantone), or WT protein (black). (C) The mean amplitudes of RRP and SRP and their corresponding time constants τRRP and τSRP are depicted for the fast burst component. The mean sustained release rates describe the linear release component. The exocytic delay indicates the time interval between flash application and secretion onset. n is depicted in panel B. All data is plotted as mean ± SEM, statistical analysis was done with student's t-test.

1.15 Spacer insertions between SN1 and the linker affect fusion triggering, but do not interfere with force transduction

In all vertebrate orthologs of SNAP-25, the linker acylation motif directly adjoins the end of the SNARE motif SN1, thus placing the SNAP-25 membrane anchors in direct vicinity of the C-terminal end of the assembling SNARE complex. Given the conspicuous triggering phenotype of SN25-cys, we wondered whether linker-mediated membrane contacts contribute to the SNARE force-induced membrane straining that is believed to initiate bilayer merger. To investigate this mechanistic idea in detail, we

generated linker mutants, in which the mechanical coupling between SN1 and acylation motif was inhibited by insertion of short flexible spacer peptides. In detail, we constructed three linker insertion mutants, in which 6, 10 or 14 residues of varied GGS sequence were inserted before K^{82} (named SN25-shift 6aa, SN25-shift 10aa, SN25-shift 14aa respectively; Figure 28A). While total secretion remained unchanged in cells expressing the different spacer mutants, we found graded kinetic changes of the secretory responses, wherein spacer insertions of increasing length inducing a progressively intensifying slowdown of release kinetics (Figure 28 B-D).

To better compare the different mutants, we normalized the results of our detailed kinetic analysis to the corresponding WT values (Figure 28 C and D). While both primed vesicles pools (RRP and SRP) were similar to controls for all three mutants, we found that the time constants for release of vesicles from RRP and SRP were significantly prolonged, and that effect size increased in a correlated fashion with spacer length [norm. τ_{RRP} (SN25-shift 6aa) = 1.49 ± 0.11, n = 26; norm. τ_{RRP} (SN25-shift 10aa) = 1.7 ± 0.14, n = 43; norm. τ_{RRP} (SN25-shift 14aa) = 3.5 ± 0.36, n = 34; P = 0.008 for (6aa vs. WT), P < 0.001 for (10aa vs. WT), and P < 0.001 for (14aa vs. WT); norm. τ_{SRP} (SN25-shift 6aa) = 1.5 ± 0.17; norm. τ_{SRP} (SN25-shift 10aa) = 1.75 ± 0.16; norm. τ_{SRP} (SN25-shift 14aa) = 1.7 ± 0.16; p = 0.008 for (6aa vs. WT), P < 0.001 for (10aa vs. WT), and P < 0.001 for (14aa vs. WT)]. Similarly, the onset of secretion was progressively delayed with the length of the insertion [norm. delay (SN25-shift 6aa) = 1.76 ± 0.24; P = 0.014, norm. delay (SN25-shift 10aa) = 2.62 ± 0.24; P < 0.001 norm. delay (SN25-shift 14aa) = 5.571 ± 1.11; p < 0.001]; Figure 28 B-D. Thus, altering the relative position of the membrane anchors within the linker clearly affects fusion triggering, causing a slowdown of release that was reminiscent of the kinetic changes in SN25-cys. This slowdown cannot not be explained by a general effect of linker length on SNARE complex function, as similar-sized insertions within the linker (SN25 ext7aa/14aa) were inconsequential for secretion.

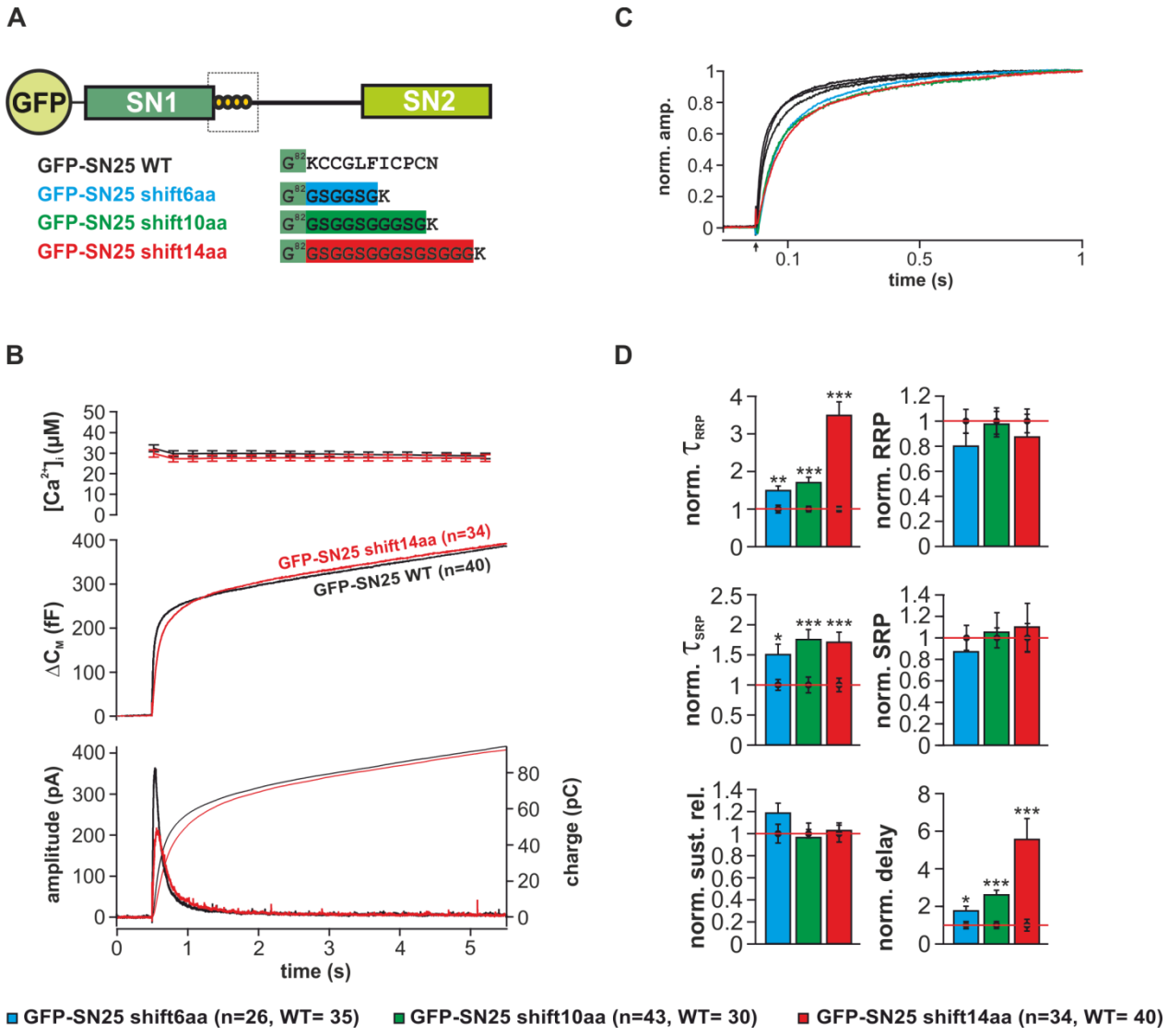

Figure 28 Uncoupling the SN1 from the linker results in delayed secretion.
(A) Structure of the three tested uncoupling mutants, SN25 shift6/10/14aa in blue, green and red respectively. (B) Characterization of secretion in KO cells expressing GFP-SN25 shift14aa in red; and WT in black). Shown are averaged $[Ca^{2+}]_i$ measurements (top), capacitance traces (middle) and amperometric recordings (bottom). (C) Normalized first second of capacitance traces illustrating slow down kinetics of the uncoupling mutants and their corresponding WT controls (D) Quantification of kinetic parameters for the three uncoupling mutations. n is depicted in panel B. Statistical analyses were only performed between mutant and according control measurements (Student's t-test).

The triggering defects of mutants carrying spacer insertions would in principle be consistent with reduced force transfer from the core complex onto the plasma membrane. However, contrary to our findings, spacer insertions in the juxta-membrane domain of Syb-2 have been previously been reported to dramatically diminish secretion (Kesavan et al., 2007), which may indicate that the linker-mediated facilitatory process is distinct from the general force transduction mechanism. To directly test the idea that the acyl anchors of SNAP-25 are indeed used to strain the plasma membrane, we inserted the largest spacer into the acylated-

deficient SN25-cys variant, thereby generating a double mutant called SN25-cys shift14aa (Figure 29A). If our mechanistic notion was indeed true, removal of the membrane anchor should preclude any further interference by spacer insertions, thus preventing an exacerbated secretion phenotype of the double mutant. Intriguingly, however, our functional characterization clearly demonstrated more pronounced secretion deficits in SN25-cys shift14aa compared to the original SN25-cys variant (Figure 29 B-D): While the mutant only showed tendentially smaller primed vesicle pools [RRP(SN25-cys shift14aa) = 17.3 ± 7.4 fF, n = 26 vs. RRP(SN25-cys) = 37 ± 5.2 fF, n = 24 vs. RRP(WT) = 108.3 ± 8 fF, n = 29; SRP(SN25-cys shift14aa) = 86 ± 12.9 fF vs. SRP(SN25-cys) = 117.9 ± 10.2 fF vs. SRP(WT) = 121 ± 8.3 fF; $P < 0.001$ (WT vs SN25-cys, and WT vs SN25-cys shift14aa, $P = 0.27$ (SN25-cys vs SN25-cys shift14aa)], we found significantly increased time constants for release from both pools in comparison to SN25-cys [τ_{RRP}(SN25-cys) = 24.7 ± 3 ms vs. τ_{RRP}(SN25-cys shift14aa) = 39 ± 5.9; $P < 0.001$, and τ_{SRP}(SN25-cys) = 177 ± 12 ms vs. τ_{SRP}(SN25-cys shift14aa) = 299 ± 28, $P < 0.001$]. Moreover, the exocytotic delay was prolonged in the double mutant compared to the original variant SN25-cys [delay(SN25-cys) = 5.3 ± 0.5 ms vs delay(SN25-cys shift14aa) = 11.1 ± 1.5 ms, $P < 0.001$], which is in agreement with the apparent weakening of stimulus-secretion coupling. Sustained release was however indistinguishable between both mutants, but significantly lower than in WT controls [sust. rel. (SN25-cys shift14aa) = 22.9 ± 2.8 fF/s vs. sust. rel.(SN25-cys) = 23.1 ± 1.39 fF/s vs. sust.rel.(WT) = 30 ± 1.6 fF/s; $P < 0.05$ for both mutants vs. WT]; Figure 29 D.

In summary, we demonstrate here that the positioning of the acylation site within the SN25 linker is crucial for fast vesicle, and specific membrane contacts of the linker at the C-terminal end of the core complex likely play a mechanistic role in fusion triggering. However, the membrane anchors within the linker are not part of the force transduction machinery that putatively induces membranes merger by molecular straining of lipid bilayers.

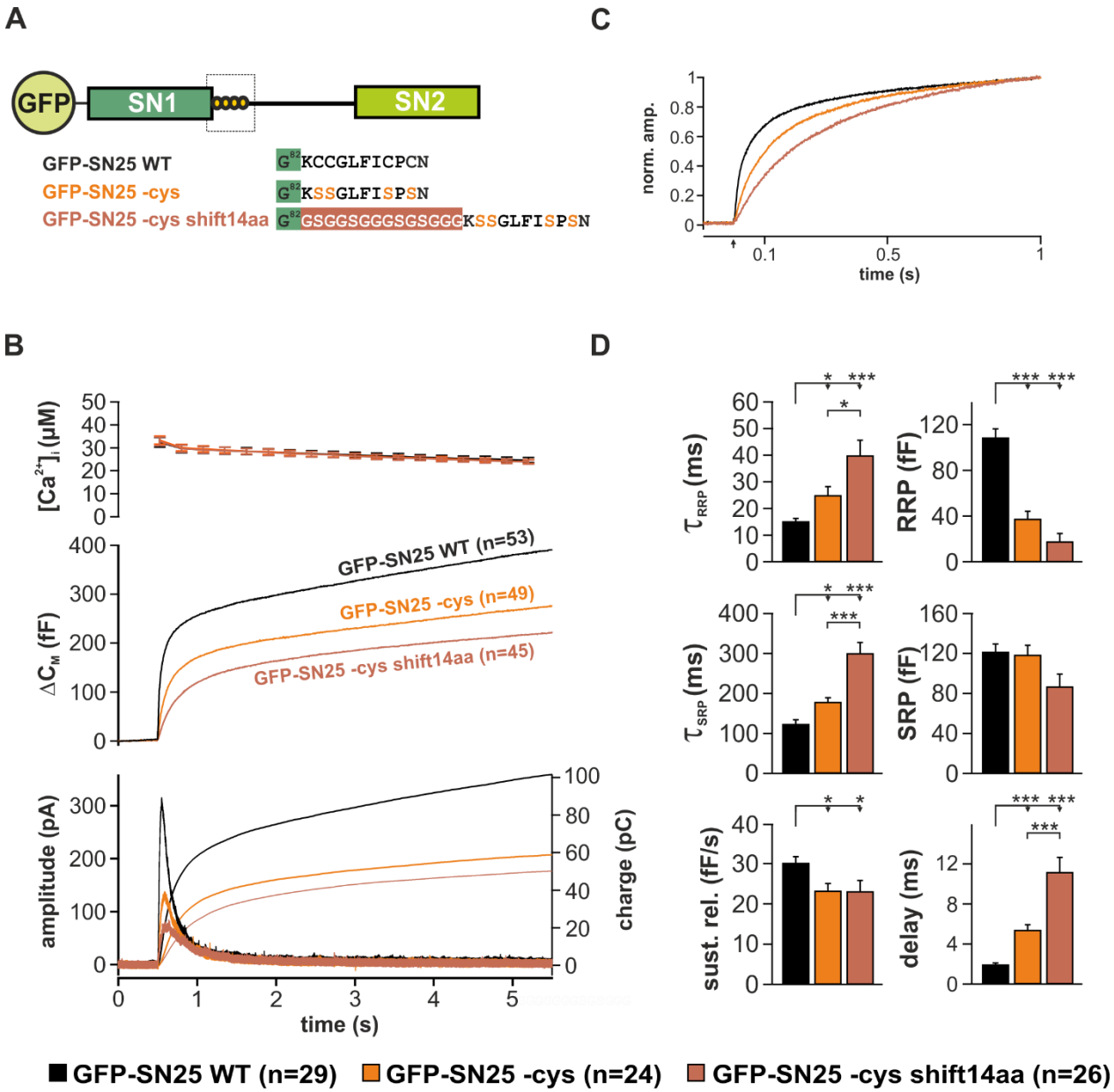

Figure 29 Acylated linker does not participate in SNARE-mediated force transfer.
(A) Cartoon showing GFP-SNAP-25 WT (black) vs the mutants GFP-SN25-cys and GFP-SN25-cys shift14aa (brick red). (B) Characterization of secretion in KO cells expressing GFP-SNAP-25 WT or mutants. Shown are averaged $[Ca^{2+}]_i$ measurements (top), capacitance traces (middle) and amperometric recordings (bottom). (C) A normalized plot of the secretory burst component further highlights the changed kinetics in the double mutant. All data are mean ± SEM, n is indicated in the corresponding panel. (D) Comparative electrophysiological analysis of secretion in GFP-SN25-cys (orange), GFP-SN25-cys shift14aa (cinnabar), and WT protein-expressing KO cells (black). The quantitative analysis of kinetic parameters showed an exacerbated phenotype. n is depicted in panel B. Multiple comparisons were performed using ANOVA and Tukey-Kramer test.

1.16 Supportive role of positively charged residues in the N-terminal linker region

The exacerbated kinetic phenotype of SN25-cys shift14aa indicates that spacer insertion disrupts an acylation-independent residual function of the N-terminal linker segment in fusion triggering. One interpretation might be that the corresponding linker region still engages in interactions with the lipid bilayers by an alternative mechanism. Indeed, positively charged amino acids within this region have been suspected to interact with phospholipid head groups, allowing for transient membrane contacts (Weber et al., 2017). To test the functional relevance of these potential interactions for release in SN25-cys-expressing cells, we mutated five lysine residues in the very N-terminal linker segment (K^{83}, K^{94}, K^{96}, K^{101}, K^{102}), substituting each position by alanine (Figure 30 A). The corresponding variant, SN25-cys 5K/A, was tested in Ca^{2+}-uncaging experiments and showed a noticeable slowdown compared to SN25-cys mutant (Figure 30 B). Our kinetic analysis revealed that τ_{RRP}(SN25-cys 5K/A) = 49.4 ± 7, n = 37, which was significantly lower than τ_{RRP}(SN25-cys) that was 28.3 ± 4 ms, n = 36; P = 0.035. Indeed, τ_{RRP}(SNAP-25 WT) = 14.3 ± 1.4 ms was significantly faster than both mutants (P < 0.001 compared to both mutants). Pool sizes were not significantly different between both mutants with RRP(SN25-cys 5K/A) = 37.4 ± 14.1 fF vs RRP(SN25-cys) = 25.8 ± 6.3 fF, ; P = 0.74 [RRP(SNAP-25 WT) = 122 ± 11.8 fF, which is significantly higher than both mutants; P < 0.001]. SRP(SN25-cys 5K/A) = 122 ± 23 fF vs SRP(SN25-cys) = 122 ± 20 fF; P = 0.893; Figure 30 C.

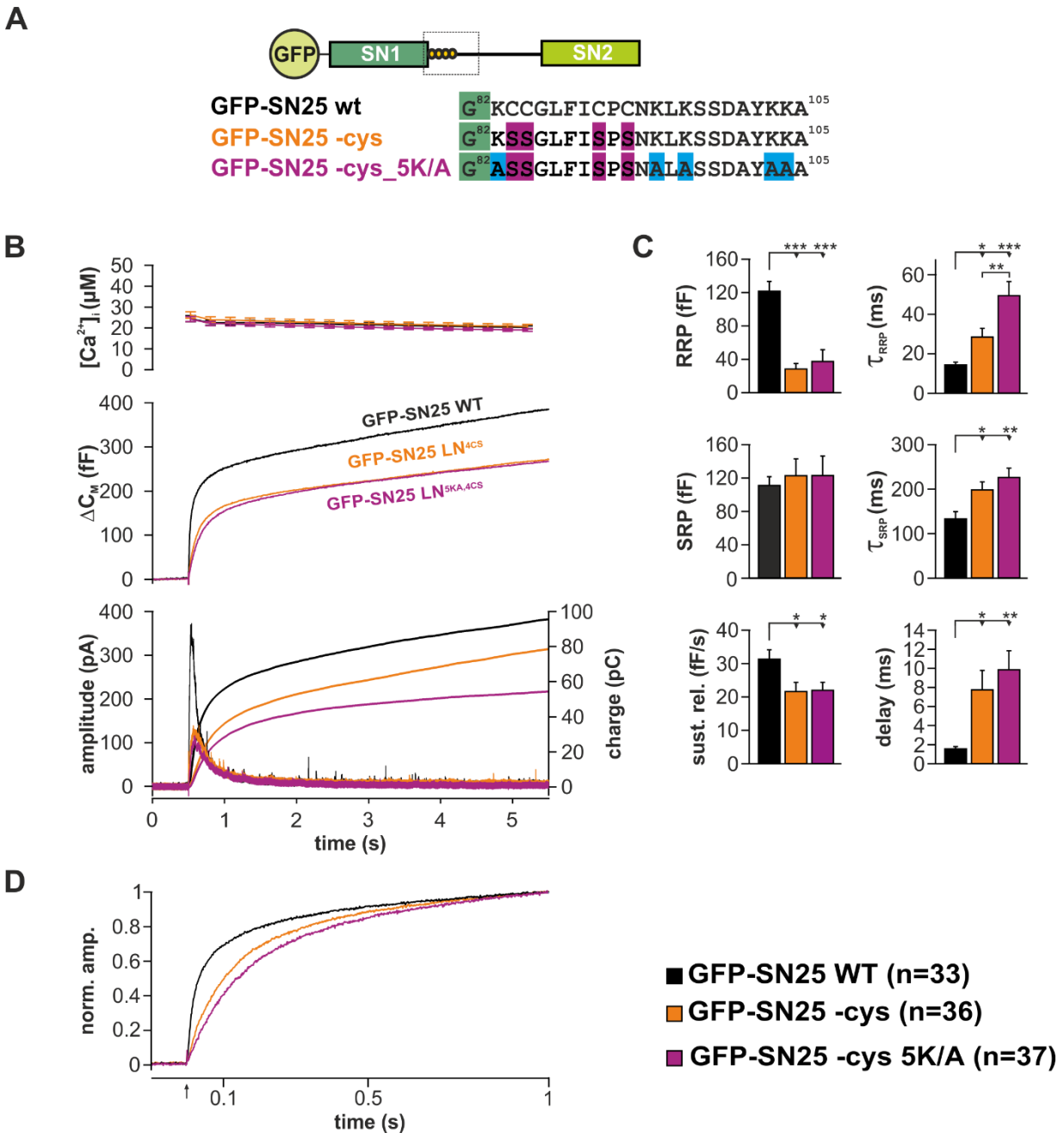

Figure 30 Charged amino acids at the N-terminal region of the linker partially stabilizes secretion. (A) Cartoon showing GFP-SNAP-25 WT (black) vs GFP-SN25-cys (orange) and GFP-SN25-cys 5K/A (violet). (B) Characterization of secretion in KO cells expressing GFP-SNAP-25 WT or mutants. Shown are averaged $[Ca^{2+}]_i$ measurements (top), capacitance traces (middle) and amperometric recordings (bottom). (C) Comparative electrophysiological analysis of secretion in GFP-SNAP-25 WT (black), GFP-SN25-cys (orange) and GFP-SN25-cys 5K/A expressing KO cells (violet). Comparison was performed using ANOVA and post-hoc Tukey test. (D) Normalized capacitance traces showing relative slowdown of release in GFP-SNAP-25 5K/A, expressing cells compared to palmitoylation mutant GFP-SN25-cys. n is depicted in the lower right panel.

In summary, our results indicate that the flanking lysine residues hold some functional role if the cysteine cluster and membrane anchorage of SNAP-25 are eliminated. In comparison to SN25-cys shift14aa, the

phenotypical exacerbation in SN25-cys 5K/A appears milder, which suggests that other residues in the N-terminal region also contribute to the function of the N-terminal linker segment. It would be interesting to investigate whether the loss of the five positively charged lysine residues would affect secretion more severely, if the cysteine cluster remains intact. However, results may also reflect changes in acylation level.

1.16.1 Core complex interactions of the C-terminal linker are required for efficient secretion

Structural analysis of the crystalized SNARE complex indicated that several bulky non-polar residues within the very C-terminal SN25 linker may interact with a hydrophobic groove on the complex (Sutton et al., 1998). To address the importance of these interactions, we generated a linker mutant denoted SN25 LC 4G, in which the corresponding residues, F^{133}, $I^{134}4$, V^{137} and A^{141}, were substituted by glycine residues (Figure 31 A). When tested in SNAP-$25^{-/-}$ cells, SN25 LC 4G-mediated release exhibited a substantial reduction of the RRP as well as decelerated RRP release kinetics (Figure 31 B). RRP was 105.1 ± 10.4 fF for WT controls (n = 26), but was reduced to 38.9 ± 5.6 fF in cells expressing GFP-SN25 LC 4G (n = 29; $P < 0.001$). The corresponding time constant for release from the RRP was significantly increased to 22.8 ± 2.9 ms in GFP-SN25 LC 4G compared to 15.9 ± 1.5 ms in controls ($P < 0.05$). In contrast, secretion from the SRP was largely unaffected [SRP(WT) = 109.1 ± 10 vs. SRP(SN25 LC 4G) = 90.9 ± 11.2 fF; τ_{SRP}(WT) = 138.2 ± 11.9 vs. τ_{SRP} (SN25 LC 4G) = 177.4 ± 23.0 ms]. The sustained release component also appeared normal in SN25 LC 4G-expressing cells [sust.rel. (WT) = 27.3 ± 2.1 fF/s vs. sust.rel. (SN25 LC 4G) = 26.5 ± 2.5 fF/s], indicating that forward priming was unchanged. However, in line with altered triggering of RRP vesicle fusion, the onset of the secretory response in SN25 LC 4G-expressing cells was significantly delayed in comparison to controls [delay (WT) = 2.5 ± 0.3 ms vs. delay (SN25 LC 4G) = 3.8 ± 0.37 ms; $P < 0.01$] (Figure 31 C).

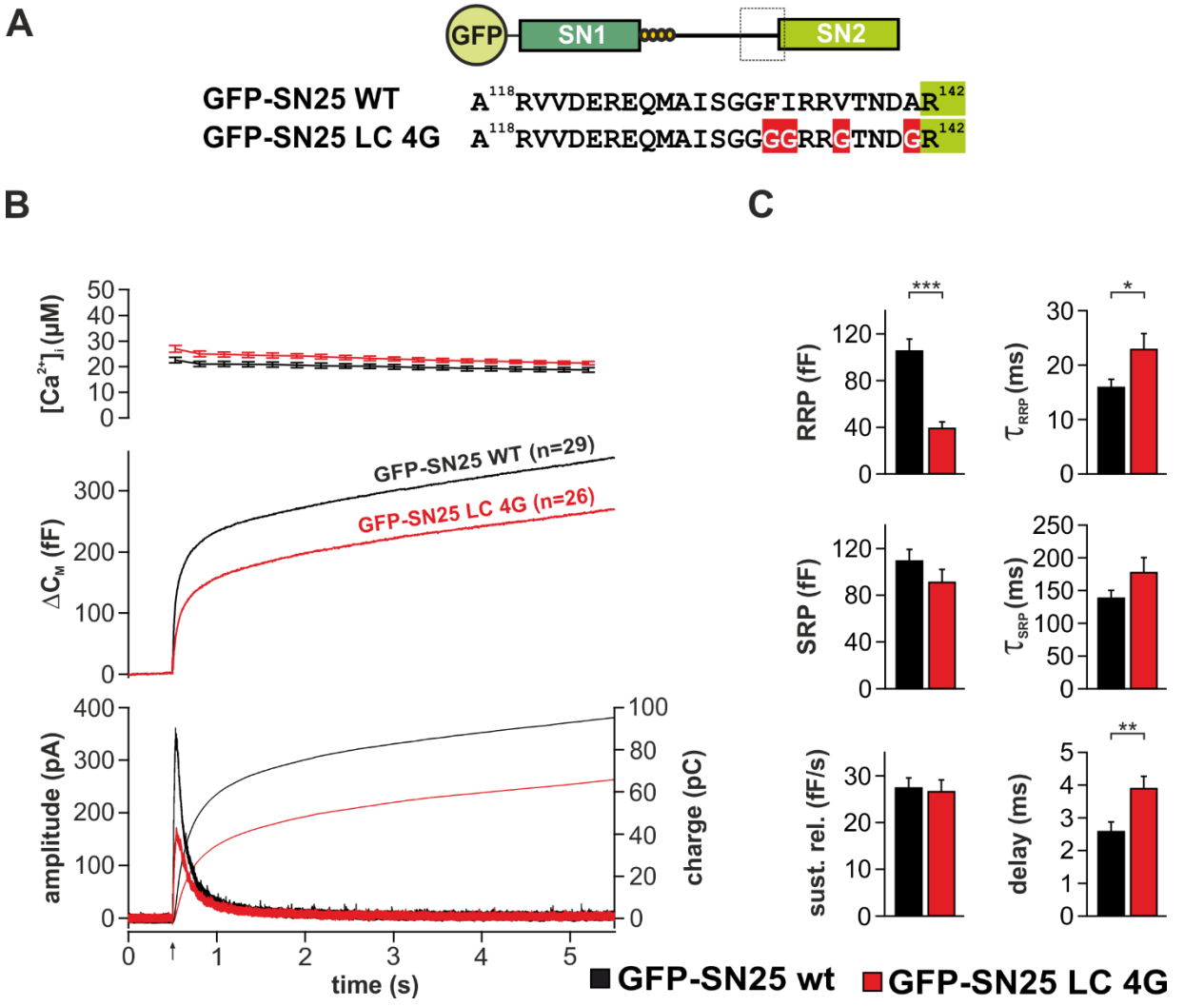

Figure 31 C-terminal mutation deteriorates pool stability as well as release kinetics.
(A) Cartoon showing GFP-SNAP-25 WT (black) and GFP-SN25 LC 4G mutant structure. (B) Characterization of secretion in SNAP-25 KO cells expressing GFP-SNAP-25 WT or mutant. Shown are averaged $[Ca^{2+}]_i$ measurements (top), capacitance traces (middle) and amperometric recordings (bottom). (C) Comparative electrophysiological analysis of secretion in GFP-SNAP-25 WT (black) and GFP-SN25 LC 9G expressing KO cells (black). n is depicted in panel B. All data are given as mean ± SEM. n is depicted in each panel. Statistical testing was done using Student's t-test.

The release defects of SN25 LC 4G indicate that core interactions of this linker region are important for effective secretion. Given the selective decrease of the RRP component, with no detectable effect on sustained release, we conclude that these interactions are important for stabilization of highly fusogenic vesicle states, likely preventing depriming. To investigate whether further residues in this particular C-terminal linker region are involved in the process, we also exchanged five additional surrounding amino acids by glycine residues resulting in SN25 LC 9G (Figure 32 A). Interestingly, the mutant exhibited an incremental exacerbation of the phenotype (Figure 32 B): The size of the RRP in KO cells expressing the

mutant remained strongly decreased [RRP(SN25 LC 9G = 59 ± 11 fF, n = 34 vs. RRP (WT) = 134 ± 19.6 fF, n = 27, P < 0.001], while the corresponding time constant of release was even further elongated to 37 ± 3.8 ms [τ_{RRP} (WT) = 17.1 ± 1.7 ms, P < 0.001]. Interestingly, we found that the size of the SRP was not significantly changed [SRP(SN25 LC 9G) = 75.9 ± 11.5 fF vs. SRP (WT) = 100.1 ± 11.8, p = 0.15], while its release kinetics were substantially slowed-down [τ_{SRP}(SN25 LC 9G) = 218.4 ± 38.5 ms vs. τ_{SRP} (WT) = 115.1 ± 9.8 ms, p = 0.017]. In line with a triggering defect, the onset of secretion was also significantly delayed [delay (SN25 LC9G = 7.2 ± 0.72 ms vs. delay(WT) = 4 ± 0.83 ms, p < 0.001]. Sustained release was however not changed in the mutant [sust.rel. (SN25 LC 9G) = 19.2 ± 1.9 fF/s vs. sust.rel. (WT) = 20 ± 2.28], suggesting again that forward priming is not affected; Figure 32 C.

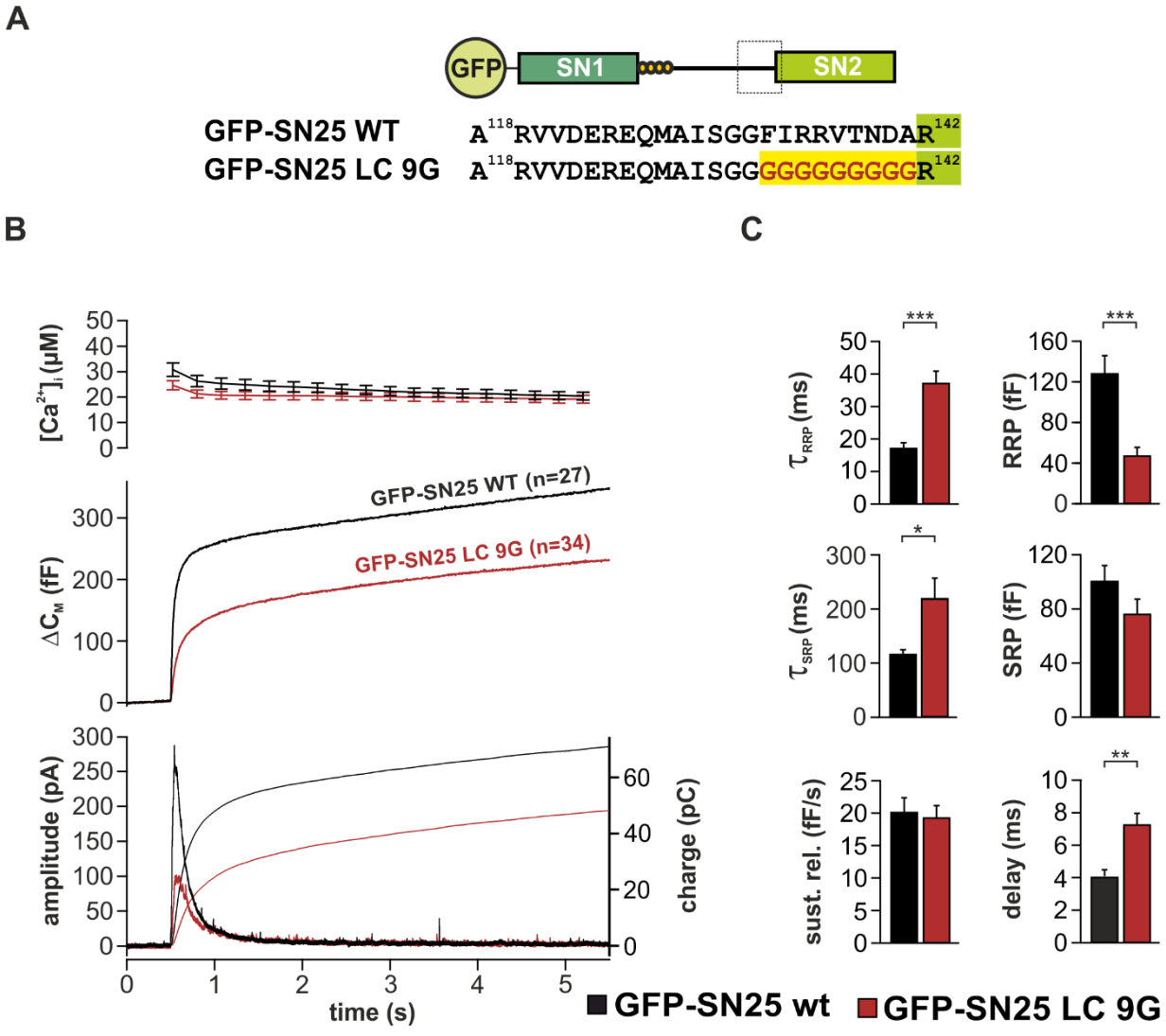

Figure 32 C-terminal mutation deteriorates pool stability as well as release kinetics.
(A) Cartoon showing GFP-SNAP-25 WT (black) and GFP-SN25 LC 9G mutant structure. (B) Characterization of secretion in KO cells expressing GFP-SNAP-25 WT or mutant. Shown are averaged $[Ca^{2+}]_i$ measurements (top),

capacitance traces (middle) and amperometric recordings (bottom). (C) Comparative electrophysiological analysis of secretion in GFP-SNAP-25 WT (black) and GFP-SN25 LC 9G expressing KO cells (black). All data are given as mean ± SEM. n is depicted in each panel. Statistical testing was using.Student's t-test.

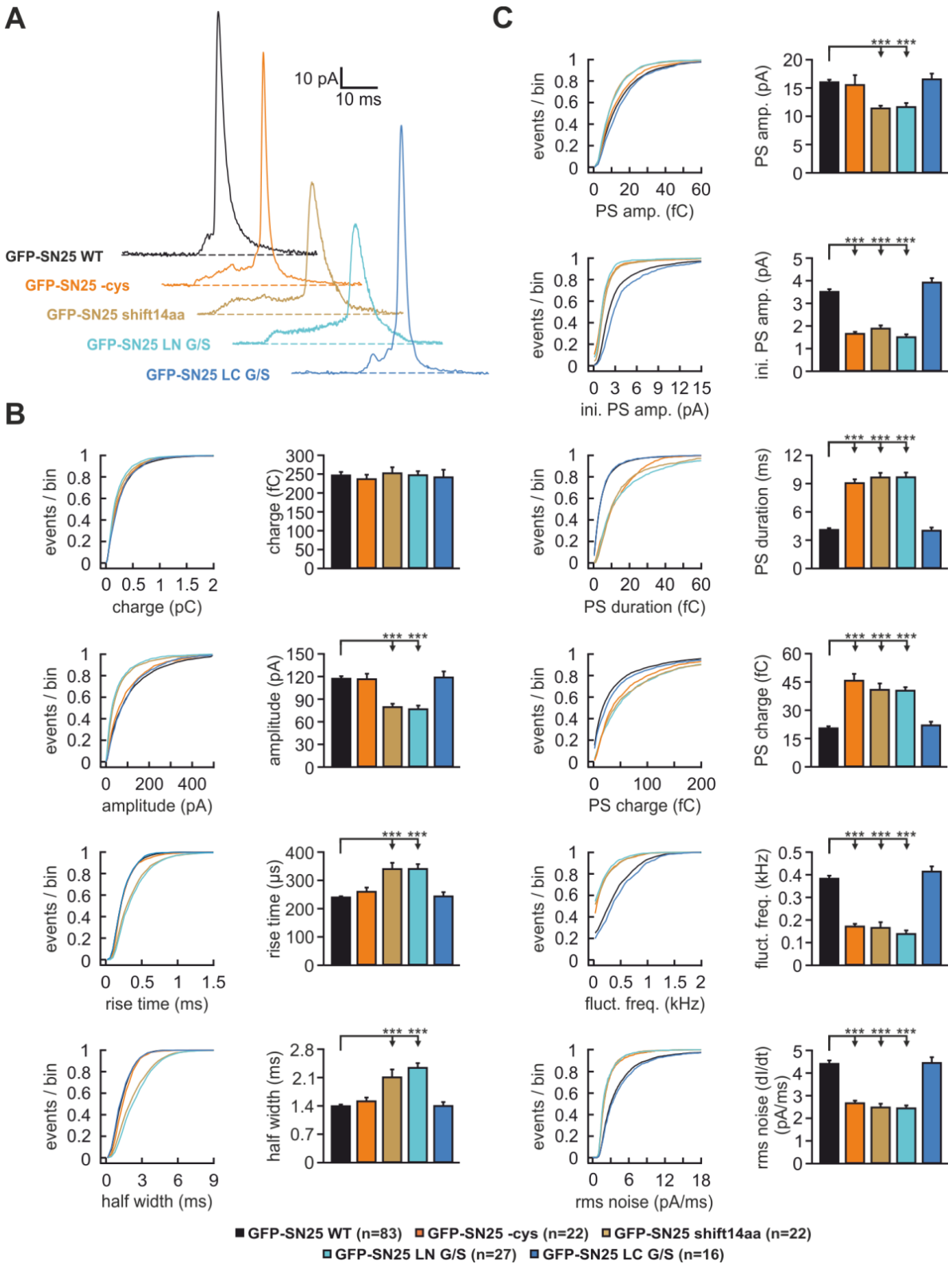

Figure 33 N- and C- terminal linker regions have different roles in controlling fusion pore initiation and expansion.
(A) Representative traces of amperometric spikes in overexpressed SNAP-25 WT or mutants in SNAP-25$^{-/-}$ cells. (B) Left panel; analysis of single fusion events of (events/number of cells): GFP-SNAP-25 WT in black (11011/83), GFP-SN25-cys in orange (1419/22), GFP-SN25 shift14aa in olive (2377/22), GFP-SN25 LN G/S in cyan (1986/27), and GFP-SN25 LC G/S in blue (1014/16). Right panel; Bar graphs of spike charge (fC), amplitude (pA), 50-90% rise time of the spike, and half width of the spike. (C) Left panel; cumulative frequency of the pre-spike foot characteristics: initial pre-spike foot amplitude (pA), pre-spike foot amplitude (pA), duration, charge (fC), fluctuation frequency (kHz), and root mean square noise (pA/ms). Right panel; bar graphs showing mean of the medians of cumulative distribution curves of the left panel. n is depicted in bottom panel, statistical comparisons were performed by ANOVA with post-hoc Tukey's test.

1.17 N-terminal motifs in the SN25 linker determine fusion pore evolution

Since the cysteine deficient mutant and the extension mutants were shown to work via two independent mechanisms, we wanted to determine the characteristic features of single fusion events by these mutants. Using 5 µm carbon fibers, we were able to detect single vesicle fusion events. The cells were stimulated with 19 µM free Ca^{2+} to drive the chromaffin cells to secrete efficient number of vesicles to reliably study differences in the mode of fusion pore initiation, vesicle fusion as well as fusion pore expansion.

	Charge (fC)	Amplitude (pA)	Rise time (µs)	Half width (ms)
WT	246.4 ± 9.32	117.04 ± 3.3521	239.5 ± 4.0191	1.3936 ± 0.0385
SN25-cys	236.5 ± 11.84	116.36 ± 7.25	259.5 ± 14.81	1.5144 ± 0.0922
SN25 shift14aa	252.01 ± 16.15	79.38 ± 4.50; P < 0.001	340.0448 ± 21.9334; P < 0.001	2.1033 ± 0.1963; P < 0.001
SN25 LN G/S	246.96 ± 10.6221	76.69 ± 4.81; P < 0.001	340.05 ± 17.13; P < 0.001	2.3392 ± 0.1154; P < 0.001
SN25 LC G/S	241.43 ± 20.14	118.65 ± 8.00	243.2530 ± 15.00	1.3987 ± 0.0971

Table 2 Single spike (fusion) event features from amperometric recordings.

SNAP-25$^{-/-}$ expressing either WT or SNAP-25 mutant proteins. Signal was filtered at 3 KHz and single spikes were analyzed as charge (fC), peak current amplitude (pA), rise time as the time needed for the spike to reach from 50-90% of the maximum spike amplitude, and half width defined as the time needed for the spike between 50% of its initial phase and 50% of its decay phase (all P values are direct comparison to WT via ANOVA using Tukey's post-hoc test).

Interestingly, the SN25-cys mutant showed a prolonged pre-spike foot (PSF) with no further change in the spike properties compared to SNAP-25 WT (for values, look at Table 2 and 3); Figure 33 A. On the other hand, the SN-25 shift14aa showed not only prolonged PSF, but also slower expansion of the fusion pore. This confirms the qualitative difference between the cysteine deficient mutant and the extension mutants.

The SN25 LN G/S showed slowed PSF as well as fusion pore expansion problem (Table 2). SN25 LC G/S in contrast did not show any vesicle fusion defect compared to WT over expressed SNAP-25. Thus, the N-terminal region of the linker located at the C-terminal region of the SNARE complex is crucial for the proper fusion of vesicles. All amperometric measurements were kindly provided by Dr. Madhurima Dhara.

	Prespike (PS) initial Foot Amplitude (pA)	**Prespike (PS) Foot Amplitude (pA)**	**Prespike foot duration**	**Prespike foot charge (fC)**	**Prespike foot fluctuation frequency (kHz)**	**Prespike foot rms noise (pA/ms)**
WT	3.51 ± 0.12	16.01 ± 0.43	4.09 ± 0.18	20.39 ± 1.07	0.38 ± 0.0135	4.40 ± 0.15
SN25-cys	1.65 ± 0.08	15.52 ± 1.73; P < 0.001	9.05 ± 0.41; P < 0.001	45.62 ± 3.61; P < 0.001	0.17 ± 0.012; P < 0.001	2.66 ± 0.12; P < 0.001
SN25 shift14aa	1.88 ± 0.14 P < 0.001	11.39 ± 0.47; P < 0.001	9.64 ± 0.50; P < 0.001	40.83 ± 3.32; P < 0.001	0.1652 ± 0.0251; P < 0.001	2.4782 ± 0.1646; P < 0.001
SN25 LN G/S	1.50 ± 0.12 P < 0.001	11.63 ± 0.71; P < 0.001	9.6719 ± 0.4901; P < 0.001	40.3784 ± 1.8143; P < 0.001	0.1381 ± 0.0160; P < 0.001	2.4399 ± 0.1263; P < 0.001
SN25 LC G/S	3.9169 ± 0.1950	16.5168 ± 1.0225	4.0093 ± 0.3346	21.9677 ± 1.9570	0.4140 ± 0.0229	4.4413 ± 0.2571

Table 3 Pre-spike foot (PSF) characteristics from amperometric recordings.
PSF amplitude, duration, and charge were calculated reflecting the initial fusion pore opening (all P values are direct comparison to WT via ANOVA using Tukey test).

1.18 Hydrogen bonding at the C-terminal linker region stabilizes the fast pool and delays triggering

According to the crystal structure of the SNARE complex, the two amino acids Arg^{136} and Asp^{140} form number of hydrogen bonds that might aid the linker in the formation and stabilization of the loop turn (Sutton et al., 1998). Thus, these two amino acids were substituted by alanine residues in order to destabilize

the loop and test the consequences of such mutation on secretion (Figure 34 A). When these two amino acids were mutated (named SN25 LC RADA), the RRP size was slightly reduced and there was a slight but significant triggering effect (Figure 34 B and C). WT_{RRP} was 156.6 ± 29.5 fF, while SN25 LC $RADA_{RRP}$ was 101 ± 14.4 fF ($P < 0.05$). WT_{TRRP} was 17.2 ± 2.7 ms and SN25 LC $RADA_{TRRP}$ was 14.9 ± 1.3 ms. WT_{SRP} was 108.9 ± 16.9 fF while SN25 LC $RADA_{SRP}$ was 169 ± 22.1 fF. WT_{TSRP} was 154 ± 26.4 ms, while SN25 LC $RADA_{TSRP}$ was 200.3 ± 38.9 ms. WT_{sus} was 32.1 fF/s, and SN25 LC $RADA_{sus}$ was 35.5 fF/s. WT_{delay} was 1.1 ± 0.3 ms, and SN25 LC $RADA_{delay}$ was 2.7 ± 0.4 ms ($P < 0.01$) (Figure 34 C). This indicated that these two amino acids are indeed important to stabilize the pool likely with the help of other neighboring amino acids. To conclude, the C-terminal end probably stabilizes the N-terminal part of the complex in its semi-zippered form allowing for fast and efficient exocytosis upon receiving a stimulus trigger.

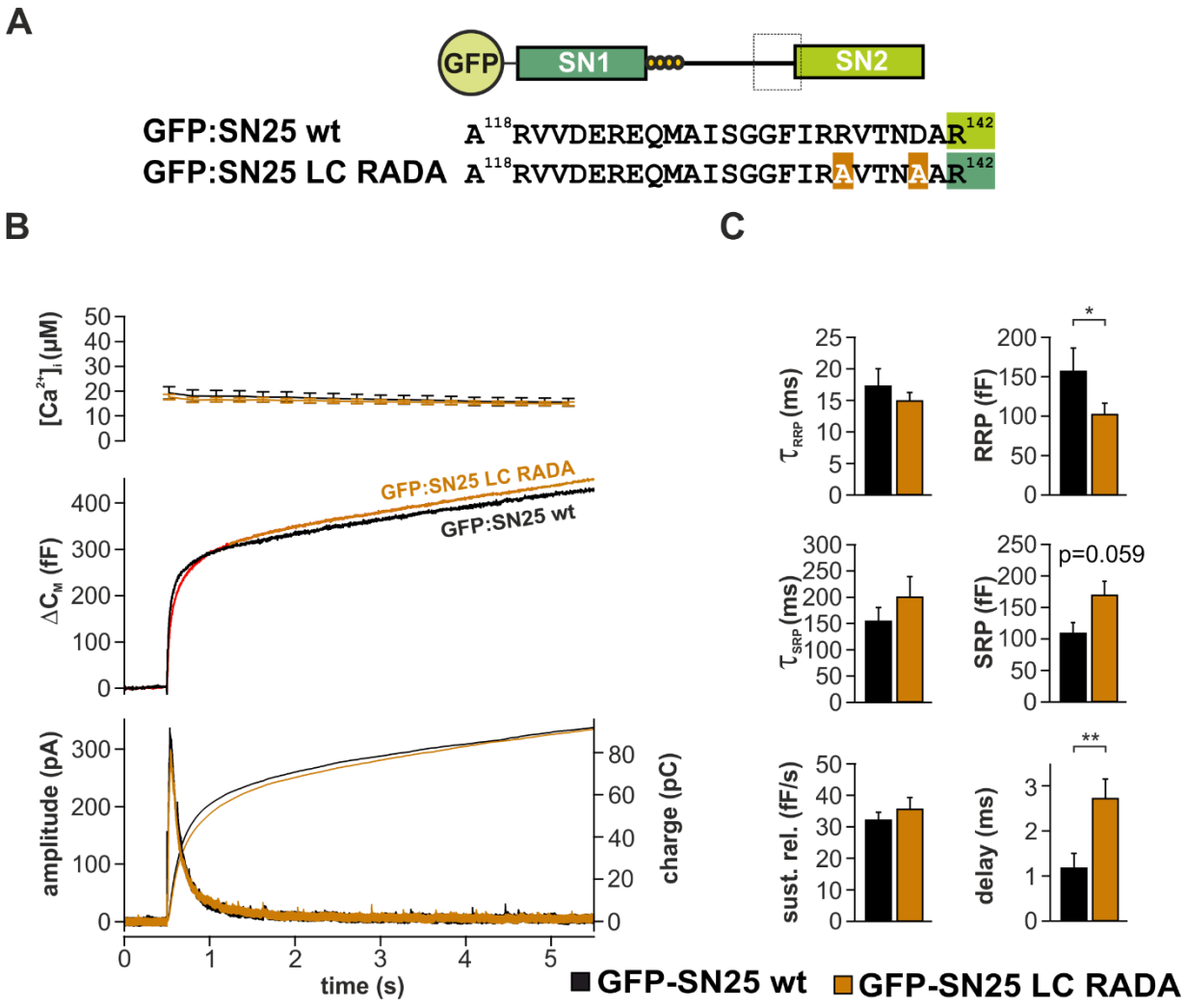

Figure 34 Amino acids at the C-terminal end stabilizes the turning loop of the linker.
(A) Cartoon showing GFP-SNAP-25 WT (black) and GFP-SN25 LC RADA mutant structure. (B) Characterization of secretion in KO cells expressing GFP-SNAP-25 WT or mutant. Shown are averaged $[Ca^{2+}]_i$ measurements (top),

capacitance traces (middle) and amperometric recordings (bottom). (C) Comparative electrophysiological analysis of secretion in GFP-SNAP-25 WT (black) and GFP-SN25 LC RADA expressing KO cells (black). Comparison was performed using Student's t test.

As a final control experiment, expression of all used constructs (except split mutants) was measured using epi-fluorescence microscopy and showed similar expression levels compared to WT SNAP-25 (Figure 35A and B). Thus, the phenotypes depicted were not due to difference in expression levels that might lead to a false phenotype.

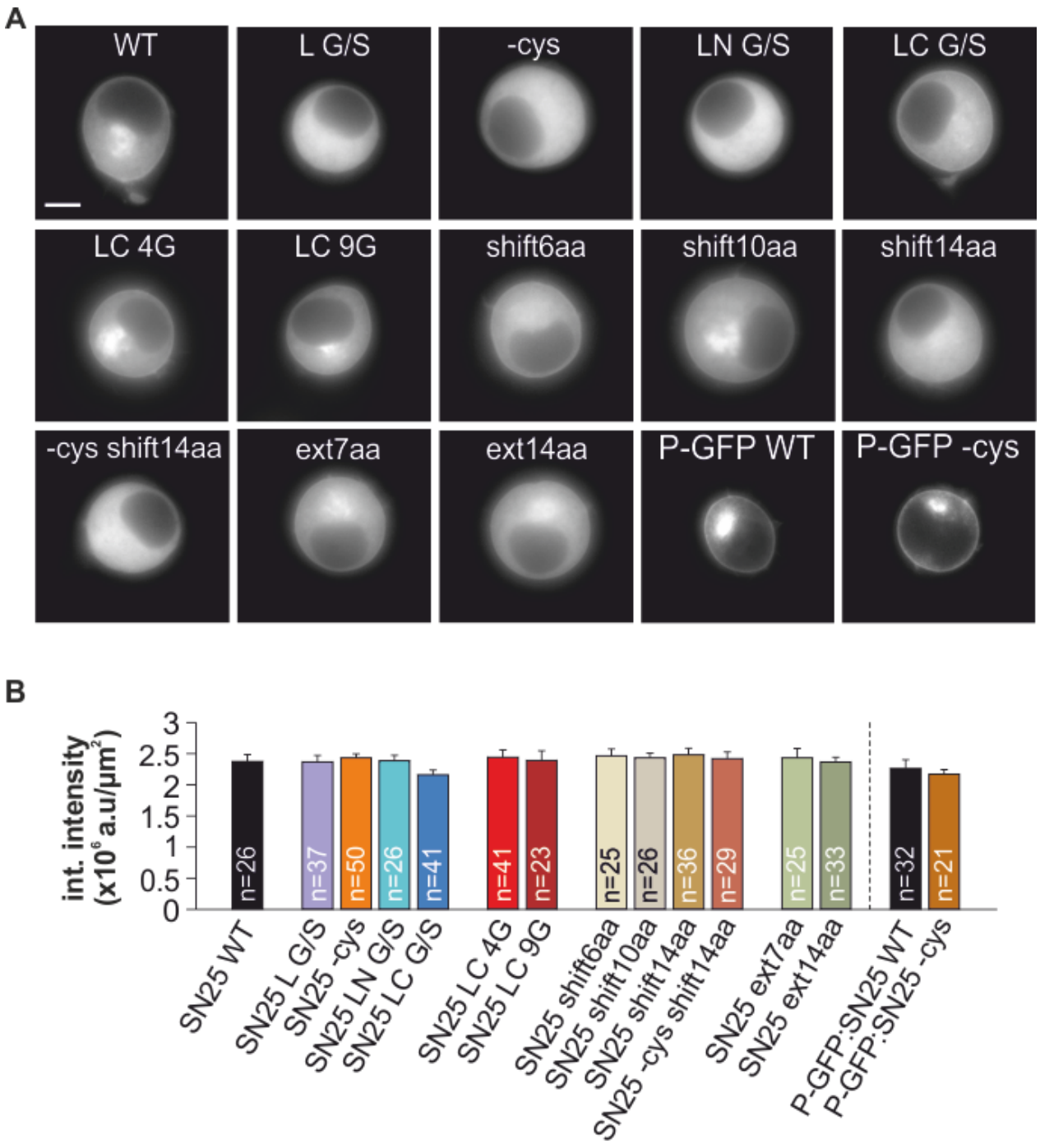

Figure 35 Expression analysis of SNAP-25 linker mutants.
(A) Exemplary epifluorescence pictures of KO cells expressing the characterized GFP-tagged SNAP-25 mutants. Abbreviated mutant labels are used ("GFP" skipped). Scale bar is 5 µm. (B) Mean integrated fluorescence of GFP over the whole cell body is quantified and did not show any significant differences in SNAP-25 expression. Error is SEM. n is indicated in bar graph of panel B. Statistical significance was tested using ANOVA with Tukey test.

Discussion

The fusion machinery of vesicle exocytosis has been extensively studied in neurons as well as neuroendocrine cells. While SNARE motifs and their mechanistic role in Ca^{2+}-regulated exocytosis has been investigated in detail, comparatively little is known about the role of a tandem-like structure of the Q_b/Q_c motifs of SNAP-25. Four main mechanistic points have been addressed here using various electrophysiological and biochemical experiments in order to fully understand the role of linked SNAP-25 SNARE motifs. Firstly, we examined the general importance of SNAP-25 linker integrity and its primary structure in SNARE complex formation and Ca^{2+}-triggering of release. Secondly, we investigated the mechanistic role of different SN25 linker sub-regions and their role in supporting exocytosis. Thirdly, we checked for the role of linker in transducing the force exerted by SNARE motifs to the membranes in promoting fusion. Our last point of interest was to test for linker-mediated lipid interplay crucial for membrane fusion. These four points will be explained in details in the coming sections.

1.19 The SNAP-25 linker is a functional part of the fusion complex

1.19.1 Linker integrity is essential for fast Ca^{2+}-triggered secretion

Unlike exocytosis of SVs and LDCVs, intracellular membrane fusion is driven by SNARE complexes that comprise two separate Q_b and Q_c SNARE proteins instead of a single tandem-like Q_{bc}-SNAREs (Liu and Barlowe, 2002; Weimbs et al., 1998), raising the question whether the linkage of SNARE motifs in Q_{bc}-SNARE represent an adaptation to meet the specific requirements of fast neuronal/neuroendocrine exocytosis. Interestingly, it has previously been questioned whether a physical linkage of Q_b/Q_c SNARE motifs in SNAP-25 is a strict prerequisite of exocytosis (Chen et al., 1999; Wang et al., 2008): Chen et al. (1999) were able to restore norepinephrine release from BoNT/E-treated (cutting the last 26 amino acids at the C-terminal end of the SNAP-25), cracked PC12 cells by infusion of intact SN2 fragment at high concentrations (up to 100 µM). Wang et al. (2008) also observed a reconstitution of secretion when expressing separate (BoNT/E-insensitive) SNAP-25 fragments in permeabilized BoNT/E-treated bovine chromaffin cells. However, this rescue effect succeeded only under certain secretion protocols after an initial rundown of secretion. Challenging the results of these rescue experiments, we co-expressed SNAP-25Δ26 and SN2 fragments in intact live chromaffin cells using SNAP-$25^{-/-}$ background in order to investigate the necessity of the linked SN1/SN2 motifs under tightly controlled conditions. Using single cell capacitance measurements combined with high-resolution amperometric recordings, our experiments not only showed a complete failure of the fragments to rescue exocytosis, but also demonstrated an inhibitory effect on secretion compared to the residual release observed in uninfected SNAP-$25^{-/-}$

chromaffin cells. The lack of any significant rescue might be explained by the formation of SN25Δ26-containing SNARE complexes, which are stable enough to prevent the efficient incorporation of the intact SN2 fragment but cannot support fusion due to disrupted C-terminal assembly (Lu, 2015). While the formation of stable SN25Δ26-containing SNARE complexes has been previously confirmed, the resulting complexes are not SDS resistant (Hayashi et al., 1994; Lu, 2015). Although the SN2 fragment was already expressed at much higher levels than the SNAP-25Δ26 fragment in our experiments, the possibility of a partial restoration at much higher concentrations (in the high micro molar range) of SN2 fragment cannot be fully excluded by our data. It has been also reported that the interaction of SN25Δ26 with Stx is not tight enough to allow for productive interaction with Syb (Wang et al., 2008). The observed inhibitory effect on residual secretion in SNAP-25$^{-/-}$ cells probably reflects a dominant-negative effect of the SN25Δ26 fragment on release mediated by SNAP-23 (SNAP-23), another member of the Q_{bc} SNARE family expressed in chromaffin cells. SN25Δ26 may compete with endogenous SNAP-23 in Stx binding, basically excluding SNAP-23 from binary SNARE interaction due to its high viral expression level. A clear dominant-negative effect of SN25Δ26 has already been shown by Sorensen et al (2006) for the viral overexpression of the fragment in WT chromaffin cells.

In order to avoid the dominant-negative effect of SN25Δ26, we co-expressed a shorter, C-terminally truncated SNAP-25 fragment (SN25ΔC) together with SN2. Expression of this fragment combination resulted in a clear restoration of secretion upon Ca^{2+}-uncaging. Total secretion was, however, strongly reduced when compared to the secretory response in WT SN25-expressing SNAP-25$^{-/-}$ cells. Interestingly, we not only observed a severe priming defect (reflected by complete abolishment of the RRP) but also noticed that secretion kinetics were prominently delayed. This observation indicated that a physical linkage between both SNARE motifs is not obligatory for successful fusion but clearly increases the efficiency and speed of LDCVs exocytosis in adrenal chromaffin cells. In a third rescue paradigm, an even shorter truncated fragment, SN25$^{1\text{-}118}$, was co-expressed together with SN2, and release was tested by capacitance/amperometric recordings upon Ca^{2+}-uncaging. Surprisingly, co-expression of these fragments resulted in a secretory response whose burst component (ΔC_M at 1 s post-flash) was significantly more decreased than in the case of the "SN25ΔC/SN2" experiment. This is a striking observation, as it implies that the C-terminal sections of the linker exert a facilitating effect on SNARE-mediated exocytosis despite their physical detachment from SN2. Interestingly, proteolytic assays on fully assembled SNARE complexes had previously suggested that major sections of the linker are only loosely attached with the helical linker core (Fasshauer et al., 1998a), thus suggesting that detachment of the linker at the C-terminal will likely result in its dislocation. Accordingly, we expected that a dislocated linker will be of little functional consequence in its full form as in SN25ΔC or truncated as in SN25$^{1\text{-}118}$. Our results, however,

show that the linker indeed is playing a role in stabilizing the primed pool, probably via interacting with the core complex. Recent structural analysis by electron microscopy has delivered evidence for a diffuse structure of the C- and N- terminal linker sections of the fully formed complex imaged (White et al., 2018), possibly indicating the existence of functional interaction sites.

Previous reconstitution experiments with SNAP-25 fragments suggested little relevance for linker integrity in SNARE complex function (Chen et al., 1999; Parlati et al., 1999). Some of these controversial findings might be explained by the use of less sensitive experimental techniques in older studies, especially the use of BoNT/E-based reconstitution paradigms and population-based release assays. Unlike our single cell capacitance/amperometric recordings that deliver secretion data based on single cells at high temporal resolution, these assays do not provide detailed results on release kinetics. Moreover, the concentration of infused protein (SN2) used by (Chen et al., 1999) was fairly high (up to 100 µM), which may have masked the lowered efficiency of SN2 to drive fusion in this experimental paradigm. Our rescue experiments were performed via Ca^{2+}-uncaging over a duration of only 5s, during which capacitance and amperometry from single cells were recorded. In contrast, Wang et al. (2008) described the recovery of secretion in permeabilized cells after initial rundown of release, lasting around 30 min. Thus, release observed in these permeabilized cells may have at least in part followed non-canonical pathways, disguising the functional consequences of linker manipulation.

1.19.2 The naïve SN25 linker is required for efficient secretion

Given the absence of a detectable secondary structure (Margittai et al., 2001), the SNAP-25 linker has been frequently considered as a simple flexible connector without functional motifs or interaction sites. To investigate whether its conformational flexibility is the only decisive feature of the linker peptide, we constructed a SNAP-25 mutant, in which the linker was substituted by a flexible "GGS"-peptide of equal length (mutant SN25 L G/S). Intriguingly, SN25 L G/S completely failed to rescue exocytosis in SNAP-$25^{-/-}$ cells (Figure 15 B), when using Ca^{2+}-uncaging to stimulate cells. The SN25 L G/S mutant also showed no rescue in experiments with a prolonged strong stimulus (infusion of 19 µM Ca^{2+} for up to 3 min; Figure 15 D) rendering delayed secretion or weakened stimulus-secretion coupling unlikely. This dramatic effect on secretion stresses the importance of the primary linker sequences and suggests that specific biophysical properties or the presence of specific interaction motifs in the linker are required for proper function of SNAP-25. That said, it may also be argued that a complete substitution of 60 aa could disrupt the function of the adjoining SNARE motifs, thus un-specifically disturbing SNARE complex function. Several lines of argument render such scenario unlikely: firstly, the SN25 L G/S mutant could form SNARE

complexes *in vitro* as shown in (Figure 16 B) indicating the capability of this protein to interact with its SNARE partners. That said, the rate of SNARE complex formation observed with this mutant was significantly slower than WT SNAP-25 protein - possibly partly due to the high glycine content in the introduced linker, which may have altered the relative spontaneous movement and orientation of the two SNAP-25 SNARE motifs during complex initiation. Interestingly, the rate of SNARE complex formation for SN25 L G/S was still much faster than using separated Q_b/Q_c SNARE motifs confirming the necessity of a connected SNAP-25 structure in order to efficiently engage with Stx and Syb. Secondly, the SN25 L G/S mutant showed a dominant negative effect when expressed in WT adrenal chromaffin cells (Figure 15 B, C), inducing slower release and lower secretion amplitude, again confirming the fact that SN25 L G/S mutant still interacts with Syb and Stx and competes with endogenous WT SNAP-25 in complex formation. Finally, progressively larger substitution in the SNAP-25 linker produced correlated specific changes in release properties, suggesting that the severe phenotype of SN25 L G/S represents the endpoint of an incremental loss of functional linker motifs.

A proper membrane localization of SNAP-25 is ensured by N-terminal linker acylation (Gonzalo and Linder, 1998; Greaves et al., 2010b; Hess et al., 1992). Since linker substitution in SN25 L G/S also eliminated the acylated cycteine cluster in the linker, the mutant protein is mislocalized when expressed in SNAP-25$^{-/-}$ cells (Figure 35). However, the lack of membrane expression of SN25 L G/S cannot fully explain its dysfunctional nature, as an acylation-deficient mutant, in which only the 4 cysteine amino acids were substituted by serines (SN25-cys) could drive considerable secretion despite improper localization (Figure 18; Figure 35). While SN25-cys mutant showed slower release and decreased amplitude in the RRP indicating reduced fusion rate and primed pool size in comparison to WT SNAP-25 protein, around 70% of the total secretion could be elicited by the SN25-cys compared to WT protein. Thus, the dysfunctional nature of the SN25 L G/S is not due to simple protein mislocalization.

Partial N- or C-terminal substitutions within the linker also severely affected release properties, resulting in a dramatically diminished secretory response. Intriguingly, replacement of non-overlapping sequences in both regions caused a similar complex secretion phenotype (Figure 18 B; Figure 19 B), that is characterized by a pronounced loss of primed vesicle pools and a general slow-down of release. Noteworthy, also the general onset of release was delayed in both mutants, indicating that triggering of release and general stimulus secretion coupling were affected in both linker mutants.

The N-terminal substitution “SN25 LN G/S” showed an augmented phenotype compared to the cysteine deficient mutant (Figure 18 B). The RRP component was completely lost and the SRP was significantly delayed together with a delay in the stimulation-secretion coupling, such a complex phenotype showed that the fusion process is being altered through numerous mechanistic levels. From the electrophysiological data,

we can speculate that this mutant showed an altered priming rate as well as defects in stabilizing the primed pool, and finally fusion triggering. It comes to attention that the SN25 LN G/S mutant lacks the cysteine residues which resulted in a priming/triggering defect, but also they lack important residues that indeed affect both fusion pore initiation and expansion (Figure 33). The fact that N-terminal end of the linker is in very close proximity to the fusion pore according to our proposed model (Figure 36) could serve as a possible explanation. Therefore, we believe that the N-terminal linker domain negatively affected exocytosis at different mechanistic aspects including stability of the primed pool, fusion triggering, and fusion pore initiation and expansion.

On the other hand, the C terminal end substitution of the linker had no influence on either fusion pore expansion or initiation. However, this C terminal substitution led to reduced interaction with Stx-1A which resulted in a reduced amount of acceptor complex formation (Figure 21). This diminished interaction could lead to a pool defect as the acceptor complex formation is the primary step for the full complex formation and subsequent vesicle priming (Fasshauer and Margittai, 2004; Pobbati et al., 2006). Moreover, the C-terminal substitution comprises a sensitive stretch ^{119}VVDEREQMAI^{128} that has been showed by Nagy et al. (2008) to have a regulatory role in exocytosis.

The N-terminal end is engaged with the C-terminal end of the complex, support fusion triggering, possibly interacting with the membrane phospholipids supporting the fusion pore initiation and expansion. The C-terminal end on the other hand is placed near the N-terminal end of the SNARE complex, supporting acceptor complex formation with Stx and possibly preventing excess depriming. Therefore, we speculate that the similar phenotypes mediated by SN25 LN G/S or SN25 LC G/S arose from two mechanistically different steps. As both motifs of the linker are connected, they can act interdependently. For example, a dislocated N-terminal region, due to lack of palmitoylation, could spatially distort the whole linker region and subsequently induce functional disability. The same applies to the C-terminal region, which could possibly lead to a very similar effect on the functional level. This idea is supported by recent work showing for the first time that the SNAP-25 linker is present in a diffuse density that is strongest at the stretches near SN1 and SN2 motifs and weakest in the middle of the linker (White et al., 2018). Moreover, the C-terminal end of the linker was shown to stabilize the entire SNARE complex formation (Jiang et al., 2019).

1.20 Linker motifs support binary and ternary SNARE interactions

1.20.1 The SN25 linker as an organizer of SNARE assembly?

Experiments with substitution mutants indicated a mechanistic requirement for the naïve amino acid sequence of the SNAP-25 linker. The complex secretion phenotypes of the corresponding SNAP-25 mutants may highlight priming and triggering deficits due to altered SNARE assembly. Indeed, we have demonstrated in this work that purified SN25 L G/S protein exhibited a delayed formation of SNARE complexed, when mixed with its binding partners (Figure 16). Obviously, these kinetic alterations may reflect [1] hindered complex nucleation and/or a [2] decelerated folding of the core complex due to diminished external interactions with the linker. Our data on SNAP-25: Stx-1A interactions in combination with the results of SNARE complex formation experiments using partial linker substitution mutants suggest contributions of both mechanistic effects.

1.20.2 The linker facilitates SN2 association with Stx H3:SN1 assemblies

Initial studies on SNARE interactions showed that the SNARE motifs of the cognate SNARE proteins spontaneously adopt α-helical conformation and interact with each other, when mixed in different combinations (Fasshauer et al., 1998a). That said, SNAP-25 in isolation exhibits low helicity, with its SN1 motif possibly possessing the highest propensity to assume a helical conformation (Chapman et al., 1994; Fasshauer and Margittai, 2004). Interestingly, it has been demonstrated that truncated SNAP-25 fragments containing the full SN1 motif bind to and are retained on immobilized Stx-1A, while SN2 seems uninvolved in Stx-1A interactions (Chapman et al., 1994). To investigate the role of the linker in t-SNARE interactions, we tested SNAP-25 fragments with or without linker in binding assays with Stx-1A. Intriguingly, we found that only SN1 showed any retention, when a mixture of linker-less SN1 and SN2 fragments was incubated with immobilized Stx-1A. However, our further experiments demonstrated that SN2 was retained with SN1 on Stx-1A, when the linker was left attached to the SN2 fragment (Figure 17). As a continuous SN1-linker fragment and separated SN2 did not allow for significant SN2 retention in the reverse setup, we consider the continuous linker-SN2 fragment as a functional unit that promotes the recruitment of SN2 into t-SNARE assemblies. Given the low helical character of SN2 in solution (Fasshauer and Margittai, 2004), it might be speculated that the linker supports the SN2 motif to assume a suitable helical conformation for interactions with SN1:Stx1A H3. The C-terminal linker segment might be of particular relevance for the stabilizing interactions, as substitution of the linker region in SN25 LC G/S impacted the efficiency of Stx-1A binding. In line with this idea, Jiang et al. (2019) showed that the C-terminal end of the linker interacts with Stx in membrane environments via electrostatic interactions to stabilize the acceptor (binary) complex formation.

In seminal work of Weninger et al. (2008), the conformational dynamics of a binary t-SNARE complex has been investigated using single molecule FRET experiments. Interestingly, they demonstrated that binary t-SNARE complexes dynamically transit through different conformational states, in which only SN1, both SNAP-25 SNARE motifs, or SN2 interact with the Stx-H3 SNARE motif. Syb binding stabilizes the assembly, in line with the idea that t-SNARE complexes serve as acceptors for Syb and thus mediate complex nucleation. Given the dynamic properties of the binary t-SNARE complex, the linker should putatively serve two supporting functions according to our results: [1] Concatenation via the linker should retain SNAP-25 SNARE motifs in a critical distance to bihelical complexes after spontaneous dissociation, therefore facilitating (re-)entry of the free motif and (re-)formation of the trihelical state. Some of the release deficits observed in reconstitutions experiments with unlinked SNAP-25 fragments might be explained by unstable acceptor complexes due to the loss of this function. [2] Interactions of the C-terminal linker motif facilitate the recruitment of SN2 onto the relatively stable SN1:Stx H3 assembly, thus shifting dynamics to the trihelical conformation. A hindered entry of SN2 into the assembly would likely decrease complex lifetime and prevent productive Syb interactions in SN25 L G/S and SN25 LC G/S, respectively. Our results on linker-mediated assembly of binary complexes are therefore of functional significance for successful vesicle priming.

1.20.3 Altered core complex dimerization in linker mutants

SNARE complexes formed by separate SN1/SN2 fragments, SN25 L G/S or SN25 LN G/S exhibit a higher apparent molecular weight than those containing SNAP-25 WT (Figure 16 A-C), which may indicate that the loss of N-terminal linker motifs affects biochemical properties and/or composition of complexes. Interestingly, it has been previously demonstrated by Fdez et al. (2008) that SNARE complexes containing linker-less SN1 and SN2 fragments have a high propensity to form wing-shaped dimers, in which two fully formed complexes interact with each other via their C-terminal ends, possibly also involving residues of the juxta-membrane domain of Syb-2 in the binding interface. Given that we observed a characteristic size shift of SNARE complexes formed by the very same combination of fragments, it stands to reason that the linker-less core complex in our experiments also forms SDS-resistant SNARE dimers. Noteworthy, the presence of the N-terminal linker motif prevents the apparent increase in molecular weight, implying that this linker segment masks surfaces that are required for dimerization.

Fdez et al. (2008), identified two tryptophan residues (W^{89}, W^{90}) and an arginine residue (R^{86}) in the juxta-membrane domain of Syb-2 as essential for the observed dimerization activity. Since mutation of these residues decreased the rescue of human growth hormone release in a BoNT/E reconstitution experiment, the authors proposed that SNARE complex dimerization via these residues is functionally important for exocytosis. Following this sentiment, however, it is incomprehensible, why the disinhibited dimerization in

SN25 LN G/S would then result in strong release deficits. Therefore, it seems more likely that the SNARE dimers observed by Fdez et al. (2008) do not serve as a productive intermediate *en route* to membrane fusion. Rather, compromised exocytosis in Syb-2 variants with mutated juxta-membrane domains should reflect other mechanistic defects. Intriguingly, Borisovska et al. (2012) indeed delivered an alternative explanation for the phenotype by showing in molecular dynamic simulations that the two tryptophan residues in Syb-2 affect the electrostatic surface potential by determining the orientation of neighboring charged amino acids (lysine and arginine) at the membrane water interface. Moreover, they demonstrated a characteristic priming defect for Syb-2 mutants, in which both tryptophan residues were mutated.

It might be speculated that the observed dimerization of SNAP-25 linker mutants *in vitro* could itself impose an obstacle to the fusion process. As the two tryptophan residues, which have been considered essential for dimerization, likely engage in membrane interactions under physiological conditions (Borisovska et al., 2012), it is however doubtful whether dimer formation actually occurs *in vivo*. Moreover, if aberrant dimerization would be responsible for compromised secretion in SN25 LN G/S-expressing KO cells, it would be expected that exocytosis mediated by SN25 LC G/S-containing complexes with "normal" dimerization propensity should be largely unaffected. The similarity of the phenotypical features of both linker substitution mutants however suggest that other mechanistic reasons cause the low secretion rates and reduced primed pool size in these mutants.

1.21 The role of acylated linker segment in exocytosis

1.21.1 Intramolecular acylation is crucial for efficient Ca^{2+}-dependent exocytosis

Substituting the cysteine residues with serine residues led to loss of membrane localization together with a triggering deficit upon stimulation, a phenotype that was previously observed by Nagy et al. (2008). Other reports, however, found a different effect upon cysteine abolition. For example, SNAP-25 mutants lacking cysteine residues were unable to support release in PC12 cells (Washbourne et al., 2001). Washbourne and colleagues co-transfected the PC12 cells with human growth hormone construct together with BoNT/E resistant mutant of SNAP-25. PC12 were then treated with BoNT/E and assayed as a population for the release of the growth hormone. The observed result could be due to low concentration of the co-expressed SNAP-25 BoNT/E resistant mutant. As this neurotoxin mutant when combined with cysteine-negative mutant did not yield release in neither BoNT/E treated PC12 cells nor showed any dominant-negative effect in non-treated cells. This questions the general effect of the expressed protein. In another experimental paradigm, the cysteine-deficient mutant showed partial rescue of exocytosis (Nagy et al., 2008). This experiment was performed in pancreatic beta-cells and the results were again based on a

population assay after permeabilization of cells and rushing in Ca^{2+} for 8 min. Therefore, we provided with our single cell based measurements more accurate and direct correlation of stimulation and secretion. This discrepancy in the literature stimulated us to investigate to which degree does the mislocalization of the cysteine-deficient mutant leads to the observed phenotype. Interestingly, addition of an extra acylation sequence led to the proper localization of either the SNAP-25 WT or the cysteine-negative proteins (Figure 26 B). The retargeting of the SN25-cys mutant with an extra acylation sequence (DP-SN25-cys; Figure 27) did not rescue the phenotype of the substituted cysteine moieties. This is a direct evidence that the four cysteine residues are not just of anchoring purpose but indeed play a role in modulation of exocytosis.

As the retargeting experiment confirmed that the cysteine moieties function beyond just membrane targeting of the SN25, we wondered about a special mechanistic role in triggering vesicle fusion. Looking at different SN25 orthologs, the palmitolytion motif is located directly after the Q_b motif. In fact, the first cysteine residue is separated from the end of the Q_b SNARE motif by just one lysine amino acid. This lysine residue was shown to interact with the phospholipid bilayer of the cell membrane (Weber et al., 2017). Thus, this structure could position the linker at the interface between the Q_b/Q_c SNARE motifs and the membrane, facilitating the transfer of the force produced by the SNARE motifs to the membrane, and finally aiding in fast release.

To test this postulation, we inserted linker extensions between SN1 and the linker in order to mechanically "uncouple" the linker membrane anchors from the core complex, thus interfering with a potential molecular straining of the plasma membrane via linker membrane contacts. As insertions at the juxta-membrane domain of either Stx (Wang et al., 2001) or Syb (Kesavan et al., 2007) resulted in diminished vesicle exocytosis, we expected a similar phenotype when inserting similar sizes of insertions between SN1 and the linker domain. Surprisingly, inserting 6, 10, or 14 amino acids showed also a mild triggering phenotype with decelerated release rates, but with no effect on the total pool sizes. These insertion mutants phenotypes were clearly distinctive from the cysteine-negative mutant (compare Figure 18 to Figure 28) raising more doubts about the initial idea of force transduction.

To pinpoint the role of the acylated linker in force transduction, we combined the palmitoylation deficient mutant (SN25-cys) with the extension mutant producing a new mutant lacking the cysteine residues with a linker extension of 14 amino acids between the SN1 and the linker. This double mutation, SN25-cys shift14aa, was compared against the SN25-cys mutant (Figure 29). The SN25-cys shift14aa mutation showed an exacerbated phenotype with slower release rates and decreased pool compared to the SN25-cys mutation. As the linker acyl anchors act as the main pivot by which the SNAP-25 protein is attached to the membrane, the loss of this pivot in the cysteine-negative mutant should have ruled out the upstream effect of any linker insertion. Therefore, with this augmented phenotype, we can conclude that spacer insertions

negatively affects the facilitatory role of the N-terminal end of the linker in exocytosis in a palmitoylation independent fashion. It could be speculated that the N-terminal insertions render the whole linker out of register with its possible interaction partners, showing the mild triggering effect. The juxta-membrane domains of either syx or syb are possibly positioned during fusion at close proximity to the SN25 linker N-terminal region, as it is believed that the SNARE complex continues zippering through the juxta-membrane domain (Stein et al., 2009). Therefore, the Stx/Syb juxta-membrane domains could be possible interaction partners with the N-terminal domain of the linker.

To follow up the facilitatory role of the N-terminal domain of the linker, we checked for the possible contribution to release by the lysine moieties positioned around the cysteine cluster. These basic lysine residues are interesting as they can interact with acidic lipids in the membrane (Weber et al., 2017). In agreement to the previous experiment, a mutant lacking the cysteines and surrounding lysines, SN25-cys 5K/A, showed a slower release rate and more delayed response when compared to the cysteine-deficient mutant (Figure 30). Thus, the positively charged amino acids at the vicinity of the fusion pore supports fast release in the absence of any palmitoylated protein. Therefore, the position of the linker i.e. having the linker in very close proximity to the end of the SN1 together with the amino acids present at this N-terminal end of the linker, ensures efficient secretion. These experiments hint to the fact that force transduced from the SN1 towards the linker region plays a small role. This suggests another scenario by which the cysteine and lysine residues in the palmitoylation motif form collectively a protein-lipid interface that is crucial to ensure proper interaction with the membrane, keeping the core complex in register, and stabilizing the partially assembled complex to ensure proper fusion with no delay upon stimulation.

Recently, the cysteine residues was shown to exert a direct effect on SNARE complex formation as substituting either two or the whole four residues resulted in inhibition of the SNARE complex assembly (Jiang et al., 2019). This inhibition could be related to the priming and triggering defects that we observed by the cysteine-negative mutant. Moreover, we showed that retargeting the whole SNAP-25 protein with an extra acylation sequence did not rescue the pool. In addition, we investigated the role of the lysine amino acids and their role in exocytosis. The lysine residues also supported last stages of fusion pore expansion (Shaaban et al., 2019). Our observation is supported by the work of Weber et al. (2017) confirmed that the lysines with their basic nature could bind to acidic PIPs, even enhancing the palmitoylation of SNAP-25 on the membranes. This shows the interdependence of the charged lysine amino acids and the neighboring cysteine cluster. As the lysine amino acids increase the dwell time on the membrane, this could allow for the SNAP-25 cysteine residues to become properly palmitoylated. Therefore, the stretch of the linker flanking its N-terminal end comprising of cysteine and neighboring lysine residues are working hand in hand to ensure proper [1] SNARE complex assembly, [2] protein-lipid interaction and [3] maintenance of

the whole complex in the proper arrangement needed for efficient delivery of the free energy produced by the SNARE motifs.

1.22 The role of C-terminal linker segment in exocytosis

The N-terminal stretch of the linker had a significant contribution in supporting SNARE complex assembly as well as the release magnitude and kinetics. The more amino acids substituted at the N-terminal side of the linker, the more severe deficits observed until reaching complete abolishment of the RRP together with triggering defect and fusion pore deficits upon complete N-terminal linker exchange. The N- and C- terminal substitutions of the linker showed very similar phenotypes in response to Ca^{2+}-uncaging. Thus, we wanted to perform a structure function analysis to further dissect the mechanisms and amino acids that support secretion at the linker C-terminus. Looking into the details of the C-terminal region (amino acids$^{119\text{-}141}$) of the linker, we started with substitution of four residues (F^{133}, I^{134}, V^{137}, A^{141}; denoted "SN25 LC 4G") that had been suggested to interact with the core SNARE complex through their non-polar side chain (Figure 31). The SN25 LC 4G mutant showed mainly diminished RRP pool with a slight change in the kinetics of release. This hints that these hydrophobic interactions are necessary to stabilize the RRP pool, preventing vesicle depriming. As zippering of SNARE proteins is believed to happen from N- to C- terminal ends of the core complex, this positions the C-terminal end of the linker at the N-terminal side of the complex and thereby having a direct effect on the first phase of priming/depriming stages.

Mutating the entire last 9 amino acids stretch with glycines, SN25 LC 9G, (Figure 32) exacerbated the deficits causing lower RRP and much slower kinetics of the release with a noticeable delay. In the SN25 LC 9G mutant, Argenine (R)^{135}, R^{136} Threonine (T)^{138}, Asparagine (N)^{139}, and Aspartate (D)^{140} were additionally mutated compared to SN25 LC 4G. R^{135} and R^{136} were mutated in a recent study to aspartate in order to reverse their charge from positive to negative. Flipping the charge of the argenine residues ($R^{1358}A/R^{136}A$) yielded a protein less capable of engaging with Stx to form acceptor complexes, and even less efficient to form SNARE complexes compared to WT protein (Jiang et al., 2019). The same phenotype was observed when the polar uncharged T^{138} was mutated to the nonpolar negatively charged aspartate. The mechanism postulated is this threonine undergoes phosphorylation which in turn affects the electrostatic interaction with Stx. This eventually affects the SNARE complex assembly. Although the C-terminal mutations should have an effect on the stability of the primed vesicle pool, it was surprising that a triggering phenotype was also observed in our SN25 LC 9G mutant as this end of the linker is relatively far from the fusion pore and the C-terminal end of the core complex. Therefore, it is apparent that the tight connection between the C-terminus of the linker and the SN2 motif is crucial to enable the multiple mechanistic

functions (i.e. priming and triggering) performed by this linker loop. Mutating only one arginine (R^{136}) of the two together with the D^{140}, both to alanine, decreased the readily releasable pool and produced a delayed phenotype which again pinpoints the necessity of such polar amino acids for SNAP-25 to properly interact with its SNARE partners. It would be interesting to further investigate the engagement of this mutant with syx to form acceptor complexes and in full SNARE complex assembly. Exchanging the whole C-terminal part of the linker produced a compound phenotype as the SN25 LC G/S even lacks important sequence ^{119}VVDEREQMAI^{128} that is needed for proper exocytosis (Nagy et al., 2008).

1.23 Does the acylated linker region serve as a membrane interface that controls fusion pore evolution?

Using amperometric recordings, we were able to gain more information about a potential contribution of the SN25 linker in fusion pore opening and expansion. We checked the impact of either the N- or C- terminal end of the linker on the fusion pore. In Ca^{2+}-uncaging experiments, the phenotypes of SN25 LN G/S and SN25 LC G/S. Interestingly, via studying single fusion events, we observed different impact from SN25 LN G/S and SN25 LC G/S mutants. The N- terminal linker substitution had delayed discharge kinetics of neurotransmitters, while the C- terminal linker substitution had, surprisingly, no impact on the kinetics of single fused vesicles. This suggests that the N-terminal part exerts its impact on the fusion pore characteristics through its interactions with membrane components.

The effect of the linker on the fusion pore was incremental. Amperometric spikes elicited via infusion of 19 µM Ca^{2+} through the patch pipette were studied. The initial PSF duration was increased in the case of the cysteine deficient mutant. The change observed in the PSF properties elicited by the cysteine deficient mutant could be attributed to the ability of the cysteine moieties to interact with the lipid bilayer, and possibly modifying local membrane properties. Previous studies were able to accelerate or decelerate the PSF duration by using membrane perturbing agents such as lysophosphatidylcholine (LPC) or arachidonic acid (AA). When applying LPC and AA exogenously on to chromaffin cells, they observed faster feet in case of LPC and slower in case of AA without affecting the overall frequency of observed spike with feet. This affect was attributed to the modified membrane curvature induced by those introduced fatty acids (Amatore et al., 2007). The main spike characteristics were affected when the whole N- terminal linker region was rendered out of position using the 14 amino acids shift mutant in addition to the delayed kinetics of the PSF (Figure 33). In this case, the kinetics of transmitter discharge were significantly slowed down. This slowdown indicates that the dilatation of the fusion pore was delayed. The same effect was observed when the N-terminal stretch was completely substituted with a flexible GGS peptide with the SN25 LN G/S

mutant. Therefore, we can observe from the data two mechanistically different effects: [1] the effect on the nascent fusion pore and the local lipid properties, reflected in the PSF, and the cysteine residues playing role in that especially as they are situated very close to the contact point between the vesicle and the plasma membrane; [2] the effect mediated by the entire structure of the N-terminal part of the linker as it directly affects the fusion pore expansion itself in addition to the initial PSF. The effect on the fusion pore could be related to a different scenario by which the protein-protein interaction is affected.

One scenario could be the N-terminal linker region of SNAP-25 is actively interacting with the JMD domains of either syx or syb. Alternatively, the N-terminal linker stretch could have some interaction with accessory proteins such as synaptotagmin and/or complexin known for having some effect on the fusion pore expansion (Dhara et al., 2014). Lysine residues surrounding the cysteine amino acids at the N-terminus of the linker are probably responsible for this additional impact on the main spike; the lysine residues could be of greatest impact due to their charged nature as well as the proximity from the fusion pore (Figure 36). Mutation of lysine amino acids in the JMD region of syb caused a marked reduction in release upon Ca^{2+}-uncaging, thus having a great impact in stabilizing the primed pool of vesicles in chromaffin cells (Borisovska et al., 2012). Therefore, we assume that the lysine residues residing in the SN25 linker at the fusion pore are indeed of importance in supporting protein-lipid interaction and subsequently fusion pore expansion.

Our experiments revealed that not only the primary structure of the linker is needed, but also the close contact of the N-terminus of the SN25 linker to the SN1 (and the fusion pore at the C-terminal end of the complex). The SN25 shift 14 aa mutant put the linker in a disadvantageous position where the N-terminus cannot be in the vicinity of the fusion pore anymore. This deregistered position yielded severe deficits in the single spike properties as mentioned before. The deficits were surprisingly as severe as exchanging the entire N-terminal linker sequence with a flexible peptide confirming the need of the whole stretch to support fast fusion of vesicles in chromaffin cells. In addition, the C-terminal linker exchange with a flexible peptide did not yield any changes in either the PSF or the spike characterizes. In the case of late stages of fusion, the C-terminal part of the linker is facing the half-zippered SNARE complex (Jahn and Fasshauer, 2012) and therefore might not have any contribution in mediating fusion. The N-terminal end of the linker is, however, positioned at the neck of the fusion where proper protein-lipid interaction is crucial in order to ensure fast opening and expansion of the pore. Our data provides new evidence of the SN25 linker contribution to the late stages of fusion through a protein:membrane interface formed mainly through its N-terminal end.

1.24 Effects of conformational tension within the SN25 linker

The crystal structure of fully assembled core SNARE complex showed that its coiled-coil structure extends for a total length of 12 nm (Sutton et al., 1998), with the linker putatively stretching out along the length of the complex. While linker length is considered to be sufficient to just cover this distance, there have been speculations that crosslinking of cysteine residues in the palmitoylation site due to oxidative stress could hinder normal assembly (Bock et al., 2010; Foley et al., 2012). Given the considerations that min changes in linker length could affect SNARE complex structure, we wondered whether conformational tension in the linker may play a role in stabilizing the primed intermediate before the Ca^{2+}-trigger induces membrane merger. However, addition of a flexible peptide of either 7aa or 14aa length in the middle of the linker did not show any triggering or pool deficits and was rather well tolerated by the overall linker structure.

The SN25 linker was extended by either 7 or 14 amino acid peptide after $A^{118.}$ The extension left the whole N-terminal part of the linker (needed by DHHC acyl-transferase enzymes) intact and could be subsequently efficiently targeted to the membrane. The first 7 amino acids added were of similar sequence to that extra amino acids in the linker of SNAP-23, while the other 7 amino acids were the "GGS" flexible peptide sequence as denoted in (Figure 22 A, Figure 23 A; respectively). Surprisingly, the release kinetics from both mutants were similar to that of WT (Figure 22 B, C; Figure 23 B, C). Therefore, we conclude that the overall length of the linker is not a major factor in performing its function. In fact, it seems that the SN25 linker can perform its function fully when the N-terminal motif is directly attached to the SN1 and the C-terminal motif attached to the SN2, independent of the inserted peptides.

This left us with another interesting phenotype elicited by the SN25 -4AA mutant, where four non-conserved amino acids from the SN25 linker were deleted producing a shorter linker. We observed a boost (almost doubled) effect for the slowly releasable pool of the SN25 -4AA mutant compared to WT SNAP-25. Looking into the states of SNAREs assembly, Gao et al. (2012) showed that there are three distinct states of SNAREs zippering using optical tweezers. A metastable state was described as the "half-zippered" conformation where the N-terminal domain of the SNAREs is zippered and the remaining C-terminal domain free. This conformation stabilizes the ready-releasable pool of neurotransmitter filled vesicles (Walter et al., 2010). Given already the very short distance that the whole complex occupies (12 nm), we would speculate that the SN25 -4AA mutant shifts the equilibrium of the whole complex into a half-zippered and more ready to fuse state at which less force is needed to overcome the energy barrier of vesicle fusion. Probably in the case of chromaffin cells lacking specialized active zones, the SRP would be more affected

in this case as the RRP would be more sensitive to Ca^{2+} concentrations and proximity of the vesicles to the neighboring Ca^{2+} channels.

Another postulation is that shortening of the linker could produce a more rigid structure with less ability to move. Subsequently, spontaneous fusion of vesicles could be hampered by having a more thermostable SNARE complex that is not fusogenic under submicromolar calcium concentrations which is the case in unstimulated cells. In syb mutants with two highly conserved tryptophan residues substituted in the juxta-membrane domain, diminished secretion was observed in chromaffin cells and was attributed to the high degree of flexibility between the SNARE motif and TMD of syb. However, the calcium sensitivity was unchanged compared to WT syb weakening this clamping/unclamping theory. An interesting experiment in that sense would be to check the clamping potency of SN25 -4AA mutant at different submicromolar Ca^{2+} concentrations to assess a possible clamping effect. The clamping effect would lead eventually to more accumulation of vesicles that could be in turn released upon Ca^{2+}-uncaging eliciting the boosted phenotype. Another possible scheme would be the ability of the SNAP-25 to modulate the process of "priming/depriming" through the post-translational modification, in this case phosphorylation. Nagy et al. (2004) showed that SNAP-25 phosphorylation by protein kinase A (PKA) reduces the depriming rate from the unprimed pool to the SRP/RRP. Despite that phosphorylation occurs at threonine T^{138} in the C-terminal linker region, it cannot be excluded that such shortening in the overall length of the linker could render the whole linker in a configuration that is more prone to phosphorylation by PKA.

To conclude, we showed here that the linker could enhance the exocytotic burst, 0-0.5 s after the Ca^{2+}-uncaging trigger, by shortening the linker either by clamping the release at resting stage leading to higher pool build up and release upon triggering, or via stabilizing an intermediate state of half-zippered SNARE complex that is less energy demanding to fuse vesicles. Either way, this is the first shortening experiment to the linker yielding this augmented effect. Studying the ultrastructure of the LDCVs in chromaffin cells or SVs in neurons expressing this mutant protein would be helpful in giving more insights about the distribution of the vesicles and their proximity from their release sites.

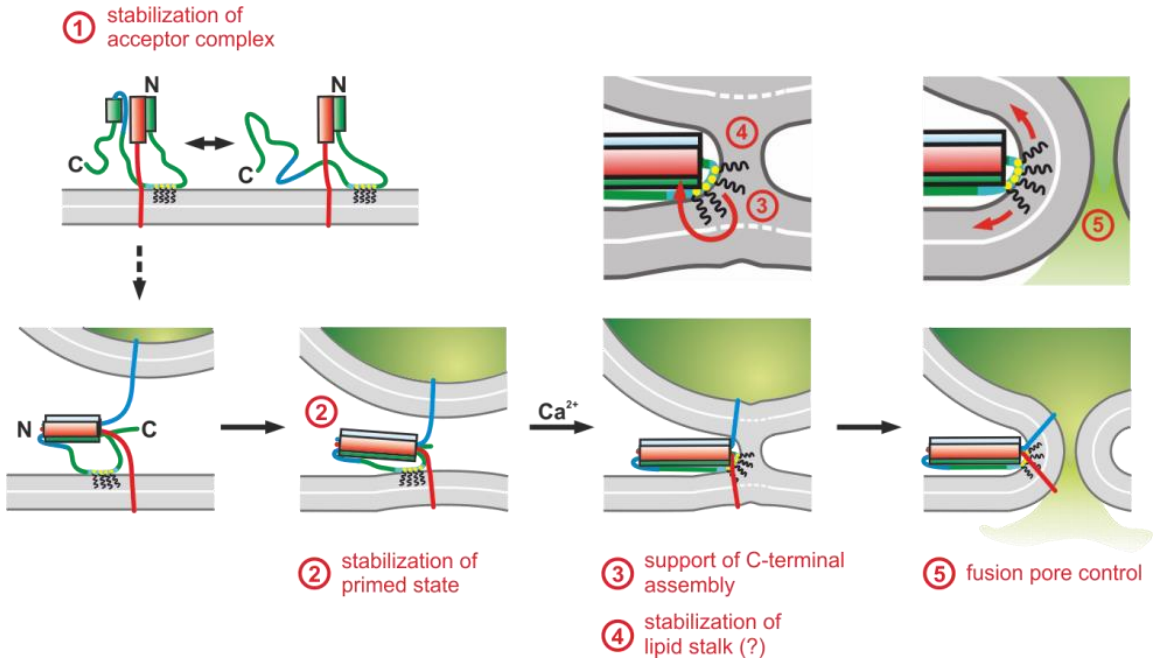

Figure 36 Mechanistic model of SNAP-25 linker function in exocytosis.
The cartoon summarizes putative mechanistic functions of the SN25 linker in acceptor complex formation (1), stabilization of the primed pool (2), fusion triggering (3,4), and fusion pore expansion (5). Syb-2 is shown in blue, Stx-1A in red, and SNAP-25 in green. The acylated N-terminal linker segment is indicated by the cyan region; the blue section represents the back-folding C-terminal loop of SNAP-25. Helical segments are shown as boxes. Yellow circles indicate cysteine residues that were modified by acylation (black wavy lines). For clarity, only the SNARE motif of Syb-2 and Stx-1A are shown in the magnified views.

Conclusion and perspectives

In summary, our data show a completely new view about the mechanistic role of the SN25 linker, delineating its functional relevance in multiple steps of the fusion mechanism. N- and C- linker mutations showed severe secretion phenotypes, confirming that the linker is involved in different stages of exocytosis such as priming, primed pool stabilization, and fusion triggering. Mechanistically, our experiments hint that the full linker acts as regulator to the full SNARE complex assembly with the C-terminal linker region stabilizing the t-SNARE complexes and thereby may serve as a supporting element anchoring the linker to the N-terminal end of the SNARE complex. On the other hand, the N-terminal end of the linker modulates fusion triggering step as well as maintaining the primed fusion intermediates and subsequently control the zippering of the C-terminus of the SNARE complex and fusion pore expansion. The linker, however, is not involved in force transduction. To sum up, the multi-level facilitatory functions of the SN25 linker support the operation of the exocytotic machinery, enabling it to meet the speed and accuracy requirements of neuronal as well as neuroendocrine secretion.

Appendix for all statistical analysis of the presented data.

Figure 11 D										
ΔCM (5s)	Label	Mean (F)	SD (F)	SEM (F)	n	Number of preps	Comparison	P	Significant	ANOVA
	SNAP-25 WT	3.90E-13	1.63E-13	2.97E-14	30	6	WT vs. SN25Δ26	<0.05	Yes	Dunn's post hoc
	SN25Δ26+mCh-SN2	-4.29E-16	1.46E-14	2.81E-15	27	6	WT vs. KO	<0.05	Yes	
	KO	3.074E-14	1.411E-14	2.942E-15	23	6	KO vs. SN25Δ26	<0.05	Yes	
ΔCM (1s)	Label	Mean (F)	SD (F)	SEM (F)	n	Number of preps	Comparison	P	Significant	ANOVA
	SNAP-25 WT	2.73E-13	1.25E-13	2.28E-14	30	6	WT vs. SN25Δ26	<0.05	Yes	Dunn's post hoc
	SN25Δ26+mCh-SN2	-1.80E-17	5.55E-15	1.07E-15	27	6	WT vs. KO	<0.05	Yes	
	KO	1.57E-14	1.07E-14	2.24E-15	23	6	KO vs. SN25Δ26	<0.05	Yes	
Sust. Rel.	Label	Mean (F)	SD (F)	SEM (F)	n	Number of preps	Comparison	P	Significant	ANOVA
	SNAP-25 WT	2.95E-14	1.68E-14	3.06E-15	30	6	WT vs. SN25Δ26	<0.05	Yes	Dunn's post hoc
	SN25Δ26+mCh-SN2	-1.03E-16	3.32E-15	6.39E-16	27	6	WT vs. KO	<0.05	Yes	
	KO	3.75E-15	4.09E-15	8.53E-16	23	6	KO vs. SN25Δ26	<0.05	Yes	
Figure 13 D										
ΔCM (5s)	Label	Mean (F)	SD (F)	SEM (F)	n	Number of preps	Comparison	P	Significant	ANOVA
	SNAP-25 WT	3.23E-13	1.52E-13	2.93E-14	27	4	WT vs. KO	<0.001	Yes	Tukey's post hoc
	SN25ΔC+mCh-SN2	1.11E-13	8.06E-14	1.76E-14	21	4	WT vs. SN25ΔC+mCh-SN2	<0.001	Yes	
	KO	2.96E-14	3.03E-14	5.35E-01	32	4	Split 5s vs. KO 5s	0.013	Yes	
ΔCM (1s)	Label	Mean (F)	SD (F)	SEM (F)	n	Number of preps	Comparison	P	Significant	ANOVA
	SNAP-25 WT	2.31E-13	1.19E-13	2.29E-14	27	4	WT vs. KO	<0.001	Yes	Tukey's post hoc
	SN25ΔC+mCh-SN2	6.57E-14	5.68E-14	1.24E-14	21	4	WT vs. SN25ΔC+mCh-SN2	<0.001	Yes	
	KO	1.27E-14	1.32E-14	2.32E-15	32	4	SN1-L+SN2 vs. KO	0.038	Yes	
Sust. Rel.	Label	Mean (F)	SD (F)	SEM (F)	n	Number of preps	Comparison	P	Significant	ANOVA
	SNAP-25 WT	2.30E-14	1.47E-14	2.83E-15	27	4	WT vs. KO	<0.001	Yes	Tukey's post hoc
	SN25ΔC+mCh-SN2	1.13E-14	8.29E-15	1.81E-15	21	4	WT vs. SN25ΔC+mCh-SN2	<0.001	Yes	
	KO	4.24E-15	5.71E-15	1.01E-15	32	4	SN1-L+SN2 vs. KO	0.041	Yes	

Figure 15 C

ΔCM (5s)	Label	Mean (F)	SD (F)	SEM (F)	n	Number of preps	Comparison	P	Significant	ANOVA
	SNAP-25 WT	3.26E-13	1.12E-13	2.25E-14	25	3	WT vs. SN25 L G/S	<0.001	Yes	Tukey's post hoc
	SN25 L G/S	4.38E-14	3.44E-14	6.75E-15	26	3	WT vs. KO	<0.001	Yes	
	KO	3.70E-14	2.84E-14	5.92E-15	23	3	KO vs. SN25 L G/S	0.939	No	
ΔCM (1s)	Label	Mean (F)	SD (F)	SEM (F)	n	Number of preps	Comparison	P	Significant	ANOVA
	SNAP-25 WT	2.36E-13	9.40E-14	1.88E-14	25	3	WT vs. SN25 L G/S	<0.001	Yes	Tukey's post hoc
	SN25 L G/S	1.85E-14	1.43E-14	2.81E-15	26	3	WT vs. KO	<0.001	Yes	
	KO	2.06E-14	1.75E-14	3.65E-15	23	3	KO vs. SN25 L G/S	0.991	No	
Sust. Rel.	Label	Mean (F/s)	SD (F/s)	SEM (F/s)	n	Number of preps	Comparison	P	Significant	ANOVA
	SNAP-25 WT	2.24E-14	1.12E-14	2.24E-15	25	3	WT vs. SN25 L G/S	<0.001	Yes	Tukey's post hoc
	SN25 L G/S	6.33E-15	6.15E-15	1.21E-15	26	3	WT vs. KO	<0.001	Yes	
	KO	4.10E-15	4.80E-15	1.00E-15	23	3	KO vs. SN25 L G/S	0.593	No	

Figure 15 E upper panel

ΔCM (5s)	Label	Mean (F)	SD (F)	SEM (F)	n	Number of preps	Comparison	P	Significant	ANOVA
	SNAP-25 WT	2.51E-12	7.70E-13	1.82E-13	18	4	WT vs. SN25 L G/S	<0.001	Yes	Tukey's post hoc
	SN25 L G/S	2.55E-13	3.03E-13	8.11E-14	14	4	WT vs. KO	<0.001	Yes	
	KO	3.86E-13	3.33E-13	1.00E-13	11	4	KO vs. SN25 L G/S	0.829	No	
	lower panel									
ΔCM (5s)	Label	Mean (F)	SD (F)	SEM (F)	n	Number of preps	Comparison	P	Significant	Student's t-test
	OE SNAP-25 WT	2.64E-12	7.41E-13	2.05E-13	18	2	OE WT vs. OE SN25 L G/S	0.0115	Yes	
	OE SN25 L G/S	1.86E-12	4.71E-13	1.57E-13	14	2				

Figure 17 B

Rel. Retention	Label	Mean	SD	SEM	n		Comparison	P	Significant	ANOVA
	SNAP-25 WT	0.715254	0.0493654	0.0201534	6		WT vs. SN25 L G/S	<0.001	Yes	Tukey's post hoc
	SN25 L G/S	0.36817	0.0710886	0.0290218	6		WT vs. SN1(+SN2)	<0.001	Yes	
	SN1 (+SN2)	0.468687	0.0674548	0.0275383	6		WT vs. SN2 (+SN1)	<0.001	Yes	
	SN2 (+SN1)	0.0813838	0.049238	0.0201013	6		WT vs. SN1-L (+SN2)	<0.001	Yes	
	SN1-L (+SN2)	0.394348	0.122381	0.0499617	6		WT vs. SN2 (+SN1-L)	<0.001	Yes	
	SN2 (+SN1-L)	0.12315	0.0735802	0.030039	6		WT vs. SN1 (+SN2-L)	>0.05	No	
	SN1 (+SN2-L)	0.701219	0.153008	0.0624651	6		WT vs. SN2-L (+SN1)	<0.001	Yes	
	SN2-L (+SN1)	0.419321	0.0974562	0.0397863	6		WT vs. SN2-L (alone)	<0.001	Yes	

	SN2-L (alone)	0.0564529	0.0269573	0.0110053	6		WT vs. WT (GST-GFP)	<0.001	Yes	
	SNAP-25 WT (GST-GFP)	0.0240377	0.0268464	0.01096	6		SN25 L G/S vs. SN1 (+SN2)	>0.05	No	
							SN25 L G/S vs. SN2 (+SN1)	<0.001	Yes	
							SN25 L G/S vs. SN1-L (+SN2)	>0.05	No	
							SN25 L G/S vs. SN2 (+SN1-L)	<0.001	Yes	
							SN25 L G/S vs. SN1 (+SN2-L)	<0.001	Yes	
							SN25 L G/S vs SN2-L (+SN1)	>0.05	No	
							SN25 L G/S vs. SN2-L (alone)	<0.001	Yes	
							SN25 L G/S vs. WT (GST-GFP)	<0.001	Yes	
							SN1 (+SN2) vs. SN2 (+SN1)	<0.001	Yes	
							SN1 (+SN2) vs. SN1-L (+SN2)	>0.05	No	
							SN1 (+SN2) vs. SN2 (+SN1-L)	<0.001	Yes	
							SN1 (+SN2) vs. SN1 (+SN2-L)	<0.001	Yes	
							SN1 (+SN2) vs. SN2-L (+SN1)	>0.05	No	
							SN1 (+SN2) vs. SN2-L (alone)	<0.001	Yes	
							SN1 (+SN2) vs. WT (GST-GFP)	<0.001	Yes	
							SN2 (+SN1) vs. SN1-L (+SN2)	<0.001	Yes	
							SN2 (+SN1) vs. SN2 (+SN1-L)	>0.05	No	
							SN2 (+SN1) vs. SN1 (+SN2-L)	<0.001	Yes	
							SN2 (+SN1) vs. SN2-L (+SN1)	<0.001	Yes	
							SN2 (+SN1) vs. SN2-L (alone)	>0.05	No	
							SN2 (+SN1) vs. WT (GST-GFP)	>0.05	No	
							SN1-L (+SN2) vs. SN2 (+SN1-L)	<0.001	Yes	
							SN1-L(+SN2) vs. SN1 (+SN2-L)	<0.001	Yes	
							SN1-L (+SN2) vs. SN2-L (+SN1)	>0.05	No	
							SN1-L (+SN2) vs. SN2-L (alone)	<0.001	Yes	
							SN1-L (+SN2) vs. WT (GST-GFP)	<0.001	Yes	
							SN2 (+SN1-L) vs. SN1 (+SN2-L)	<0.001	Yes	
							SN2(+SN1-L) vs. SN2-L (+SN1)	<0.001	Yes	
							SN2 (+SN1-L) vs. SN2-L (alone)	>0.05	No	
							SN2 (+SN1-L) vs. WT (GST-GFP)	>0.05	No	
							SN1 (+SN2-L) vs. SN2-L (+SN1)	<0.001	Yes	
							SN1(+SN2-L) vs. SN2-L (alone)	<0.001	Yes	
							SN1 (+SN2-L) vs. WT (GST-GFP)	<0.001	Yes	
							SN2-L (+SN1) vs. SN2-L (alone)	<0.001	Yes	
							SN2-L (+SN1) vs. WT (GST-GFP)	<0.001	Yes	
							SN2-L (alone) vs. WT(GST-GFP)	>0.05	No	

Figure 18 C

RRP	Label	Mean (F)	SD (F)	SEM (F)	n	Number of preps	Comparison	P	Significant	ANOVA
	SNAP-25 WT	9.17E-14	6.03E-14	8.89E-15	46	7	WT vs. SN25 LN G/S	<0.001	Yes	Tukey's post hoc

	SN25 -cys	1.86E-14	3.80E-14	5.22E-15	53	7	WT vs. SN25 -cys	n.d.		
	SN25 LN G/S	0	0	0	22	7	SN25 -cys vs. SN25 LN G/S	n.d.		
τRRP	Label	Mean (ms)	SD (ms)	SEM (ms)	n	Number of preps	Comparison	P	Significant	ANOVA
	SNAP-25 WT	0.0126	0.00612	0.000922	46	7	WT vs. SN25 LN G/S	n.d.		Tukey's post hoc
	SN25 -cys	0.0239	0.0114	0.00295	53	7	WT vs. SN25 -cys	<0.001	Yes	
	SN25 LN G/S	n.d.	n.d.	n.d.	22	7	SN25 -cys vs. SN25 LN G/S	n.d.		
sust. rel.	Label	Mean (F/s)	SD (F/s)	SEM (F/s)	n	Number of preps	Comparison	P	Significant	ANOVA
	SNAP-25 WT	3.05E-14	1.88E-14	2.76E-15	46	7	WT vs. SN25 LN G/S	0.024	Yes	Tukey's post hoc
	SN25 -cys	1.99E-14	1.29E-14	1.77E-15	53	7	WT vs. SN25 -cys	0.003	Yes	
	SN25 LN G/S	1.98E-14	1.35E-14	2.87E-15	22	7	SN25 -cys vs. SN25 LN G/S	1	No	
SRP	Label	Mean (F)	SD (F)	SEM (F)	n	Number of preps	Comparison	P	Significant	ANOVA
	SNAP-25 WT	9.73E-14	4.95E-14	7.29E-15	46	7	WT vs. SN25 LN G/S	0.006	Yes	Tukey's post hoc
	SN25 -cys	1.14E-13	8.08E-14	1.11E-14	53	7	WT vs. SN25 -cys	0.459	No	
	SN25 LN G/S	4.18E-14	6.68E-14	1.42E-14	22	7	SN25 -cys vs. SN25 LN G/S	<0.001	Yes	
τSRP	Label	Mean (ms)	SD (ms)	SEM (ms)	n	Number of preps	Comparison	P	Significant	ANOVA
	SNAP-25 WT	0.132	0.0723	0.0108	46	7	WT vs. SN25 LN G/S	0.015	Yes	Tukey's post hoc
	SN25 -cys	0.241	0.243	0.0334	53	7	WT vs. SN25 -cys	0.019	Yes	
	SN25 LN G/S	0.307	0.263	0.073	22	7	SN25 -cys vs. SN25 LN G/S	0.527	No	
delay	Label	Mean (ms)	SD (ms)	SEM (ms)	n	Number of preps	Comparison	P	Significant	ANOVA
	SNAP-25 WT	0.00242	0.00272	0.000401	46	7	WT vs. SN25 LN G/S	<0.001	Yes	Tukey's post hoc
	SN25 -cys	0.00651	0.00488	0.00067	53	7	WT vs. SN25 -cys	0.012	Yes	
	SN25 LN G/S	0.019	0.0141	0.00301	22	7	SN25 -cys vs. SN25 LN G/S	<0.001	Yes	
Figure 19 C										
RRP	Label	Mean (F)	SD (F)	SEM (F)	n	Number of preps	Comparison	P	Significant	Student's t-Test
	SNAP-25 WT	1.25E-13	5.97E-14	1.17E-14	26	6	WT vs. SN25 LC G/S	<0.001	Yes	
	SN25 LC G/S	5.66E-15	1.57E-14	2.87E-15	31	6				
τRRP	Label	Mean (ms)	SD (ms)	SEM (ms)	n	Number of preps	Comparison	P	Significant	Student's t-Test

	SNAP-25 WT	0.0131	0.00365	0.00073	26	6	WT vs. SN25 LC G/S	<0.001	Yes	
	SN25 LC G/S	0.0572	0.0168	0.00842	31	6				
sust. rel.	Label	Mean (F/s)	SD (F/s)	SEM (F/s)	n	Number of preps	Comparison	P	Significant	Student's t-Test
	SNAP-25 WT	3.10E-14	1.78E-14	3.50E-15	26	6	WT vs. SN25 LC G/S	0.0147	Yes	
	SN25 LC G/S	1.91E-14	1.78E-14	3.19E-15	31	6				
SRP	Label	Mean (F)	SD (F)	SEM (F)	n	Number of preps	Comparison	P	Significant	Student's t-Test
	SNAP-25 WT	9.35E-14	5.41E-14	1.06E-14	26	6	WT vs. SN25 LC G/S	<0.001	Yes	
	SN25 LC G/S	2.80E-14	4.50E-14	8.21E-15	31	6				
τSRP	Label	Mean (ms)	SD (ms)	SEM (ms)	n	Number of preps	Comparison	P	Significant	Student's t-Test
	SNAP-25 WT	0.123	0.0548	0.0108	26	6	WT vs. SN25 LC G/S	0.00148	Yes	
	SN25 LC G/S	0.272	0.211	0.0565	31	6				
delay	Label	Mean (ms)	SD (ms)	SEM (ms)	n	Number of preps	Comparison	P	Significant	Student's t-Test
	SNAP-25 WT	0.0016	0.00156	0.000307	26	6	WT vs. SN25 LC G/S	<0.001	Yes	
	SN25 LC G/S	0.0175	0.0232	0.00465	31	6				
Figure 20 B										
Membrane fluorescence	Label	Mean (a.u.)	SD	SEM	n	Number of preps	Comparison	P	Significant	ANOVA
	SNAP-25 WT	16844.536	5100.885	1063.608	23	3	SNAP-25 WT vs SN25 -cys	0.027	Yes	Tukey's post hoc
	SN25-cys	12436.518	4971.471	1036.623	23	3	SN25 LN G/S vs SN25 LC G/S	0.037	Yes	
	SN25 LN G/S	13200.776	4907.929	1046.374	22	3	SN25 LN G/S vs SN25 -cys	0.692	No	
	SN25 LC G/S	17484.796	5888.779	1227.895	23	3	SNAP-25 WT vs SN25 LC G/S	0.976	No	
Figure 21 B										
Rel. Retention	Label	Mean	SD	SEM	n		Comparison	P	Significant	ANOVA
	SNAP-25 WT	0.707	0.0699	0.0202	12		WT vs. SN25 LN G/S	>0.05	No	Tukey's post hoc
	SN25 LN G/S	0.69	0.1035	0.0299	12		WT vs. SN25 LC G/S	<0.001	Yes	
	SN25 LC G/S	0.512	0.0854	0.0246	12		SN25 LN G/S vs. SN25 LC G/S	<0.001	Yes	
Figure 22 C										
RRP	Label	Mean (F)	SD (F)	SEM (F)	n	Number of preps	Comparison	P	Significant	Student's t-test

	SNAP-25 WT	1.40E-13	1.06E-13	2.12E-14	25	5	WT vs. SN25 ext7aa	0.864	No	
	SN25 ext7aa	1.44E-13	9.81E-14	1.96E-14	28	5				
τRRP	Label	Mean (ms)	SD (ms)	SEM (ms)	n	Number of preps	Comparison	P	Significant	Student's t-test
	SNAP-25 WT	0.0224	0.0101	0.00214	25	5	WT vs. SN25 ext7aa	0.48	No	
	SN25 ext7aa	0.0248	0.0128	0.00268	28	5				
sust. rel.	Label	Mean (F/s)	SD (F/s)	SEM (F/s)	n	Number of preps	Comparison	P	Significant	Student's t-test
	SNAP-25 WT	3.08E-14	1.81E-14	3.61E-15	25	5	WT vs. SN25 ext7aa	0.787	No	
	SN25 ext7aa	3.21E-14	1.48E-14	2.95E-15	28	5				
SRP	Label	Mean (F)	SD (F)	SEM (F)	n	Number of preps	Comparison	P	Significant	Student's t-test
	SNAP-25 WT	1.12E-13	1.16E-13	2.33E-14	25	5	WT vs. SN25 ext7aa	0.899	No	
	SN25 ext7aa	1.16E-13	1.25E-13	2.51E-14	28	5				
τSRP	Label	Mean (ms)	SD (ms)	SEM (ms)	n	Number of preps	Comparison	P	Significant	Student's t-test
	SNAP-25 WT	0.152	0.0992	0.0207	25	5	WT vs. SN25 ext7aa	0.512	No	
	SN25 ext7aa	0.174	0.119	0.0254	28	5				
delay	Label	Mean (ms)	SD (ms)	SEM (ms)	n	Number of preps	Comparison	P	Significant	Student's t-test
	SNAP-25 WT	0.00374	0.00312	0.000756	17	5	WT vs. SN25 ext7aa	0.889	No	
	SN25 ext7aa	0.00359	0.00262	0.000756	21	5				
Figure 23 C										
RRP	Label	Mean (F)	SD (F)	SEM (F)	n	Number of preps	Comparison	P	Significant	Student's t-test
	SNAP-25 WT	1.73E-13	1.45E-13	3.52E-14	17	5	WT vs. SN25 ext14aa	0.905	No	
	SN25 ext14aa	1.68E-13	9.77E-14	2.82E-14	21	5				
τRRP	Label	Mean (ms)	SD (ms)	SEM (ms)	n	Number of preps	Comparison	P	Significant	Student's t-test
	SNAP-25 WT	0.0302	0.0237	0.00574	17	5	WT vs. SN25 ext14aa	0.843	No	
	SN25 ext14aa	0.0317	0.0118	0.00341	21	5				
sust. rel.	Label	Mean (F/s)	SD (F/s)	SEM (F/s)	n	Number of preps	Comparison	P	Significant	Student's t-test

	SNAP-25 WT	3.05E-14	1.12E-14	2.88E-15	17	5	WT vs. SN25 ext14aa	0.0751	No	
	SN25 ext14aa	4.21E-14	2.09E-14	6.04E-15	21	5				
SRP	Label	Mean (F)	SD (F)	SEM (F)	n	Number of preps	Comparison	P	Significant	Student's t-test
	SNAP-25 WT	8.95E-14	6.08E-14	1.47E-14	17	5	WT vs. SN25 ext14aa	0.662	No	
	SN25 ext14aa	7.99E-14	5.23E-14	1.51E-14	21	5				
τSRP	Label	Mean (ms)	SD (ms)	SEM (ms)	n	Number of preps	Comparison	P	Significant	Student's t-test
	SNAP-25 WT	0.154	0.1	0.0269	17	5	WT vs. SN25 ext14aa	0.327	No	
	SN25 ext14aa	0.196	0.104	0.033	21	5				
delay	Label	Mean (ms)	SD (ms)	SEM (ms)	n	Number of preps	Comparison	P	Significant	Student's t-test
	SNAP-25 WT	0.00406	0.00482	0.000964	25	5	WT vs. SN25 ext14aa	0.806	No	
	SN25 ext14aa	0.00375	0.00388	0.000777	28	5				
Figure 25 C										
RRP	Label	Mean (F)	SD (F)	SEM (F)	n	Number of preps	Comparison	P	Significant	Student's t-test
	SNAP-25 WT	1.95E-13	1.42E-13	2.63E-14	29	6	WT vs. SN25 -4AA	0.393	No	
	SN25 -4AA	2.25E-13	1.33E-13	2.35E-14	32	6				
τRRP	Label	Mean (ms)	SD (ms)	SEM (ms)	n	Number of preps	Comparison	P	Significant	Student's t-test
	SNAP-25 WT	0.0194	0.00608	0.00113	29	6	WT vs. SN25 -4AA	0.0274	Yes	
	SN25 -4AA	0.0239	0.00905	0.00163	32	6				
sust. rel.	Label	Mean (F/s)	SD (F/s)	SEM (F/s)	n	Number of preps	Comparison	P	Significant	Student's t-test
	SNAP-25 WT	2.18E-14	1.16E-14	2.14E-15	29	6	WT vs. SN25 -4AA	0.121	No	
	SN25 -4AA	2.82E-14	1.88E-14	3.33E-15	32	6				
SRP	Label	Mean (F)	SD (F)	SEM (F)	n	Number of preps	Comparison	P	Significant	Student's t-test
	SNAP-25 WT	9.37E-14	5.44E-14	1.01E-14	29	6	WT vs. SN25 -4AA	<0.001	Yes	
	SN25 -4AA	1.90E-13	9.37E-14	1.66E-14	32	6				
τSRP	Label	Mean (ms)	SD (ms)	SEM (ms)	n	Number of preps	Comparison	P	Significant	Student's t-test

	SNAP-25 WT	0.121	0.0629	0.0117	29	6	WT vs. SN25 -4AA	0.0993	No	
	SN25 -4AA	0.154	0.0873	0.015	32	6				
delay	Label	Mean (ms)	SD (ms)	SEM (ms)	n	Number of preps	Comparison	P	Significant	Student's t-test
	SNAP-25 WT	0.00334	0.00194	0.000361	29	6	WT vs. SN25 -4AA	0.0587	No	
	SN25 -4AA	0.00442	0.0024	0.000424	32	6				
Figure 26 C										
Fpeak	Label	Mean (a.u.)	SD (a.u.)	SEM (a.u.)	n	Number of preps	Comparison	P	Significant	Student's t-Test
	P-GFP-SN25 WT	5845.594	2843.409	620.483	21	3	P-GFP-WT vs. P-GFP-SN25 -cys	0.117	No	
	P-GFP-SN25 -cys	7680.798	4495.048	937.282	23	3				
Figure 27 C										
RRP	Label	Mean (F)	SD (F)	SEM (F)	n	Number of preps	Comparison	P	Significant	Student's t-Test
	P-GFP-SN25 WT	1.03E-13	6.40E-14	1.19E-14	26	5	P-GFP-WT vs. P-GFP-SN25 -cys	0.0194	Yes	
	P-GFP-SN25 -cys	6.06E-14	6.34E-14	1.27E-14	25	5				
τRRP	Label	Mean (ms)	SD (ms)	SEM (ms)	n	Number of preps	Comparison	P	Significant	Student's t-Test
	P-GFP-SN25 WT	0.0187	0.013	0.0025	26	5	P-GFP-WT vs. P-GFP-SN25 -cys	0.021	Yes	
	P-GFP-SN25 -cys	0.0319	0.0245	0.00548	25	5				
sust. rel.	Label	Mean (F/s)	SD (F/s)	SEM (F/s)	n	Number of preps	Comparison	P	Significant	Student's t-Test
	P-GFP-SN25 WT	3.69E-14	2.03E-14	3.78E-15	26	5	P-GFP-WT vs. P-GFP-SN25 -cys	0.273	No	
	P-GFP-SN25 -cys	3.16E-14	1.30E-14	2.60E-15	25	5				
SRP	Label	Mean (F)	SD (F)	SEM (F)	n	Number of preps	Comparison	P	Significant	Student's t-Test
	P-GFP-SN25 WT	1.38E-13	8.70E-14	1.62E-14	26	5	P-GFP-WT vs. P-GFP-SN25 -cys	0.136	No	
	P-GFP-SN25 -cys	1.07E-13	5.99E-14	1.20E-14	25	5				
τRRP	Label	Mean (ms)	SD (ms)	SEM (ms)	n	Number of preps	Comparison	P	Significant	Student's t-Test
	P-GFP-SN25 WT	0.159	0.0976	0.0184	26	5	P-GFP-WT vs. P-GFP-SN25 -cys	0.0396	Yes	
	P-GFP-SN25 -cys	0.214	0.0838	0.0179	25	5				

delay	Label	Mean (ms)	SD (ms)	SEM (ms)	n	Number of preps	Comparison	P	Significant	Student's t-Test
	P-GFP-SN25 WT	0.0032	0.00324	0.000601	26	5	P-GFP-WT vs. P-GFP-SN25 -cys	0.444	No	
	P-GFP-SN25 -cys	0.00394	0.00382	0.000763	25	5				
Figure 28 D										
non-normalized data										
RRP	Label	Mean (F)	SD (F)	SEM (F)	n	Number of preps	Comparison	P	Significant	Student's t-Test
	SNAP-25 WT	1.208E-13	6.598E-14	1.132E-14	35	7	WT vs. SN25 Shift6aa	0.154	No	
	SN25 shift6aa	9.665E-14	6.543E-14	1.236E-14	26	7				
τRRP	Label	Mean (ms)	SD (ms)	SEM (ms)	n	Number of preps	Comparison	P	Significant	Student's t-Test
	SNAP-25 WT	0.0174	0.0102	0.00178	35	7	WT vs. SN25 Shift6aa	0.00853	Yes	
	SN25 shift6aa	0.025	0.0117	0.00221	26	7				
sust. rel.	Label	Mean (F/s)	SD (F/s)	SEM (F/s)	n	Number of preps	Comparison	P	Significant	Student's t-Test
	SNAP-25 WT	2.97E-14	1.472E-14	2.524E-15	35	7	WT vs. SN25 Shift6aa	0.0688	No	
	SN25 shift6aa	3.525E-14	1.408E-14	2.661E-15	26	7				
SRP	Label	Mean (F)	SD (F)	SEM (F)	n	Number of preps	Comparison	P	Significant	Student's t-Test
	SNAP-25 WT	9.655E-14	6.549E-14	1.123E-14	35	7	WT vs. SN25 Shift6aa	0.564	No	
	SN25 shift6aa	8.719E-14	5.879E-14	1.131E-14	26	7				
τSRP	Label	Mean (ms)	SD (ms)	SEM (ms)	n	Number of preps	Comparison	P	Significant	Student's t-Test
	SNAP-25 WT	0.111	0.0568	0.0102	35	7	WT vs. SN25 Shift6aa	0.00861	Yes	
	SN25 shift6aa	0.166	0.0949	0.019	26	7				
delay	Label	Mean (ms)	SD (ms)	SEM (ms)	n	Number of preps	Comparison	P	Significant	Student's t-Test
	SNAP-25 WT	0.00184	0.00197	0.000337	35	7	WT vs. SN25 Shift6aa	0.0146	Yes	
	SN25 shift6aa	0.00323	0.0024	0.000454	26	7				
RRP	Label	Mean (F)	SD (F)	SEM (F)	n	Number of preps	Comparison	P	Significant	Student's t-Test
	SNAP-25 WT	1.599E-13	9.011E-14	1.673E-14	30	7	WT vs. SN25 Shift10aa	0.505	No	
	SN25 shift10aa	1.439E-13	1.054E-13	1.626E-14	43	7				

τRRP	Label	Mean (ms)	SD (ms)	SEM (ms)	n	Number of preps	Comparison	P	Significant	Student's t-Test
	SNAP-25 WT	0.023	0.00915	0.0017	30	7	WT vs. SN25 Shift10aa	4.61E-07	Yes	
	SN25 shift10aa	0.0433	0.0179	0.0029	43	7				
sust. rel.	Label	Mean (F/s)	SD (F/s)	SEM (F/s)	n	Number of preps	Comparison	P	Significant	Student's t-Test
	SNAP-25 WT	2.792E-14	1.435E-14	2.665E-15	30	7	WT vs. SN25 Shift10aa	0.768	No	
	SN25 shift10aa	2.694E-14	1.326E-14	2.045E-15	43	7				
SRP	Label	Mean (F)	SD (F)	SEM (F)	n	Number of preps	Comparison	P	Significant	Student's t-Test
	SNAP-25 WT	9.231E-14	6.612E-14	1.228E-14	30	7	WT vs. SN25 Shift10aa	0.726	No	
	SN25 shift10aa	1.016E-13	1.317E-13	2.032E-14	43	7				
τSRP	Label	Mean (ms)	SD (ms)	SEM (ms)	n	Number of preps	Comparison	P	Significant	Student's t-Test
	SNAP-25 WT	0.129	0.0835	0.017	30	7	WT vs. SN25 Shift10aa	0.000661	Yes	
	SN25 shift10aa	0.227	0.12	0.0216	43	7				
delay	Label	Mean (ms)	SD (ms)	SEM (ms)	n	Number of preps	Comparison	P	Significant	Student's t-Test
	SNAP-25 WT	0.00269	0.00272	0.000505	30	7	WT vs. SN25 Shift14aa	4.23E-06	Yes	
	SN25 shift10aa	0.00706	0.00432	0.000667	43	7				
RRP	Label	Mean (F)	SD (F)	SEM (F)	n	Number of preps	Comparison	P	Significant	Student's t-Test
	SNAP-25 WT	1.428E-13	8.46E-14	1.338E-14	40	4	WT vs. SN25 Shift14aa	0.517	No	
	SN25 shift14aa	1.246E-13	1.513E-13	2.594E-14	34	4				
τRRP	Label	Mean (ms)	SD (ms)	SEM (ms)	n	Number of preps	Comparison	P	Significant	Student's t-Test
	SNAP-25 WT	0.0137	0.00615	0.000973	40	4	WT vs. SN25 Shift14aa	1.2E-11	Yes	
	SN25 shift14aa	0.0478	0.0251	0.00493	34	4				
sust. rel.	Label	Mean (F/s)	SD (F/s)	SEM (F/s)	n	Number of preps	Comparison	P	Significant	Student's t-Test
	SNAP-25 WT	2.961E-14	1.439E-14	2.276E-15	40	4	WT vs. SN25 Shift14aa	0.787	No	
	SN25 shift14aa	3.046E-14	1.187E-14	2.036E-15	34	4				

SRP	Label	Mean (F)	SD (F)	SEM (F)	n	Number of preps	Comparison	P	Significant	Student's t-Test
	SNAP-25 WT	9.601E-14	5.633E-14	8.907E-15	40	4	WT vs. SN25 Shift14aa	0.787	No	
	SN25 shift14aa	1.011E-13	1.015E-13	1.741E-14	34	4				
τSRP	Label	Mean (ms)	SD (ms)	SEM (ms)	n	Number of preps	Comparison	P	Significant	Student's t-Test
	SNAP-25 WT	0.121	0.0844	0.0135	40	4	WT vs. SN25 Shift14aa	0.00049	Yes	
	SN25 shift14aa	0.206	0.0996	0.0203	34	4				
delay	Label	Mean (ms)	SD (ms)	SEM (ms)	n	Number of preps	Comparison	P	Significant	Student's t-Test
	SNAP-25 WT	0.00111	0.00217	0.000344	40	4	WT vs. SN25 Shift14aa	6.46E-05	Yes	
	SN25 shift14aa	0.00617	0.00717	0.00123	34	4				
Figure 29 D										
RRP	Label	Mean (F)	SD (F)	SEM (F)	n	Number of preps	Comparison	P	Significant	ANOVA
	SNAP-25 WT	1.08E-13	6.27E-14	8.09E-15	29	5	WT vs. SN25 LN^{4CS}	<0.001	Yes	Tukey's post hoc
	SN25 -cys	3.71E-14	5.22E-14	7.17E-15	24	5	WT vs. SN25 shift14aaLN^{4CS}	<0.001	Yes	
	SN25 -cys shift 14aa	1.73E-14	3.95E-14	7.47E-15	26	5	SN25 LN^{4CS} vs. SN25 shift14aaLN^{4CS}	0.27	No	
τRRP	Label	Mean (ms)	SD (ms)	SEM (ms)	n	Number of preps	Comparison	P	Significant	ANOVA
	SNAP-25 WT	0.0149	0.01	0.00134	29	5	WT vs. SN25 LN^{4CS}	0.01	Yes	Tukey's post hoc
	SN25 -cys	0.0247	0.0192	0.00345	24	5	WT vs. SN25 shift14aaLN^{4CS}	<0.001	Yes	
	SN25 -cys shift 14aa	0.0397	0.0197	0.00593	26	5	SN25 LN^{4CS} vs. SN25 shift14aaLN^{4CS}	0.013	Yes	
sust. rel.	Label	Mean (F/s)	SD (F/s)	SEM (F/s)	n	Number of preps	Comparison	P	Significant	ANOVA
	SNAP-25 WT	3.05E-14	1.28E-14	1.65E-15	29	5	WT vs. SN25 LN^{4CS}	0.044	Yes	Tukey's post hoc
	SN25 -cys	2.31E-14	1.40E-14	1.92E-15	24	5	WT vs. SN25 shift14aaLN^{4CS}	0.012	Yes	
	SN25 -cys shift 14aa	2.30E-14	1.50E-14	2.83E-15	26	5	SN25 LN^{4CS} vs. SN25 shift14aaLN^{4CS}	0.999	No	
SRP	Label	Mean (F)	SD (F)	SEM (F)	n	Number of preps	Comparison	P	Significant	ANOVA
	SNAP-25 WT	1.21E-13	6.43E-14	8.30E-15	29	5	ANOVA	0.075	No	Tukey's post hoc
	SN25 -cys	1.18E-13	7.46E-14	1.02E-14	24	5				

	SN25 -cys shift 14aa	8.62E-14	6.86E-14	1.30E-14	26	5				
τSRP	Label	Mean (ms)	SD (ms)	SEM (ms)	n	Number of preps	Comparison	P	Significant	ANOVA
	SNAP-25 WT	0.122	0.0911	0.0119	29	5	WT vs. SN25 LN^{4CS}	0.012	Yes	Tukey's post hoc
	SN25 -cys	0.177	0.0887	0.0124	24	5	WT vs. SN25 shift14aaLN^{4CS}	<0.001	Yes	
	SN25 -cys shift 14aa	0.299	0.139	0.0283	26	5	SN25 LN^{4CS} vs. SN25 shift14aaLN^{4CS}	<0.001	Yes	
delay	Label	Mean (ms)	SD (ms)	SEM (ms)	n	Number of preps	Comparison	P	Significant	ANOVA
	SNAP-25 WT	0.00189	0.00171	0.000219	29	5	WT vs. SN25 LN^{4CS}	<0.001	Yes	Tukey's post hoc
	SN25 -cys	0.00534	0.00431	0.000591	24	5	WT vs. SN25 shift14aaLN^{4CS}	<0.001	Yes	
	SN25 -cys shift 14aa	0.0111	0.00811	0.00153	26	5	SN25 LN^{4CS} vs. SN25 shift14aaLN^{4CS}	<0.001	Yes	
Figure 30 C										
RRP	Label	Mean (F)	SD (F)	SEM (F)	n	Number of preps	Comparison	P	Significant	ANOVA
	SNAP-25 WT	1.22E-13	6.77E-14	1.18E-14	33	6	WT vs. SN25 -cys 5K/A	<0.001	Yes	Tukey's post hoc
	SN25 -cys	2.58E-14	3.81E-14	6.35E-15	36	6	WT vs. SN25 -cys	<0.001	Yes	
	SN25 -cys 5K/A	3.74E-14	8.89E-14	1.41E-14	37	6	SN25 LN^{4CS} vs. SN25 $LN^{5kA,4CS}$	0.746	No	
τRRP	Label	Mean (ms)	SD (ms)	SEM (ms)	n	Number of preps	Comparison	P	Significant	ANOVA
	SNAP-25 WT	0.0143	0.00792	0.0014	33	6	WT vs. SN25 $LN^{5KA,4CS}$	0.004	Yes	Tukey's post hoc
	SN25 -cys	0.0283	0.0196	0.00462	36	6	WT vs. SN25 LN^{4CS}	<0.001	Yes	
	SN25 -cys 5K/A	0.0494	0.0294	0.00712	37	6	SN25 LN^{4CS} vs. SN25 $LN^{5kA,4CS}$	0.035	Yes	
sust. rel.	Label	Mean (F/s)	SD (F/s)	SEM (F/s)	n	Number of preps	Comparison	P	Significant	ANOVA
	SNAP-25 WT	3.13E-14	1.62E-14	2.81E-15	33	6	WT vs. SN25 $LN^{5KA,4CS}$	0.038	Yes	Tukey's post hoc
	SN25 -cys	2.16E-14	1.66E-14	2.76E-15	36	6	WT vs. SN25 LN^{4CS}	0.034	Yes	
	SN25 -cys 5K/A	2.20E-14	1.51E-14	2.39E-15	37	6	SN25 LN^{4CS} vs. SN25 $LN^{5kA,4CS}$	0.994	No	
SRP	Label	Mean (F)	SD (F)	SEM (F)	n	Number of preps	Comparison	P	Significant	ANOVA
	SNAP-25 WT	1.111E-13	6.049E-14	1.053E-14	33	6	ANOVA	0.893	No	
	SN25 -cys	1.228E-13	1.21E-13	2.016E-14	36	6				
	SN25 -cys 5K/A	1.229E-13	1.486E-13	2.35E-14	37	6				

τSRP	Label	Mean (ms)	SD (ms)	SEM (ms)	n	Number of preps	Comparison	P	Significant	ANOVA
	SNAP-25 WT	0.133	0.0913	0.0161	33	6	WT vs. SN25 $LN^{5KA,4CS}$	0.002	Yes	Tukey's post hoc
	SN25 -cys	0.193	0.104	0.0181	36	6	WT vs. SN25 LN4CS	0.035	Yes	
	SN25 -cys 5K/A	0.226	0.116	0.0208	37	6	SN25 LN^{4CS} vs. SN25 $LN^{5KA,4CS}$	0.533	No	
delay	Label	Mean (ms)	SD (ms)	SEM (ms)	n	Number of preps	Comparison	P	Significant	ANOVA
	SNAP-25 WT	0.00155	0.00138	0.000241	33	6	WT vs. SN25 $LN^{5KA,4CS}$	0.659	No	Tukey's post hoc
	SN25 -cys	0.00774	0.0122	0.00204	36	6	WT vs. SN25 LN^{4CS}	0.041	Yes	
	SN25 -cys 5K/A	0.00984	0.0127	0.00201	37	6	SN25 LN^{4CS} vs. SN25 $LN^{5KA,4CS}$	0.003	Yes	
Figure 31 C										
RRP	Label	Mean (F)	SD (F)	SEM (F)	n	Number of preps	Comparison	P	Significant	Student's t-Test
	SNAP-25 WT	1.25E-13	5.97E-14	1.17E-14	26	6	WT vs. SN25 LC 4G	<0.001	Yes	
	SN25 LC 4G	7.03E-14	8.79E-14	1.63E-14	29	6				
τRRP	Label	Mean (ms)	SD (ms)	SEM (ms)	n	Number of preps	Comparison	P	Significant	Student's t-Test
	SNAP-25 WT	0.0131	0.00365	0.00073	26	6	WT vs. SN25 LC 4G	0.002	Yes	
	SN25 LC 4G	0.0301	0.0152	0.0034	29	6				
sust. rel.	Label	Mean (F/s)	SD (F/s)	SEM (F/s)	n	Number of preps	Comparison	P	Significant	Student's t-Test
	SNAP-25 WT	3.10E-14	1.78E-14	3.50E-15	26	6	WT vs. SN25 LC 4G	0.002	Yes	
	SN25 LC 4G	2.74E-14	1.74E-14	3.23E-15	29	6				
SRP	Label	Mean (F)	SD (F)	SEM (F)	n	Number of preps	Comparison	P	Significant	Student's t-Test
	SNAP-25 WT	9.35E-14	5.41E-14	1.06E-14	26	6	WT vs. SN25 LC 4G	<0.001	Yes	
	SN25 LC 4G	7.58E-14	6.54E-14	1.21E-14	29	6				
τRRP	Label	Mean (ms)	SD (ms)	SEM (ms)	n	Number of preps	Comparison	P	Significant	Student's t-Test
	SNAP-25 WT	0.123	0.0548	0.0108	26	6	WT vs. SN25 LC 4G	0.005	Yes	
	SN25 LC 4G	0.175	0.144	0.0307	29	6				
delay	Label	Mean (ms)	SD (ms)	SEM (ms)	n	Number of preps	Comparison	P	Significant	Student's t-Test
	SNAP-25 WT	0.0016	0.00156	0.000307	26	6	WT vs. SN25 LC 4G	<0.001	Yes	
	SN25 LC 4G	0.00392	0.00441	0.000819	29	6				

Figure 32 C										
RRP	Label	Mean (F)	SD (F)	SEM (F)	n	Number of preps	Comparison	P	Significant	Student's t-test
	SNAP-25 WT	1.34E-13	1.02E-13	1.96E-14	27	6	WT vs. SN25 LC 9G	0.000871	Yes	
	SN25 LC 9G	5.91E-14	6.65E-14	1.12E-14	34	6				
τRRP	Label	Mean (ms)	SD (ms)	SEM (ms)	n	Number of preps	Comparison	P	Significant	Student's t-test
	SNAP-25 WT	0.0171	0.0087	0.00171	27	6	WT vs. SN25 LC 9G	1.75E-05	Yes	
	SN25 LC 9G	0.037	0.0196	0.00384	34	6				
sust. rel.	Label	Mean (F/s)	SD (F/s)	SEM (F/s)	n	Number of preps	Comparison	P	Significant	Student's t-test
	SNAP-25 WT	2.01E-14	1.19E-14	2.28E-15	27	6	WT vs. SN25 LC 9G	0.775	No	
	SN25 LC 9G	1.92E-14	1.14E-14	1.92E-15	34	6				
SRP	Label	Mean (F)	SD (F)	SEM (F)	n	Number of preps	Comparison	P	Significant	Student's t-test
	SNAP-25 WT	1.00E-13	6.11E-14	1.18E-14	27	6	WT vs. SN25 LC 9G	0.15	No	
	SN25 LC 9G	7.59E-14	6.78E-14	1.15E-14	34	6				
τSRP	Label	Mean (ms)	SD (ms)	SEM (ms)	n	Number of preps	Comparison	P	Significant	Student's t-test
	SNAP-25 WT	0.115	0.0514	0.0099	27	6	WT vs. SN25 LC 9G	0.0179	Yes	
	SN25 LC 9G	0.218	0.215	0.0385	34	6				
delay	Label	Mean (ms)	SD (ms)	SEM (ms)	n	Number of preps	Comparison	P	Significant	Student's t-test
	SNAP-25 WT	0.00401	0.00251	0.000483	27	6	WT vs. SN25 LC 9G	0.000737	Yes	
	SN25 LC 9G	0.00724	0.0041	0.000724	34	6				
Figure 32 B										
Spike charge	Label	Mean (fC)	SD (fC)	SEM (fC)	n	Number of preps	Comparison	P	Significant	ANOVA
	SNAP-25 WT	244.8583	86.5179	8.6954	100	15 (pooled)	ANOVA	0.969	No	Tukey's post hoc
	SN25 -cys	236.5146	55.5647	11.8464	22	3				
	SN25 LN G/S	246.9646	55.1938	10.6221	27	4				
	SN25 shift14aa	252.0175	75.7785	16.156	22	3				
	SN25 LC G/S	241.4312	80.5943	20.1486	16	3				

Spike amplitude	Label	Mean (pA)	SD (pA)	SEM (pA)	n	Number of preps	Comparison	P	Significant	ANOVA
	SNAP-25 WT	120.7234	33.0579	3.3394	100	15 (pooled)	SN25 -cys vs. WT	0.991	No	Tukey's post hoc
	SN25 -cys	116.3613	34.0314	7.2555	22	3	SN25 LN G/S vs. WT	<0.001	Yes	
	SN25 LN G/S	76.6957	25.0043	4.8121	27	4	SN25 shift14aa vs. WT	<0.001	Yes	
	SN25 shift14aa	79.3846	21.1245	4.5038	22	3	SN25 LC G/S vs. WT	1	No	
	SN25 LC G/S	118.6585	32.0023	8.0006	16	3				
Spike risetime	Label	Mean (µs)	SD (µs)	SEM (µs)	n	Number of preps	Comparison	P	Significant	ANOVA
	SNAP-25 WT	243.9578	39.4188	3.9617	100	15 (pooled)	SN25 -cys vs. WT	0.928	No	Tukey's post hoc
	SN25 -cys	259.546	69.4933	14.816	22	3	SN25 LN G/S vs. WT	<0.001	Yes	
	SN25 LN G/S	340.0524	89.0606	17.1397	27	4	SN25 shift14aa vs. WT	<0.001	Yes	
	SN25 shift14aa	340.0448	102.8766	21.9334	22	3	SN25 LC G/S vs. WT	1	No	
	SN25 LC G/S	243.253	60.0351	15.0088	16	3				
Spike halfwidth	Label	Mean (ms)	SD (ms)	SEM (ms)	n	Number of preps	Comparison	P	Significant	ANOVA
	SNAP-25 WT	1.4093	0.3627	0.0365	100	15 (pooled)	SN25 -cys vs. WT	0.96	No	Tukey's post hoc
	SN25 -cys	1.5144	0.4326	0.0922	22	3	SN25 LN G/S vs. WT	<0.001	Yes	
	SN25 LN G/S	2.3392	0.5995	0.1154	27	4	SN25 shift14aa vs. WT	<0.001	Yes	
	SN25 shift14aa	2.1033	0.9206	0.1963	22	3	SN25 LC G/S vs. WT	1	No	
	SN25 LC G/S	1.3987	0.3884	0.0971	16	3				
Figure 32 C										
Prespike ampl.	Label	Mean (pA)	SD (pA)	SEM (pA)	n	Number of preps	Comparison	P	Significant	ANOVA
	SNAP-25 WT	16.1493	4.283	0.4305	100	15 (pooled)	SN25 -cys vs. WT	0.992	No	Tukey's post hoc
	SN25 -cys	15.5228	8.1546	1.7386	22	3	SN25 LN G/S vs. WT	<0.001	Yes	
	SN25 LN G/S	11.63	3.6871	0.7096	27	4	SN25 shift14aa vs. WT	<0.001	Yes	
	SN25 shift14aa	11.3954	2.2134	0.4719	22	3	SN25 LC G/S vs. WT	1	No	
	SN25 LC G/S	16.5168	4.09	1.0225	16	3				
Prespike initial ampl.	Label	Mean (pA)	SD (pA)	SEM (pA)	n	Number of preps	Comparison	P	Significant	ANOVA
	SNAP-25 WT	3.5061	1.1076	0.1113	100	15 (pooled)	SN25 -cys vs. WT	<0.001	Yes	Tukey's post hoc
	SN25 -cys	1.6548	0.4128	0.088	22	3	SN25 LN G/S vs. WT	<0.001	Yes	
	SN25 LN G/S	1.5054	0.6671	0.1284	27	4	SN25 shift14aa vs. WT	<0.001	Yes	
	SN25 shift14aa	1.8843	0.6709	0.143	22	3	SN25 LC G/S vs. WT	0.546	No	
	SN25 LC G/S	3.9169	0.7798	0.195	16	3				

Prespike duration	Label	Mean (ms)	SD (ms)	SEM (ms)	n	Number of preps	Comparison	P	Significant	ANOVA
	SNAP-25 WT	4.0225	1.5819	0.159	100	15 (pooled)	SN25 -cys vs. WT	<0.001	Yes	Tukey's post hoc
	SN25 -cys	9.048	1.9129	0.4078	22	3	SN25 LN G/S vs. WT	<0.001	Yes	
	SN25 LN G/S	9.6719	2.5469	0.4901	27	4	SN25 shift14aa vs. WT	<0.001	Yes	
	SN25 shift14aa	9.6428	2.3325	0.4973	22	3	SN25 LC G/S vs. WT	1	No	
	SN25 LC G/S	4.0093	1.3383	0.3346	16	3				
Prespike charge	Label	Mean (fC)	SD (fC)	SEM (fC)	n	Number of preps	Comparison	P	Significant	ANOVA
	SNAP-25 WT	20.207	9.473	0.9521	100	15 (pooled)	SN25 -cys vs. WT	<0.001	Yes	Tukey's post hoc
	SN25 -cys	45.6229	16.9765	3.6194	22	3	SN25 LN G/S vs. WT	<0.001	Yes	
	SN25 LN G/S	40.3784	9.4272	1.8143	27	4	SN25 shift14aa vs. WT	<0.001	Yes	
	SN25 shift14aa	40.8388	15.5668	3.3189	22	3	SN25 LC G/S vs. WT	0.993	No	
	SN25 LC G/S	21.9677	7.8281	1.957	16	3				
Fluctuation freq.	Label	Mean (kHz)	SD (kHz)	SEM (kHz)	n	Number of preps	Comparison	P	Significant	ANOVA
	SNAP-25 WT	0.376	0.129	0.013	100	15 (pooled)	SN25 -cys vs. WT	<0.001	Yes	Tukey's post hoc
	SN25 -cys	0.1711	0.0566	0.0121	22	3	SN25 LN G/S vs. WT	<0.001	Yes	
	SN25 LN G/S	0.1381	0.0831	0.016	27	4	SN25 shift14aa vs. WT	<0.001	Yes	
	SN25 shift14aa	0.1652	0.1177	0.0251	22	3	SN25 LC G/S vs. WT	0.807	No	
	SN25 LC G/S	0.414	0.0914	0.0229	16	3				
rms noise	Label	Mean (pA/ms)	SD (pA/ms)	SEM (pA/ms)	n	Number of preps	Comparison	P	Significant	ANOVA
	SNAP-25 WT	4.3256	1.3794	0.1386	100	15 (pooled)	SN25 -cys vs. WT	<0.001	Yes	Tukey's post hoc
	SN25 -cys	2.6635	0.5391	0.1149	22	3	SN25 LN G/S vs. WT	<0.001	Yes	
	SN25 LN G/S	2.4399	0.6561	0.1263	27	4	SN25 shift14aa vs. WT	<0.001	Yes	
	SN25 shift14aa	2.4782	0.7721	0.1646	22	3	SN25 LC G/S vs. WT	0.999	No	
	SN25 LC G/S	4.4413	1.0285	0.2571	16	3				

References

Aalto, M.K., Ronne, H., and Keranen, S. (1993). Yeast syntaxins Sso1p and Sso2p belong to a family of related membrane proteins that function in vesicular transport. The EMBO journal *12*, 4095-4104.

Alberts, B., Johnson, A., Lewis, J., Morgan, D., Raff, M., Roberts, K., Walter, P., Wilson, J., Hunt, T., and Rosengarten Family, F. (2015). Molecular biology of the cell.

Amatore, C., Arbault, S., Bonifas, I., Guille, M., Lemaitre, F., and Verchier, Y. (2007). Relationship between amperometric pre-spike feet and secretion granule composition in chromaffin cells: an overview. Biophys Chem *129*, 181-189.

Amatore, C., Arbault, S., Guille, M., and Lemaitre, F. (2008). Electrochemical monitoring of single cell secretion: vesicular exocytosis and oxidative stress. Chemical reviews *108*, 2585-2621.

Ashery, U., Betz, A., Xu, T., Brose, N., and Rettig, J. (1999). An efficient method for infection of adrenal chromaffin cells using the Semliki Forest virus gene expression system. European journal of cell biology *78*, 525-532.

Barakauskas, V.E., Moradian, A., Barr, A.M., Beasley, C.L., Rosoklija, G., Mann, J.J., Ilievski, B., Stankov, A., Dwork, A.J., Falkai, P., *et al.* (2016). Quantitative mass spectrometry reveals changes in SNAP-25 isoforms in schizophrenia. Schizophr Res *177*, 44-51.

Bark, I.C., Hahn, K.M., Ryabinin, A.E., and Wilson, M.C. (1995). Differential expression of SNAP-25 protein isoforms during divergent vesicle fusion events of neural development. Proceedings of the National Academy of Sciences of the United States of America *92*, 1510-1514.

Bark, I.C., and Wilson, M.C. (1994). Human cDNA clones encoding two different isoforms of the nerve terminal protein SNAP-25. Gene *139*, 291-292.

Baumert, M., Maycox, P.R., Navone, F., De Camilli, P., and Jahn, R. (1989). Synaptobrevin: an integral membrane protein of 18,000 daltons present in small synaptic vesicles of rat brain. The EMBO journal *8*, 379-384.

Becherer, U., and Rettig, J. (2006). Vesicle pools, docking, priming, and release. Cell and tissue research *326*, 393-407.

Bennett, M.K., Calakos, N., and Scheller, R.H. (1992). Syntaxin: a synaptic protein implicated in docking of synaptic vesicles at presynaptic active zones. Science *257*, 255-259.

Bennett, M.K., Garcia-Arraras, J.E., Elferink, L.A., Peterson, K., Fleming, A.M., Hazuka, C.D., and Scheller, R.H. (1993). The syntaxin family of vesicular transport receptors. Cell *74*, 863-873.

Bhalla, A., Tucker, W.C., and Chapman, E.R. (2005). Synaptotagmin isoforms couple distinct ranges of Ca2+, Ba2+, and Sr2+ concentration to SNARE-mediated membrane fusion. Molecular biology of the cell *16*, 4755-4764.

Binz, T., Blasi, J., Yamasaki, S., Baumeister, A., Link, E., Sudhof, T.C., Jahn, R., and Niemann, H. (1994). Proteolysis of SNAP-25 by types E and A botulinal neurotoxins. The Journal of biological chemistry *269*, 1617-1620.

Blasi, J., Chapman, E.R., Link, E., Binz, T., Yamasaki, S., De Camilli, P., Sudhof, T.C., Niemann, H., and Jahn, R. (1993). Botulinum neurotoxin A selectively cleaves the synaptic protein SNAP-25. Nature *365*, 160-163.

Bock, L.V., Hutchings, B., Grubmuller, H., and Woodbury, D.J. (2010). Chemomechanical regulation of SNARE proteins studied with molecular dynamics simulations. Biophysical journal *99*, 1221-1230.

Borisovska, M., Schwarz, Y.N., Dhara, M., Yarzagaray, A., Hugo, S., Narzi, D., Siu, S.W., Kesavan, J., Mohrmann, R., Bockmann, R.A., *et al.* (2012). Membrane-proximal tryptophans of synaptobrevin II stabilize priming of secretory vesicles. The Journal of neuroscience : the official journal of the Society for Neuroscience *32*, 15983-15997.

Brinkmalm, A., Brinkmalm, G., Honer, W.G., Frolich, L., Hausner, L., Minthon, L., Hansson, O., Wallin, A., Zetterberg, H., Blennow, K., *et al.* (2014). SNAP-25 is a promising novel cerebrospinal fluid biomarker for synapse degeneration in Alzheimer's disease. Mol Neurodegener *9*, 53.

Broadie, K., Prokop, A., Bellen, H.J., O'Kane, C.J., Schulze, K.L., and Sweeney, S.T. (1995). Syntaxin and synaptobrevin function downstream of vesicle docking in Drosophila. Neuron *15*, 663-673.

Bronk, P., Deak, F., Wilson, M.C., Liu, X., Sudhof, T.C., and Kavalali, E.T. (2007). Differential effects of SNAP-25 deletion on Ca2+ -dependent and Ca2+ -independent neurotransmission. Journal of neurophysiology *98*, 794-806.

Brunger, A.T., Weninger, K., Bowen, M., and Chu, S. (2009). Single-molecule studies of the neuronal SNARE fusion machinery. Annu Rev Biochem *78*, 903-928.

Bruns, D. (2004). Detection of transmitter release with carbon fiber electrodes. Methods *33*, 312-321.

Bucher, E.S., and Wightman, R.M. (2015). Electrochemical Analysis of Neurotransmitters. Annual review of analytical chemistry *8*, 239-261.

Burgess, R.W., Deitcher, D.L., and Schwarz, T.L. (1997). The synaptic protein syntaxin1 is required for cellularization of Drosophila embryos. The Journal of cell biology *138*, 861-875.

Burkhardt, P., Hattendorf, D.A., Weis, W.I., and Fasshauer, D. (2008). Munc18a controls SNARE assembly through its interaction with the syntaxin N-peptide. The EMBO journal *27*, 923-933.

Carr, C.M., and Rizo, J. (2010). At the junction of SNARE and SM protein function. Curr Opin Cell Biol *22*, 488-495.

Cerezo, J.R., Jimenez, F., and Moya, F. (1995). Characterization and gene cloning of Drosophila syntaxin 1 (Dsynt1): the fruit fly homologue of rat syntaxin 1. Brain research Molecular brain research *29*, 245-252.

Chamberlain, L.H., Burgoyne, R.D., and Gould, G.W. (2001). SNARE proteins are highly enriched in lipid rafts in PC12 cells: implications for the spatial control of exocytosis. Proceedings of the National Academy of Sciences of the United States of America *98*, 5619-5624.

Chapman, E.R., An, S., Barton, N., and Jahn, R. (1994). SNAP-25, a t-SNARE which binds to both syntaxin and synaptobrevin via domains that may form coiled coils. The Journal of biological chemistry *269*, 27427-27432.

Chapman, E.R., Hanson, P.I., An, S., and Jahn, R. (1995). Ca2+ regulates the interaction between synaptotagmin and syntaxin 1. The Journal of biological chemistry *270*, 23667-23671.

Charvin, N., L'Eveque, C., Walker, D., Berton, F., Raymond, C., Kataoka, M., Shoji-Kasai, Y., Takahashi, M., De Waard, M., and Seagar, M.J. (1997). Direct interaction of the calcium sensor protein synaptotagmin I with a cytoplasmic domain of the alpha1A subunit of the P/Q-type calcium channel. The EMBO journal *16*, 4591-4596.

Chen, Y.A., Scales, S.J., Patel, S.M., Doung, Y.C., and Scheller, R.H. (1999). SNARE complex formation is triggered by Ca2+ and drives membrane fusion. Cell *97*, 165-174.

Chen, Y.A., Scales, S.J., and Scheller, R.H. (2001). Sequential SNARE assembly underlies priming and triggering of exocytosis. Neuron *30*, 161-170.

Chen, Y.A., and Scheller, R.H. (2001). SNARE-mediated membrane fusion. Nature reviews Molecular cell biology *2*, 98-106.

Cole, K.S. (1968). Membranes, ions, and impulses; a chapter of classical biophysics (Berkeley,: University of California Press).

Corradini, I., Donzelli, A., Antonucci, F., Welzl, H., Loos, M., Martucci, R., De Astis, S., Pattini, L., Inverardi, F., Wolfer, D., *et al.* (2014). Epileptiform activity and cognitive deficits in SNAP-25(+/-) mice are normalized by antiepileptic drugs. Cereb Cortex *24*, 364-376.

Dawidowski, D., and Cafiso, D.S. (2013). Allosteric control of syntaxin 1a by Munc18-1: characterization of the open and closed conformations of syntaxin. Biophysical journal *104*, 1585-1594.

Delgado-Martinez, I., Nehring, R.B., and Sorensen, J.B. (2007). Differential abilities of SNAP-25 homologs to support neuronal function. The Journal of neuroscience : the official journal of the Society for Neuroscience *27*, 9380-9391.

Delgrossi, M.H., Breuza, L., Mirre, C., Chavrier, P., and Le Bivic, A. (1997). Human syntaxin 3 is localized apically in human intestinal cells. Journal of cell science *110 (Pt 18)*, 2207-2214.

Dhara, M., Yarzagaray, A., Schwarz, Y., Dutta, S., Grabner, C., Moghadam, P.K., Bost, A., Schirra, C., Rettig, J., Reim, K., *et al.* (2014). Complexin synchronizes primed vesicle exocytosis and regulates fusion pore dynamics. The Journal of cell biology *204*, 1123-1140.

Dulubova, I., Sugita, S., Hill, S., Hosaka, M., Fernandez, I., Sudhof, T.C., and Rizo, J. (1999). A conformational switch in syntaxin during exocytosis: role of munc18. The EMBO journal *18*, 4372-4382.

Eguiagaray, J.G., Egea, J., Bravo-Cordero, J.J., and Garcia, A.G. (2004). [Neurotransmitters, calcium signalling and neuronal communication]. Neurocirugia *15*, 109-118.

Ellena, J.F., Liang, B., Wiktor, M., Stein, A., Cafiso, D.S., Jahn, R., and Tamm, L.K. (2009). Dynamic structure of lipid-bound synaptobrevin suggests a nucleation-propagation mechanism for trans-SNARE complex formation. Proceedings of the National Academy of Sciences of the United States of America *106*, 20306-20311.

Fasshauer, D., Antonin, W., Margittai, M., Pabst, S., and Jahn, R. (1999). Mixed and non-cognate SNARE complexes. Characterization of assembly and biophysical properties. The Journal of biological chemistry *274*, 15440-15446.

Fasshauer, D., Eliason, W.K., Brunger, A.T., and Jahn, R. (1998a). Identification of a minimal core of the synaptic SNARE complex sufficient for reversible assembly and disassembly. Biochemistry *37*, 10354-10362.

Fasshauer, D., and Margittai, M. (2004). A transient N-terminal interaction of SNAP-25 and syntaxin nucleates SNARE assembly. The Journal of biological chemistry *279*, 7613-7621.

Fasshauer, D., Sutton, R.B., Brunger, A.T., and Jahn, R. (1998b). Conserved structural features of the synaptic fusion complex: SNARE proteins reclassified as Q- and R-SNAREs. Proceedings of the National Academy of Sciences of the United States of America *95*, 15781-15786.

Fdez, E., Jowitt, T.A., Wang, M.C., Rajebhosale, M., Foster, K., Bella, J., Baldock, C., Woodman, P.G., and Hilfiker, S. (2008). A role for soluble N-ethylmaleimide-sensitive factor attachment protein receptor complex dimerization during neurosecretion. Molecular biology of the cell *19*, 3379-3389.

Fleming, K.G., Hohl, T.M., Yu, R.C., Muller, S.A., Wolpensinger, B., Engel, A., Engelhardt, H., Brunger, A.T., Sollner, T.H., and Hanson, P.I. (1998). A revised model for the oligomeric state of the N-ethylmaleimide-sensitive fusion protein, NSF. The Journal of biological chemistry *273*, 15675-15681.

Foley, T.D., Clark, A.R., Stredny, E.S., and Wierbowski, B.M. (2012). SNAP-25 contains non-acylated thiol pairs that can form intrachain disulfide bonds: possible sites for redox modulation of neurotransmission. Cell Mol Neurobiol *32*, 201-208.

Fujita, Y., Shirataki, H., Sakisaka, T., Asakura, T., Ohya, T., Kotani, H., Yokoyama, S., Nishioka, H., Matsuura, Y., Mizoguchi, A., *et al.* (1998). Tomosyn: a syntaxin-1-binding protein that forms a novel complex in the neurotransmitter release process. Neuron *20*, 905-915.

Fukuda, R., McNew, J.A., Weber, T., Parlati, F., Engel, T., Nickel, W., Rothman, J.E., and Sollner, T.H. (2000). Functional architecture of an intracellular membrane t-SNARE. Nature *407*, 198-202.

Gaisano, H.Y., Sheu, L., Foskett, J.K., and Trimble, W.S. (1994). Tetanus toxin light chain cleaves a vesicle-associated membrane protein (VAMP) isoform 2 in rat pancreatic zymogen granules and inhibits enzyme secretion. The Journal of biological chemistry *269*, 17062-17066.

Galli, C., Piccini, A., Ciotti, M.T., Castellani, L., Calissano, P., Zaccheo, D., and Tabaton, M. (1998). Increased amyloidogenic secretion in cerebellar granule cells undergoing apoptosis. Proceedings of the National Academy of Sciences of the United States of America *95*, 1247-1252.

Gao, Y., Zorman, S., Gundersen, G., Xi, Z., Ma, L., Sirinakis, G., Rothman, J.E., and Zhang, Y. (2012). Single reconstituted neuronal SNARE complexes zipper in three distinct stages. Science *337*, 1340-1343.

Garcia-Martinez, V., Montes, M.A., Villanueva, J., Gimenez-Molina, Y., de Toledo, G.A., and Gutierrez, L.M. (2015). Sphingomyelin derivatives increase the frequency of microvesicle and granule fusion in chromaffin cells. Neuroscience *295*, 117-125.

Garcia-Palomero, E., Cuchillo-Ibanez, I., Garcia, A.G., Renart, J., Albillos, A., and Montiel, C. (2000). Greater diversity than previously thought of chromaffin cell Ca2+ channels, derived from mRNA identification studies. FEBS letters *481*, 235-239.

Geppert, M., Archer, B.T., 3rd, and Sudhof, T.C. (1991). Synaptotagmin II. A novel differentially distributed form of synaptotagmin. The Journal of biological chemistry *266*, 13548-13552.

Gerst, J.E. (1997). Conserved alpha-helical segments on yeast homologs of the synaptobrevin/VAMP family of v-SNAREs mediate exocytic function. The Journal of biological chemistry *272*, 16591-16598.

Gerst, J.E. (1999). SNAREs and SNARE regulators in membrane fusion and exocytosis. Cellular and molecular life sciences : CMLS *55*, 707-734.

Gerst, J.E., Rodgers, L., Riggs, M., and Wigler, M. (1992). SNC1, a yeast homolog of the synaptic vesicle-associated membrane protein/synaptobrevin gene family: genetic interactions with the RAS and CAP genes. Proceedings of the National Academy of Sciences of the United States of America *89*, 4338-4342.

Gonelle-Gispert, C., Molinete, M., Halban, P.A., and Sadoul, K. (2000). Membrane localization and biological activity of SNAP-25 cysteine mutants in insulin-secreting cells. Journal of cell science *113 (Pt 18)*, 3197-3205.

Gonzalo, S., and Linder, M.E. (1998). SNAP-25 palmitoylation and plasma membrane targeting require a functional secretory pathway. Molecular biology of the cell *9*, 585-597.

Greaves, J., Gorleku, O.A., Salaun, C., and Chamberlain, L.H. (2010a). Palmitoylation of the SNAP25 protein family: specificity and regulation by DHHC palmitoyl transferases. The Journal of biological chemistry *285*, 24629-24638.

Greaves, J., Prescott, G.R., Fukata, Y., Fukata, M., Salaun, C., and Chamberlain, L.H. (2009). The hydrophobic cysteine-rich domain of SNAP25 couples with downstream residues to mediate membrane interactions and recognition by DHHC palmitoyl transferases. Molecular biology of the cell *20*, 1845-1854.

Greaves, J., Prescott, G.R., Gorleku, O.A., and Chamberlain, L.H. (2010b). Regulation of SNAP-25 trafficking and function by palmitoylation. Biochem Soc Trans *38*, 163-166.

Grote, E., Hao, J.C., Bennett, M.K., and Kelly, R.B. (1995). A targeting signal in VAMP regulating transport to synaptic vesicles. Cell *81*, 581-589.

Guerini, F.R., Agliardi, C., Sironi, M., Arosio, B., Calabrese, E., Zanzottera, M., Bolognesi, E., Ricci, C., Costa, A.S., Galimberti, D., *et al.* (2014). Possible association between SNAP-25 single nucleotide polymorphisms and alterations of categorical fluency and functional MRI parameters in Alzheimer's disease. J Alzheimers Dis *42*, 1015-1028.

Guo, Z., Turner, C., and Castle, D. (1998). Relocation of the t-SNARE SNAP-23 from lamellipodia-like cell surface projections regulates compound exocytosis in mast cells. Cell *94*, 537-548.

Hanson, P.I., Roth, R., Morisaki, H., Jahn, R., and Heuser, J.E. (1997). Structure and conformational changes in NSF and its membrane receptor complexes visualized by quick-freeze/deep-etch electron microscopy. Cell *90*, 523-535.

Hayashi, T., McMahon, H., Yamasaki, S., Binz, T., Hata, Y., Sudhof, T.C., and Niemann, H. (1994). Synaptic vesicle membrane fusion complex: action of clostridial neurotoxins on assembly. The EMBO journal *13*, 5051-5061.

Hess, D.T., Slater, T.M., Wilson, M.C., and Skene, J.H. (1992). The 25 kDa synaptosomal-associated protein SNAP-25 is the major methionine-rich polypeptide in rapid axonal transport and a major substrate for palmitoylation in adult CNS. The Journal of neuroscience : the official journal of the Society for Neuroscience *12*, 4634-4641.

Inoue, A., Obata, K., and Akagawa, K. (1992). Cloning and sequence analysis of cDNA for a neuronal cell membrane antigen, HPC-1. The Journal of biological chemistry *267*, 10613-10619.

Ivanov, A.I. (2014). Exocytosis and Endocytosis (New York (N.Y.): Springer : Humana Press).

Jackson, M.B. (2010). SNARE complex zipping as a driving force in the dilation of proteinaceous fusion pores. J Membr Biol *235*, 89-100.

Jahn, R., and Fasshauer, D. (2012). Molecular machines governing exocytosis of synaptic vesicles. Nature *490*, 201-207.

Jahn, R., Lang, T., and Sudhof, T.C. (2003). Membrane fusion. Cell *112*, 519-533.

Jahn, R., and Scheller, R.H. (2006). SNAREs--engines for membrane fusion. Nature reviews Molecular cell biology *7*, 631-643.

Jahn, R., and Sudhof, T.C. (1999). Membrane fusion and exocytosis. Annu Rev Biochem *68*, 863-911.

Jeans, A.F., Oliver, P.L., Johnson, R., Capogna, M., Vikman, J., Molnar, Z., Babbs, A., Partridge, C.J., Salehi, A., Bengtsson, M., *et al.* (2007). A dominant mutation in Snap25 causes impaired vesicle trafficking, sensorimotor gating, and ataxia in the blind-drunk mouse. Proceedings of the National Academy of Sciences of the United States of America *104*, 2431-2436.

Jiang, X., Zhang, Z., Cheng, K., Wu, Q., Jiang, L., Pielak, G.J., Liu, M., and Li, C. (2019). Membrane-mediated disorder-to-order transition of SNAP25 flexible linker facilitates its interaction with syntaxin-1 and SNARE-complex assembly. FASEB J, fj201802796R.

Jockusch, W.J., Speidel, D., Sigler, A., Sorensen, J.B., Varoqueaux, F., Rhee, J.S., and Brose, N. (2007). CAPS-1 and CAPS-2 are essential synaptic vesicle priming proteins. Cell *131*, 796-808.

Karp, G. (2013). Cell and molecular biology concepts and experiments (Hoboken: J. Wiley).

Kee, Y., Lin, R.C., Hsu, S.C., and Scheller, R.H. (1995). Distinct domains of syntaxin are required for synaptic vesicle fusion complex formation and dissociation. Neuron *14*, 991-998.

Kesavan, J., Borisovska, M., and Bruns, D. (2007). v-SNARE actions during Ca(2+)-triggered exocytosis. Cell *131*, 351-363.

Kloepper, T.H., Kienle, C.N., and Fasshauer, D. (2007). An elaborate classification of SNARE proteins sheds light on the conservation of the eukaryotic endomembrane system. Molecular biology of the cell *18*, 3463-3471.

Kyoung, M., Srivastava, A., Zhang, Y., Diao, J., Vrljic, M., Grob, P., Nogales, E., Chu, S., and Brunger, A.T. (2011). In vitro system capable of differentiating fast Ca2+-triggered content mixing from lipid exchange for mechanistic studies of neurotransmitter release. Proceedings of the National Academy of Sciences of the United States of America *108*, E304-313.

Land, J., Zhang, H., Vaidyanathan, V.V., Sadoul, K., Niemann, H., and Wollheim, C.B. (1997). Transient expression of botulinum neurotoxin C1 light chain differentially inhibits calcium and glucose induced insulin secretion in clonal beta-cells. FEBS letters *419*, 13-17.

Lang, T., Bruns, D., Wenzel, D., Riedel, D., Holroyd, P., Thiele, C., and Jahn, R. (2001). SNAREs are concentrated in cholesterol-dependent clusters that define docking and fusion sites for exocytosis. The EMBO journal *20*, 2202-2213.

Leung, S.M., Chen, D., DasGupta, B.R., Whiteheart, S.W., and Apodaca, G. (1998). SNAP-23 requirement for transferrin recycling in Streptolysin-O-permeabilized Madin-Darby canine kidney cells. The Journal of biological chemistry *273*, 17732-17741.

Leveque, C., el Far, O., Martin-Moutot, N., Sato, K., Kato, R., Takahashi, M., and Seagar, M.J. (1994). Purification of the N-type calcium channel associated with syntaxin and synaptotagmin. A complex implicated in synaptic vesicle exocytosis. The Journal of biological chemistry *269*, 6306-6312.

Li, C., Takei, K., Geppert, M., Daniell, L., Stenius, K., Chapman, E.R., Jahn, R., De Camilli, P., and Sudhof, T.C. (1994). Synaptic targeting of rabphilin-3A, a synaptic vesicle Ca2+/phospholipid-binding protein, depends on rab3A/3C. Neuron *13*, 885-898.

Liu, Y., and Barlowe, C. (2002). Analysis of Sec22p in endoplasmic reticulum/Golgi transport reveals cellular redundancy in SNARE protein function. Molecular biology of the cell *13*, 3314-3324.

Lu, B. (2015). The destructive effect of botulinum neurotoxins on the SNARE protein: SNAP-25 and synaptic membrane fusion. PeerJ *3*, e1065.

Ma, C., Li, W., Xu, Y., and Rizo, J. (2011). Munc13 mediates the transition from the closed syntaxin-Munc18 complex to the SNARE complex. Nat Struct Mol Biol *18*, 542-549.

Ma, C., Su, L., Seven, A.B., Xu, Y., and Rizo, J. (2013). Reconstitution of the vital functions of Munc18 and Munc13 in neurotransmitter release. Science *339*, 421-425.

Mandon, B., Chou, C.L., Nielsen, S., and Knepper, M.A. (1996). Syntaxin-4 is localized to the apical plasma membrane of rat renal collecting duct cells: possible role in aquaporin-2 trafficking. The Journal of clinical investigation *98*, 906-913.

Margittai, M., Fasshauer, D., Pabst, S., Jahn, R., and Langen, R. (2001). Homo- and heterooligomeric SNARE complexes studied by site-directed spin labeling. The Journal of biological chemistry *276*, 13169-13177.

McMahon, H.T., Ushkaryov, Y.A., Edelmann, L., Link, E., Binz, T., Niemann, H., Jahn, R., and Sudhof, T.C. (1993). Cellubrevin is a ubiquitous tetanus-toxin substrate homologous to a putative synaptic vesicle fusion protein. Nature *364*, 346-349.

Misonou, H., Ohara-Imaizumi, M., and Kumakura, K. (1997). Regulation of the priming of exocytosis and the dissociation of SNAP-25 and VAMP-2 in adrenal chromaffin cells. Neuroscience letters *232*, 182-184.

Misura, K.M., Scheller, R.H., and Weis, W.I. (2000). Three-dimensional structure of the neuronal-Sec1-syntaxin 1a complex. Nature *404*, 355-362.

Mizuta, M., Inagaki, N., Nemoto, Y., Matsukura, S., Takahashi, M., and Seino, S. (1994). Synaptotagmin III is a novel isoform of rat synaptotagmin expressed in endocrine and neuronal cells. The Journal of biological chemistry *269*, 11675-11678.

Mohrmann, R., de Wit, H., Connell, E., Pinheiro, P.S., Leese, C., Bruns, D., Davletov, B., Verhage, M., and Sorensen, J.B. (2013). Synaptotagmin interaction with SNAP-25 governs vesicle docking, priming, and fusion triggering. The Journal of neuroscience : the official journal of the Society for Neuroscience *33*, 14417-14430.

Mohrmann, R., de Wit, H., Verhage, M., Neher, E., and Sorensen, J.B. (2010). Fast vesicle fusion in living cells requires at least three SNARE complexes. Science *330*, 502-505.

Mohrmann, R., and Sorensen, J.B. (2012). SNARE requirements en route to exocytosis: from many to few. J Mol Neurosci *48*, 387-394.

Montana, V., Liu, W., Mohideen, U., and Parpura, V. (2008). Single Molecule Probing of Exocytotic Protein Interactions Using Force Spectroscopy. Croat Chem Acta *81*, 31.

Montana, V., Liu, W., Mohideen, U., and Parpura, V. (2009). Single molecule measurements of mechanical interactions within ternary SNARE complexes and dynamics of their disassembly: SNAP25 vs. SNAP23. J Physiol *587*, 1943-1960.

Mundroff, M.L., and Wightman, R.M. (2002). Amperometry and cyclic voltammetry with carbon fiber microelectrodes at single cells. Current protocols in neuroscience *Chapter 6*, Unit 6 14.

Nagy, G., Milosevic, I., Fasshauer, D., Muller, E.M., de Groot, B.L., Lang, T., Wilson, M.C., and Sorensen, J.B. (2005). Alternative splicing of SNAP-25 regulates secretion through nonconservative substitutions in the SNARE domain. Molecular biology of the cell *16*, 5675-5685.

Nagy, G., Milosevic, I., Mohrmann, R., Wiederhold, K., Walter, A.M., and Sorensen, J.B. (2008). The SNAP-25 linker as an adaptation toward fast exocytosis. Molecular biology of the cell *19*, 3769-3781.

Nagy, G., Reim, K., Matti, U., Brose, N., Binz, T., Rettig, J., Neher, E., and Sorensen, J.B. (2004). Regulation of releasable vesicle pool sizes by protein kinase A-dependent phosphorylation of SNAP-25. Neuron *41*, 417-429.

Neher, E., and Marty, A. (1982). Discrete changes of cell membrane capacitance observed under conditions of enhanced secretion in bovine adrenal chromaffin cells. Proceedings of the National Academy of Sciences of the United States of America *79*, 6712-6716.

Nguyen Truong, C.Q., Nestvogel, D., Ratai, O., Schirra, C., Stevens, D.R., Brose, N., Rhee, J., and Rettig, J. (2014). Secretory vesicle priming by CAPS is independent of its SNARE-binding MUN domain. Cell reports *9*, 902-909.

Nicholson, K.L., Munson, M., Miller, R.B., Filip, T.J., Fairman, R., and Hughson, F.M. (1998). Regulation of SNARE complex assembly by an N-terminal domain of the t-SNARE Sso1p. Nature structural biology *5*, 793-802.

Novick, P., Field, C., and Schekman, R. (1980). Identification of 23 complementation groups required for post-translational events in the yeast secretory pathway. Cell *21*, 205-215.

Orita, S., Sasaki, T., Naito, A., Komuro, R., Ohtsuka, T., Maeda, M., Suzuki, H., Igarashi, H., and Takai, Y. (1995). Doc2: a novel brain protein having two repeated C2-like domains. Biochemical and biophysical research communications *206*, 439-448.

Oyler, G.A., Higgins, G.A., Hart, R.A., Battenberg, E., Billingsley, M., Bloom, F.E., and Wilson, M.C. (1989). The identification of a novel synaptosomal-associated protein, SNAP-25, differentially expressed by neuronal subpopulations. The Journal of cell biology *109*, 3039-3052.

Pabst, S., Margittai, M., Vainius, D., Langen, R., Jahn, R., and Fasshauer, D. (2002). Rapid and selective binding to the synaptic SNARE complex suggests a modulatory role of complexins in neuroexocytosis. The Journal of biological chemistry *277*, 7838-7848.

Parlati, F., Weber, T., McNew, J.A., Westermann, B., Sollner, T.H., and Rothman, J.E. (1999). Rapid and efficient fusion of phospholipid vesicles by the alpha-helical core of a SNARE complex in the absence of an N-terminal regulatory domain. Proceedings of the National Academy of Sciences of the United States of America *96*, 12565-12570.

Perin, M.S., Brose, N., Jahn, R., and Sudhof, T.C. (1991). Domain structure of synaptotagmin (p65). The Journal of biological chemistry *266*, 623-629.

Petrenko, A.G., Perin, M.S., Davletov, B.A., Ushkaryov, Y.A., Geppert, M., and Sudhof, T.C. (1991). Binding of synaptotagmin to the alpha-latrotoxin receptor implicates both in synaptic vesicle exocytosis. Nature *353*, 65-68.

Pinheiro, P.S., de Wit, H., Walter, A.M., Groffen, A.J., Verhage, M., and Sorensen, J.B. (2013). Doc2b synchronizes secretion from chromaffin cells by stimulating fast and inhibiting sustained release. The Journal of neuroscience : the official journal of the Society for Neuroscience *33*, 16459-16470.

Pitzurra, L., Rossetto, O., Chimienti, A.R., Blasi, E., and Bistoni, F. (1996). Tetanus toxin-sensitive VAMP-related proteins are present in murine macrophages. Cellular immunology *169*, 113-116.

Pobbati, A.V., Stein, A., and Fasshauer, D. (2006). N- to C-terminal SNARE complex assembly promotes rapid membrane fusion. Science *313*, 673-676.

Poirier, M.A., Xiao, W., Macosko, J.C., Chan, C., Shin, Y.K., and Bennett, M.K. (1998). The synaptic SNARE complex is a parallel four-stranded helical bundle. Nature structural biology *5*, 765-769.

Prekeris, R., Yang, B., Oorschot, V., Klumperman, J., and Scheller, R.H. (1999). Differential roles of syntaxin 7 and syntaxin 8 in endosomal trafficking. Molecular biology of the cell *10*, 3891-3908.

Prescott, G.R., and Chamberlain, L.H. (2011). Regional and developmental brain expression patterns of SNAP25 splice variants. BMC Neurosci *12*, 35.

Ravichandran, V., Chawla, A., and Roche, P.A. (1996). Identification of a novel syntaxin- and synaptobrevin/VAMP-binding protein, SNAP-23, expressed in non-neuronal tissues. The Journal of biological chemistry *271*, 13300-13303.

Regazzi, R., Sadoul, K., Meda, P., Kelly, R.B., Halban, P.A., and Wollheim, C.B. (1996). Mutational analysis of VAMP domains implicated in Ca2+-induced insulin exocytosis. The EMBO journal *15*, 6951-6959.

Ren, Q., Barber, H.K., Crawford, G.L., Karim, Z.A., Zhao, C., Choi, W., Wang, C.C., Hong, W., and Whiteheart, S.W. (2007). Endobrevin/VAMP-8 is the primary v-SNARE for the platelet release reaction. Molecular biology of the cell *18*, 24-33.

Rettig, J., and Neher, E. (2002). Emerging roles of presynaptic proteins in Ca++-triggered exocytosis. Science *298*, 781-785.

Rickman, C., Archer, D.A., Meunier, F.A., Craxton, M., Fukuda, M., Burgoyne, R.D., and Davletov, B. (2004). Synaptotagmin interaction with the syntaxin/SNAP-25 dimer is mediated by an evolutionarily conserved motif and is sensitive to inositol hexakisphosphate. The Journal of biological chemistry *279*, 12574-12579.

Rizo, J., and Sudhof, T.C. (2002). Snares and Munc18 in synaptic vesicle fusion. Nat Rev Neurosci *3*, 641-653.

Rossetto, O., Gorza, L., Schiavo, G., Schiavo, N., Scheller, R.H., and Montecucco, C. (1996). VAMP/synaptobrevin isoforms 1 and 2 are widely and differentially expressed in nonneuronal tissues. The Journal of cell biology *132*, 167-179.

Rossi, G., Salminen, A., Rice, L.M., Brunger, A.T., and Brennwald, P. (1997). Analysis of a yeast SNARE complex reveals remarkable similarity to the neuronal SNARE complex and a novel function for the C terminus of the SNAP-25 homolog, Sec9. The Journal of biological chemistry *272*, 16610-16617.

Rothman, J.E. (1994). Mechanisms of intracellular protein transport. Nature *372*, 55-63.

Sadoul, K., Lang, J., Montecucco, C., Weller, U., Regazzi, R., Catsicas, S., Wollheim, C.B., and Halban, P.A. (1995). SNAP-25 is expressed in islets of Langerhans and is involved in insulin release. The Journal of cell biology *128*, 1019-1028.

Saifee, O., Wei, L., and Nonet, M.L. (1998). The Caenorhabditis elegans unc-64 locus encodes a syntaxin that interacts genetically with synaptobrevin. Molecular biology of the cell *9*, 1235-1252.

Salaun, C., Gould, G.W., and Chamberlain, L.H. (2005). The SNARE proteins SNAP-25 and SNAP-23 display different affinities for lipid rafts in PC12 cells. Regulation by distinct cysteine-rich domains. The Journal of biological chemistry *280*, 1236-1240.

Schiavo, G., Gu, Q.M., Prestwich, G.D., Sollner, T.H., and Rothman, J.E. (1996). Calcium-dependent switching of the specificity of phosphoinositide binding to synaptotagmin. Proceedings of the National Academy of Sciences of the United States of America *93*, 13327-13332.

Schiavo, G., Rossetto, O., Catsicas, S., Polverino de Laureto, P., DasGupta, B.R., Benfenati, F., and Montecucco, C. (1993). Identification of the nerve terminal targets of botulinum neurotoxin serotypes A, D, and E. The Journal of biological chemistry *268*, 23784-23787.

Schiavo, G., Stenbeck, G., Rothman, J.E., and Sollner, T.H. (1997). Binding of the synaptic vesicle v-SNARE, synaptotagmin, to the plasma membrane t-SNARE, SNAP-25, can explain docked vesicles at neurotoxin-treated synapses. Proceedings of the National Academy of Sciences of the United States of America *94*, 997-1001.

Schoch, S., Deak, F., Konigstorfer, A., Mozhayeva, M., Sara, Y., Sudhof, T.C., and Kavalali, E.T. (2001). SNARE function analyzed in synaptobrevin/VAMP knockout mice. Science *294*, 1117-1122.

Schonn, J.S., Maximov, A., Lao, Y., Sudhof, T.C., and Sorensen, J.B. (2008). Synaptotagmin-1 and -7 are functionally overlapping Ca2+ sensors for exocytosis in adrenal chromaffin cells. Proceedings of the National Academy of Sciences of the United States of America *105*, 3998-4003.

Schuette, C.G., Hatsuzawa, K., Margittai, M., Stein, A., Riedel, D., Kuster, P., Konig, M., Seidel, C., and Jahn, R. (2004). Determinants of liposome fusion mediated by synaptic SNARE proteins. Proceedings of the National Academy of Sciences of the United States of America *101*, 2858-2863.

Schulze, K.L., Broadie, K., Perin, M.S., and Bellen, H.J. (1995). Genetic and electrophysiological studies of Drosophila syntaxin-1A demonstrate its role in nonneuronal secretion and neurotransmission. Cell *80*, 311-320.

Schwarz, Y., Zhao, N., Kirchhoff, F., and Bruns, D. (2017). Astrocytes control synaptic strength by two distinct v-SNARE-dependent release pathways. Nature neuroscience *20*, 1529-1539.

Shaaban, A., Dhara, M., Frisch, W., Harb, A., Shaib, A.H., Becherer, U., Bruns, D., and Mohrmann, R. (2019). The SNAP-25 linker supports fusion intermediates by local lipid interactions. Elife *8*.

Sharma, M., Burre, J., Bronk, P., Zhang, Y., Xu, W., and Sudhof, T.C. (2012). CSPalpha knockout causes neurodegeneration by impairing SNAP-25 function. The EMBO journal *31*, 829-841.

Shi, L., Shen, Q.T., Kiel, A., Wang, J., Wang, H.W., Melia, T.J., Rothman, J.E., and Pincet, F. (2012). SNARE proteins: one to fuse and three to keep the nascent fusion pore open. Science *335*, 1355-1359.

Shukla, A., Corydon, T.J., Nielsen, S., Hoffmann, H.J., and Dahl, R. (2001). Identification of three new splice variants of the SNARE protein SNAP-23. Biochemical and biophysical research communications *285*, 320-327.

Sigworth, F.J., and Neher, E. (1980). Single Na+ channel currents observed in cultured rat muscle cells. Nature *287*, 447-449.

Sinha, R., Ahmed, S., Jahn, R., and Klingauf, J. (2011). Two synaptobrevin molecules are sufficient for vesicle fusion in central nervous system synapses. Proceedings of the National Academy of Sciences of the United States of America *108*, 14318-14323.

Sollner, T., Bennett, M.K., Whiteheart, S.W., Scheller, R.H., and Rothman, J.E. (1993a). A protein assembly-disassembly pathway in vitro that may correspond to sequential steps of synaptic vesicle docking, activation, and fusion. Cell *75*, 409-418.

Sollner, T., Whiteheart, S.W., Brunner, M., Erdjument-Bromage, H., Geromanos, S., Tempst, P., and Rothman, J.E. (1993b). SNAP receptors implicated in vesicle targeting and fusion. Nature *362*, 318-324.

Sorensen, J.B., Nagy, G., Varoqueaux, F., Nehring, R.B., Brose, N., Wilson, M.C., and Neher, E. (2003). Differential control of the releasable vesicle pools by SNAP-25 splice variants and SNAP-23. Cell *114*, 75-86.

Sorensen, J.B., Wiederhold, K., Muller, E.M., Milosevic, I., Nagy, G., de Groot, B.L., Grubmuller, H., and Fasshauer, D. (2006). Sequential N- to C-terminal SNARE complex assembly drives priming and fusion of secretory vesicles. The EMBO journal *25*, 955-966.

Stein, A., Weber, G., Wahl, M.C., and Jahn, R. (2009). Helical extension of the neuronal SNARE complex into the membrane. Nature *460*, 525-528.

Sudhof, T.C., Baumert, M., Perin, M.S., and Jahn, R. (1989). A synaptic vesicle membrane protein is conserved from mammals to Drosophila. Neuron *2*, 1475-1481.

Sudhof, T.C., and Rizo, J. (2011). Synaptic vesicle exocytosis. Cold Spring Harbor perspectives in biology *3*.

Sutton, R.B., Fasshauer, D., Jahn, R., and Brunger, A.T. (1998). Crystal structure of a SNARE complex involved in synaptic exocytosis at 2.4 A resolution. Nature *395*, 347-353.

Suudhof, T.C. (2008). Neurotransmitter release. Handbook of experimental pharmacology, 1-21.

Trimble, W.S., Cowan, D.M., and Scheller, R.H. (1988). VAMP-1: a synaptic vesicle-associated integral membrane protein. Proceedings of the National Academy of Sciences of the United States of America *85*, 4538-4542.

Trimble, W.S., Gray, T.S., Elferink, L.A., Wilson, M.C., and Scheller, R.H. (1990). Distinct patterns of expression of two VAMP genes within the rat brain. The Journal of neuroscience : the official journal of the Society for Neuroscience *10*, 1380-1387.

Tucker, W.C., Weber, T., and Chapman, E.R. (2004). Reconstitution of Ca2+-regulated membrane fusion by synaptotagmin and SNAREs. Science *304*, 435-438.

Ubach, J., Zhang, X., Shao, X., Sudhof, T.C., and Rizo, J. (1998). Ca2+ binding to synaptotagmin: how many Ca2+ ions bind to the tip of a C2-domain? The EMBO journal *17*, 3921-3930.

Veit, M., Sollner, T.H., and Rothman, J.E. (1996). Multiple palmitoylation of synaptotagmin and the t-SNARE SNAP-25. FEBS letters *385*, 119-123.

Voets, T. (2000). Dissection of three Ca2+-dependent steps leading to secretion in chromaffin cells from mouse adrenal slices. Neuron *28*, 537-545.

Voets, T., Neher, E., and Moser, T. (1999). Mechanisms underlying phasic and sustained secretion in chromaffin cells from mouse adrenal slices. Neuron *23*, 607-615.

Walter, A.M., Wiederhold, K., Bruns, D., Fasshauer, D., and Sorensen, J.B. (2010). Synaptobrevin N-terminally bound to syntaxin-SNAP-25 defines the primed vesicle state in regulated exocytosis. The Journal of cell biology *188*, 401-413.

Wang, L., Bittner, M.A., Axelrod, D., and Holz, R.W. (2008). The structural and functional implications of linked SNARE motifs in SNAP25. Molecular biology of the cell *19*, 3944-3955.

Wang, W., Zhang, S.H., Li, L.M., Wang, Z.L., Cheng, J.K., and Huang, W.H. (2009). Monitoring of vesicular exocytosis from single cells using micrometer and nanometer-sized electrochemical sensors. Analytical and bioanalytical chemistry *394*, 17-32.

Wang, Y., Dulubova, I., Rizo, J., and Sudhof, T.C. (2001). Functional analysis of conserved structural elements in yeast syntaxin Vam3p. The Journal of biological chemistry *276*, 28598-28605.

Washbourne, P., Cansino, V., Mathews, J.R., Graham, M., Burgoyne, R.D., and Wilson, M.C. (2001). Cysteine residues of SNAP-25 are required for SNARE disassembly and exocytosis, but not for membrane targeting. The Biochemical journal *357*, 625-634.

Washbourne, P., Thompson, P.M., Carta, M., Costa, E.T., Mathews, J.R., Lopez-Bendito, G., Molnar, Z., Becher, M.W., Valenzuela, C.F., Partridge, L.D., *et al.* (2002). Genetic ablation of the t-SNARE SNAP-25 distinguishes mechanisms of neuroexocytosis. Nature neuroscience *5*, 19-26.

Weber, J.P., Reim, K., and Sorensen, J.B. (2010). Opposing functions of two sub-domains of the SNARE-complex in neurotransmission. The EMBO journal *29*, 2477-2490.

Weber, J.P., Toft-Bertelsen, T.L., Mohrmann, R., Delgado-Martinez, I., and Sorensen, J.B. (2014). Synaptotagmin-7 is an asynchronous calcium sensor for synaptic transmission in neurons expressing SNAP-23. PloS one *9*, e114033.

Weber, P., Batoulis, H., Rink, K.M., Dahlhoff, S., Pinkwart, K., Sollner, T.H., and Lang, T. (2017). Electrostatic anchoring precedes stable membrane attachment of SNAP25/SNAP23 to the plasma membrane. Elife *6*.

Weber, T., Zemelman, B.V., McNew, J.A., Westermann, B., Gmachl, M., Parlati, F., Sollner, T.H., and Rothman, J.E. (1998). SNAREpins: minimal machinery for membrane fusion. Cell *92*, 759-772.

Weimbs, T., Low, S.H., Chapin, S.J., Mostov, K.E., Bucher, P., and Hofmann, K. (1997). A conserved domain is present in different families of vesicular fusion proteins: a new superfamily. Proceedings of the National Academy of Sciences of the United States of America *94*, 3046-3051.

Weimbs, T., Mostov, K., Low, S.H., and Hofmann, K. (1998). A model for structural similarity between different SNARE complexes based on sequence relationships. Trends in cell biology *8*, 260-262.

Weninger, K., Bowen, M.E., Choi, U.B., Chu, S., and Brunger, A.T. (2008). Accessory proteins stabilize the acceptor complex for synaptobrevin, the 1:1 syntaxin/SNAP-25 complex. Structure *16*, 308-320.

White, K.I., Zhao, M., Choi, U.B., Pfuetzner, R.A., and Brunger, A.T. (2018). Structural principles of SNARE complex recognition by the AAA+ protein NSF. Elife *7*.

Wiederhold, K., and Fasshauer, D. (2009). Is assembly of the SNARE complex enough to fuel membrane fusion? The Journal of biological chemistry *284*, 13143-13152.

Wilson, J.H., and Hunt, T. (2015). Molecular biology of the cell : the problems book (New York, NY; Abingdon, UK: Garland Science).

Xu, T., Rammner, B., Margittai, M., Artalejo, A.R., Neher, E., and Jahn, R. (1999). Inhibition of SNARE complex assembly differentially affects kinetic components of exocytosis. Cell *99*, 713-722.

Yamasaki, S., Baumeister, A., Binz, T., Blasi, J., Link, E., Cornille, F., Roques, B., Fykse, E.M., Sudhof, T.C., Jahn, R., *et al.* (1994). Cleavage of members of the synaptobrevin/VAMP family by types D and F botulinal neurotoxins and tetanus toxin. The Journal of biological chemistry *269*, 12764-12772.

Zhang, H., Zhu, S., Zhu, Y., Chen, J., Zhang, G., and Chang, H. (2011). An association study between SNAP-25 gene and attention-deficit hyperactivity disorder. Eur J Paediatr Neurol *15*, 48-52.

Zhang, X., Rebane, A.A., Ma, L., Li, F., Jiao, J., Qu, H., Pincet, F., Rothman, J.E., and Zhang, Y. (2016). Stability, folding dynamics, and long-range conformational transition of the synaptic t-SNARE complex. Proceedings of the National Academy of Sciences of the United States of America *113*, E8031-E8040.

Zhao, Y., Fang, Q., Herbst, A.D., Berberian, K.N., Almers, W., and Lindau, M. (2013). Rapid structural change in synaptosomal-associated protein 25 (SNAP25) precedes the fusion of single vesicles with the plasma membrane in live chromaffin cells. Proceedings of the National Academy of Sciences of the United States of America *110*, 14249-14254.

List of Publications

Haas, M., **Shaaban, A.**, and Reiser, G. (2014). Alanine-(87)-threonine polymorphism impairs signaling and internalization of the human P2Y11 receptor, when co-expressed with the P2Y1 receptor. J Neurochem *129*, 602-613.

Dhara, M., Yarzagaray, A., Makke, M., Schindeldecker, B., Schwarz, Y., **Shaaban, A.**, Sharma, S., Bockmann, R.A., Lindau, M., Mohrmann, R., *et al.* (2016). v-SNARE transmembrane domains function as catalysts for vesicle fusion. Elife *5*.

Shaib, A.H., Staudt, A., Harb, A., Klose, M., **Shaaban, A.**, Schirra, C., Mohrmann, R., Rettig, J., and Becherer, U. (2018). Paralogs of the Calcium-Dependent Activator Protein for Secretion Differentially Regulate Synaptic Transmission and Peptide Secretion in Sensory Neurons. Front Cell Neurosci *12*, 304.

Shaaban, A., Dhara, M., Frisch, W., Harb, A., Shaib, A.H., Becherer, U., Bruns, D., and Mohrmann, R. (2019). The SN25 linker supports fusion intermediates by local lipid interactions. Elife *8*.

Conferences

Cell Physics 2014 (Saarbrücken, Germany): Poster presentation

Cell Physics 2016 (Saarbrücken, Germany): Poster presentation

FENS 2016: Copenhagen, Denmark: Poster presentation

DPG 2017 (Lübeck, Germany): Poster presentation

NWG 2017 (Göttingen, Germany): Poster presentation

NWG 2019 (Göttingen, Germany): Oral presentation about the “Gut-Brain axis” in the breaking news session

Acknowledgements

First and foremost, I would like to thank GOD from whom all the blessings flow. I would like to thank my mother for her great support and love during my whole life. I am grateful for what she did and I know there is no way paying her back this great support that I was luckily embraced with. I love her as a mother, as a friend, and as a sister as well. I would like also to thank my Dad for his invaluable advices since I was a child. He taught me the value of science and learning. He never stopped encouraging me when I was taking important decisions in my life to study abroad and start my professional academic career. I would like to thank my lovely sweet sisters, Nouran and Rana, who I always have great time with them. I would like to express my extreme love and gratitude to my lovely wife Nour Elazab, who has bared with me hard times without complaining and also doing her best effort in making our life in the best conditions. I want to thank my son Muhammad as he is our blessing in this life.

I would like to thank Prof. Dr. Ralf Mohrmann, who gave me the opportunity to work on this interesting project I am presenting in the thesis. He has immensely supported me with his scientific input during the entire PhD work, but also during writing this thesis. I have learned from him how to do good science and find the best approach to answer the scientific question of interest. I would like to thank Prof. Dr. Dieter Bruns who supported our team by letting us perform most of the experiments in his lab and also gave me useful advices for my work and Prof. Dr. Jens Rettig for his valuable scientific discussions during the lab meetings.

I would like to thank all the team members in the lab who enriched my stay there with many good suggestions and plenty of funny moments: Mazen Makke, Marwa Sleiman, Hawraa Bzeih, Hsin, Surya Gaya, Madhurima Dhara, and Katharina Oleinikov. Special thanks goes to Ali Shaib who is a brother to me there and to Yvonne Schwarz who was always there for me when I asked for help and Ali Harb who has been of great support to me and a helpful person in our team.

I would also like to further thank the very talented technician Walentina Frisch, who supported me with many materials (especially Semliki-Forest viruses) in the right time with very high efficiency and quality. Another special thanks goes to Marina Wirth, who was a huge support in everything in the lab, starting from breeding the mice making sure I have enough of them for my experiments, along with all the paper work and all tiny problems in the lab ending with even her emotional support acting as the "Mother of the lab".

I would like to my deep gratitude to Dr. Cordelia Imig for her unconditional and incredible support. I would like to thank Prof. Dr. Nils Brose for his very nice support and understanding. I want to thank Dr. Erinn Gideons

for helping me with my thesis. I want to thank all the lab members of the Max-Planck institute for experimental medicine for the great atmosphere they provided me.

Last but not least, many thanks to my friends, who never left me during my darkest and brightest moments in life. They never gave up trying to reach me when I was not reachable for weeks, completely focused and stuck in my work or life. They were incredibly patient and tolerant. One bless of GOD is having true friends.